



## **MODULAR PIPE RACK DESIGN AND ANALYSIS**

Lappeenranta–Lahti University of Technology LUT

Bachelor's Programme in Mechanical engineering

Bachelor's thesis

2024

Egor Kirsanov

Examiner: University lecturer Katriina Mielonen, D.Sc.

## ABSTRACT

Lappeenranta–Lahti University of Technology LUT

LUT School of Energy Systems

Mechanical Engineering

Egor Kirsanov

### **Modular Pipe Rack Design and Analysis**

Bachelor's thesis

2024

125 pages, 80 figures, 5 tables and 3 appendices

Examiner: University lecturer Katriina Mielonen, D.Sc.

**Keywords:** pipe rack, CAD, 3D, FEA, FEM, parametric modelling, design automation, modular design, structural analysis, metal structures, Inventor, Frame Analysis, RISA

The main goal of this thesis was to validate and analyse already established design of a pipe rack, as requested by Waterleau (an international wastewater treatment company). Pipe rack in question is a modular, metal structure that is used to support and guide pipes from equipment to storage or vice versa. Though the usefulness of this pipe rack has been proven in several projects, it's possible that design can be optimised further. The importance of the pipe rack is explained by its wide use, i.e. it's present in almost every company's project.

The work presents background for structures like the pipe rack, outlining general design and its challenges. Then, design automation is explained to introduce the reader to the concept of parametric modelling with an example of iLogic in Inventor Professional. Design details relevant to the topic are further demonstrated on a 3D CAD model. Next, theory and practicalities of finite element method are discussed, and the method is compared to the analytical solutions extensively. This way, finite element analysis results are validated, and shortcomings of the method and software are mentioned. The applicability of boundary conditions is argued as well.

Results such as displacements, internal forces and stresses are reported as colour maps (diagrams). The achieved results are compared in detail again, but this time with the previous findings. Reasons behind the results deviation with earlier research are studied deeply, with a conclusion that both studies are valid, and the difference is caused by different assumptions and boundary conditions. An unexpected discovery of the previous model being over dimensioned was made, confirming company's suspicions about pipe rack being overengineered. Lastly, weight and cost reduction is proposed via structural profile selection optimisation.

## ACKNOWLEDGEMENTS

I would like to thank commissioner of this work – Waterleau for giving me an opportunity to do thesis on this challenging topic and assisting me throughout the process of writing this thesis, particularly Joris van Steenwinkel, Stijn Vanderhulst, Tim Ameye, Pedro Sales, Robbe Gierts, Stefaan Verbeek and the entire CAD team in general. Special thanks go to my parents and my university friends for their continued support. I've learned a lot during these eight weeks and hope to implement obtained knowledge and understanding in the future.

## SYMBOLS AND ABBREVIATIONS

### Roman characters

$a, b, c$	parameters	-
$B$	beam depth	mm
$C_d$	drag coefficient	-
$D$	discriminant	-
$E$	Young's modulus	GPa
$f$	load vector	N
$F$	force from wind load	N
$F_{Ax}$	horizontal reaction at A	N
$F_{Ay}$	vertical reaction at A	N
$F_{Bx}$	horizontal reaction at B	N
$F_{By}$	vertical reaction at B	N
$F_R$	resultant reaction force	N
$h$	COM height from ground	m
$H$	height of the pipe rack	m
$i$	summation variable	-
$I$	second moment of area	m <sup>4</sup>
$k$	coefficient	-
$K$	stiffness matrix	N/m
$K_{ef}$	effective length factor	-
$L, l$	length	m
$m$	mass	kg
$M_A$	reaction moment at A	Nm

$M_B$	reaction moment at B	Nm
$M_l$	left corner moment	Nm
$M_r$	right corner moment	Nm
$n$	number of trans. beams	-
$N_1, N_2$	coefficients	-
$P_{cr}$	buckling critical load	N
$p$	pressure	Pa
$u$	nodal vector	m
$w$	uniform load	N/m
$W$	width of the pipe rack	m
$x$	independent variable	-
$y$	dependent variable	-

#### Greek characters

$\delta_{max}$	max beam deflection	mm
$\mu$	dynamic viscosity	Pa · s
$\rho$	density	kg/m <sup>3</sup>
$\sigma$	normal stress	MPa
$\sigma_{1,2}$	principal stresses	MPa
$\sigma_t$	Tresca stress	MPa
$\sigma_{vm}$	von Mises stress	MPa
$\tau$	shear stress	MPa
$v$	wind speed	m/s

## Constants

$g$	gravitational acceleration $9.81 \text{ m/s}^2$
$\pi$	ratio of circle's circumference to its diameter

## Dimensionless quantities

$Re$	Reynolds number
------	-----------------

## Subscripts

$1, 2, 3$	subsequent parts, e.g. lower, middle and top longitudinal beams; spacers
$beam$	variable related to the base beam
$column$	variable related to the column
$long$	variable related to the longitudinal beam
$sim$	simulation value
$spacer$	variable related to the spacer

## Abbreviations

1D	one-dimensional
2D	two-dimensional
3D	three-dimensional
API	Application Programming Interface
CAD	Computer Aided Design
CNC	Computer Numeric Control
COM	Centre Of Mass
DOF	Degree Of Freedom

FEA	Finite Element Analysis
FEM	Finite Element Method
HEA/HEB	European wide flange beams
IPE	European I beams
LC	Load Combination
LUT	Lappeenranta-Lahti University of Technology
MMAW	Manual Metal Arc Welding
NASTRAN	NASA Structural Analysis
PDE	Partial Differential Equations
S235JR	Structural steel, yield strength 235 MPa, completed Charpy V-notch test
SMAW	Shielded Metal Arc Welding
UPN	European U channels

## Table of contents

Abstract

Acknowledgements

Symbols and abbreviations

1	Introduction .....	10
1.1	Background .....	10
1.2	Research problem.....	10
1.3	Research questions .....	11
1.4	Research goals.....	11
1.5	Hypothesis.....	11
1.6	Research methods and thesis structure.....	12
2	Literature review and parametric modelling .....	13
2.1	Pipe rack design and its challenges .....	13
2.2	Parametric modelling in Inventor.....	15
3	Methods .....	23
3.1	CAD .....	23
3.1.1	3D Model .....	23
3.1.2	iLogic and pipe rack configurations .....	29
3.2	FEM.....	30
3.2.1	Theoretical background of FEM.....	30
3.2.2	Practical aspects of FEM .....	31
3.2.3	Simulation setup .....	34
3.3	Analytical solution .....	45
3.3.1	Reactions.....	45
3.3.2	Base frame .....	55
3.3.3	Beam deflection .....	59
3.3.4	Joints .....	63
3.3.5	Dead and live loads.....	66
4	Results .....	70
4.1	Configuration A .....	70



4.2	Configuration B.....	70
4.3	Configuration C.....	71
5	Discussion.....	72
5.1	Reliability and objectivity .....	72
5.2	Comparison with previous results, example 3A .....	72
5.2.1	Sensitivity and buckling analyses .....	78
5.3	Comparison with previous results, example 1C.....	83
5.4	Key results.....	85
5.5	Future improvements and usability of results .....	87
6	Conclusions .....	92
	References.....	93

## Appendices

Appendix 1. Structural profile selection sheet

Appendix 2. Pipe specifications

Appendix 3. Results of simulations

# 1 Introduction

Pipe rack is a structure used in process engineering, especially chemical, wastewater and power plants. The main task of a pipe rack is to support pipes, electrical cables and, possibly, other equipment such as valves, vessels, etc. Though pipe rack is not considered a complex structure, its design is vital, because it's a default solution in majority of process engineering applications. Furthermore, due to nature of many plant layouts, total length of a pipe rack can reach kilometres, making it one of the largest cost contributors during construction process, up to 30% of the capital cost (Moran, 2016), with Waterleau sometimes spending more than 15% of construction costs on it. Thus, standard pipe rack is preferable, which eliminates the need of detailed engineering of the structure for every new application.

## 1.1 Background

Waterleau has designed a standard pipe rack with multiple configurations, depending on the operating conditions and loads to be carried. Although the usefulness of this pipe rack has been proven in several projects, it's possible that design can be optimised further, which this work is going to investigate. As discussed earlier, pipe rack is a typical solution for process unit, wastewater treatment included, so it's used in almost every Waterleau project, having a big impact on supporting structures cost.

## 1.2 Research problem

The current industry practice for designing pipe racks often relies on conservative standards or rules of thumb that may lead to overengineering. This study investigates the design of a specific pipe rack lineup to determine if the results align with those of a previous report by an external company Advise Mechanical Solutions and to assess the potential for optimisation to reduce material use without compromising safety and integrity of the structure.

Alternatively, previous analysis can be validated by this thesis, confirming the pipe rack as an already well-established product. In case of such an outcome, no optimisation or further redesign proposal is made, but toolset used for the study's analysis is evaluated instead.

### 1.3 Research questions

This case study is going to answer the following research questions:

1. Do software results coincide with hand calculations?
2. Are achieved results similar to the previous findings?
3. What are the expected displacements, forces and stresses in the structure?
4. Can the pipe rack be optimised?
5. Can the current design be made lighter for further height increase?
6. Alternatively, how much higher loads can the pipe rack withstand?

### 1.4 Research goals

One of the research goals is to produce colour maps (diagrams) of displacements, forces and stresses distributions for all available pipe racks, so that the entire lineup is analysed, with every version (configuration) having its own validation verdict. Another objective is to analytically verify things such as reaction forces and moments, beam deflections, column buckling, comparing analytical results with the software output in the form of colour maps or beam diagrams. The end goal is to either confirm or deny company's suspicions that some pipe rack versions are overengineered.

### 1.5 Hypothesis

Waterleau raised suspicions that certain pipe rack versions are too heavy for the loads they are currently carrying. As VP Engineering Stijn Vanderhulst noted "If Third World War breaks out – everything will be destroyed. Except that pipe rack in Kenya". However, there

were no detailed investigations to support or deny these suspicions so far. Structural analysis was performed by an external company, and Waterleau believes it's worth to explore this area internally.

## 1.6 Research methods and thesis structure

First, background for the pipe rack and design automation will be given. Then, finite element method (FEM) will be used to simulate loads, with some simplified analytical solutions to confirm validity of finite element analysis (FEA). Displacements (beam deflections), internal forces and stresses from these two methods will be compared, with the support of previous report from Advise Mechanical Solutions as a reference.

Lastly, results are discussed with the conclusion being either confirming previous findings and current design viability, or possibility of redesigning the structure to improve cost efficiency. Based on that, further product proposals will be present internally for Waterleau, and due to their confidential nature, details of these proposals are not reported or mentioned in the thesis. Instead, optimisation solutions will be outlined generally.

## 2 Literature review and parametric modelling

This chapter gives reader additional information about the pipe rack and parametric modelling. Subchapter 2.1 captures main design aspects of pipe racks through literature review and Waterleau's experience. Subchapter 2.2 introduces reader to the concept of design automation in the form of parametric modelling via both mathematical and practical examples.

### 2.1 Pipe rack design and its challenges

In every project, pipes are used to transport fluids from point A to point B, e.g. from equipment to storage or vice versa. Similarly, electrical cables are used to foresee all equipment from electrical power to data-exchange. These pipes and cables need to be supported in an economical manner, considering both space and cost. It is important to note that storage racks are different kind of structures even if they are used to store pipes (Drake and Walter, 2010).

Pipe racks greatly differ in size across different industries, which includes main dimensions of width and height, number of supporting layers (tiers) and structural shapes. Typically, petrochemical pipe racks are the largest, up to 20 m wide for double bay applications (Morrison, 2018), while pipe racks used in wastewater treatment industry are significantly smaller, and the one used by Waterleau ranges from 1.2 to 2.2 m wide, taking into account 20-25% of extra space for future piping expansion. Spacing or span (distance between columns in longitudinal direction) is usually no more than 8 m, and mostly depends on the piping load and landscape, while height is directly linked to the number of supporting layers, though it is recommended to have column height to be no less than 3 m (Bausbacher and Hunt, 1994).

Despite size differences, all pipe racks are moment frames, with columns carrying transverse beams, that support piping and equipment. Pipe rack can be strutted or un-strutted (with or without longitudinal beams, latter case being cantilever columns, as Drake and Walter (2010) mention in their article), the pipe rack under consideration is strutted because it allows more transverse beams per span, thus decreasing number of required base subassemblies, as

can be seen on Figure 1 and Figure 2. Material selection is dictated by the modular nature of the design: structure can be steel, concrete or steel reinforced concrete. Last two are more expensive and more time-consuming to construct due to weather dependency, though require almost no maintenance. The main obstacle, however, is the difficulty or complete inability of pre-fabrication in a workshop. Consequently, steel is selected, allowing partial fabrication in a shop, facilitating better quality control, simpler logistics and easier assembly on-site, thanks to bolted connections between structural members, which reduce welding operations on-site.

Modular design also implies high level of customisation to satisfy different requirements, offering high cost-efficiency: for heavier loads from piping, wind or earthquakes bigger structural profiles are selected to anticipate safe operation, e.g. no yielding, while lower loads can be satisfied with smaller profiles, making pipe rack lighter and cheaper. Modularisation is further improved with base being subassembly, which also allows installation clearance.

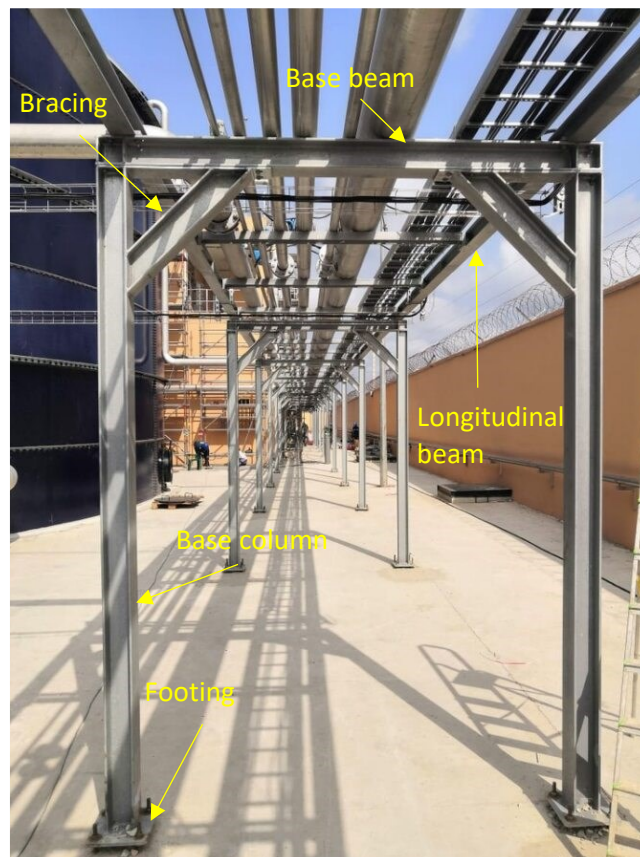


Figure 1. Pipe rack overview (Stijn Vanderhulst).



Figure 2. Pipe rack details (Stijn Vanderhulst).

## 2.2 Parametric modelling in Inventor

Parametric modelling is different from direct modelling in a way that geometry is altered via algorithms and associations, rather than direct manipulations, which allows creating theoretically an unlimited number of variations of original design in a short period of time. Parametric modelling in traditional CAD (computer aided design) programmes like Autodesk Inventor is based on direct modelling anyway, so it can be seen as a combination of two approaches. It is a very powerful tool in the right hands that can save huge amount of time during a development phase of a product which flexibility and customisation will be limited only by the complexity of the parametric model, which is essentially a system of parametric equations.

Parametric equation is an equation that has an independent variable called parameter. In such equation, dependent variable is expressed in terms of a parameter, e.g. is defined as a function of a parameter (Ucal, 2024). It's the opposite to non-parametric equations, where there is a unique value for dependent variable for every value of independent variable (CAD/CAM Machine Drawing and Computer Graphics, 2013). General equation of a parabola is an example of a parametric equation:

$$y = ax^2 + bx + c \quad (1)$$

where  $a$ ,  $b$  and  $c$  are parameters. If we substitute  $a = 1$ ,  $b = 2$  and  $c = 3$ , then:

$$y = x^2 + 2x + 3 \quad (2)$$

is no longer a parametric equation. For a deeper insight, let's find for what values of parameter  $a$  the following equation has zero, one and two solutions:

$$x^2 + 4x + a = 0 \quad (3)$$

We know that quadratic equation has zero, one and two solutions when its discriminant is less than, equal or more than zero respectively. Discriminant of the equation is:

$$D = 4^2 - 4 \cdot a \quad (4)$$

Equation has zero solutions when:

$$D < 0 \rightarrow 16 < 4a \rightarrow a > 4 \quad (5)$$

Equation has one solution when:

$$D = 0 \rightarrow 16 = 4a \rightarrow a = 4 \quad (6)$$

Equation has two solutions when:

$$D > 0 \rightarrow 16 > 4a \rightarrow a < 4 \quad (7)$$

It's also possible to solve such equations graphically – since parameter  $a$  represents shift along  $y$ -axis on the  $xy$ -plane, we can plot such parabola with different values of the parameter to see when graph doesn't cross  $x$ -axis, when it barely touches it and when it intersects it twice, representing zero, one and two solutions respectively. We can also solve for  $x$ , for example we know that equation has one solution only when  $a = 4$ , so  $x = -2$ . The problem with graphical method is that it's numeric – an initial guess for the parameter is needed, it can't be solved analytically. Autodesk Inventor is similar in this regard, since it's CAD, it also focuses on the numeric solutions. Short 2D (two-dimensional) sketch demo is presented below.

Sketch consists of two right triangles and a rectangle, with one of the triangles sharing one side with the rectangle. Triangle on the left has bottom leg of a constant length (20 mm), while another leg has length as a parameter called "a" in parameter table. Inventor



automatically calculates length of the hypotenuse (value is displaced in brackets and in the table). Then, at a distance that equals half of hypotenuse, rectangle is drawn with one side equals parameter “a” and another double the parameter. Finally, second triangle has an angle of 45 degrees, with the entire sketch and parameter table being shown on Figure 3. Changing parameter’s value will change both size and location of another two shapes. Furthermore, a short If-Else statement can be implemented with iLogic programming environment, so that second triangle changes its direction depending on the ratio of parameter to half of hypotenuse, as seen on Figure 4. Note that all created dimensions are parameters in Inventor, bottom leg of the first triangle was assumed to be constant for simplicity, but in fact it is also a parameter, changing which will affect hypotenuse and location of the remaining shapes, but not their size, since their dimensions are linked only to parameter “a”.

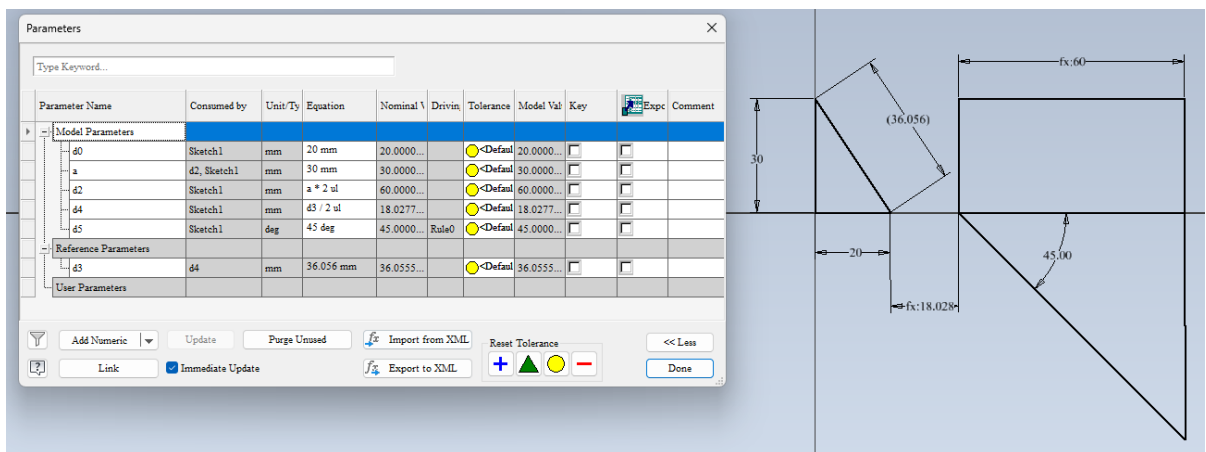


Figure 3. Initial demo sketch.

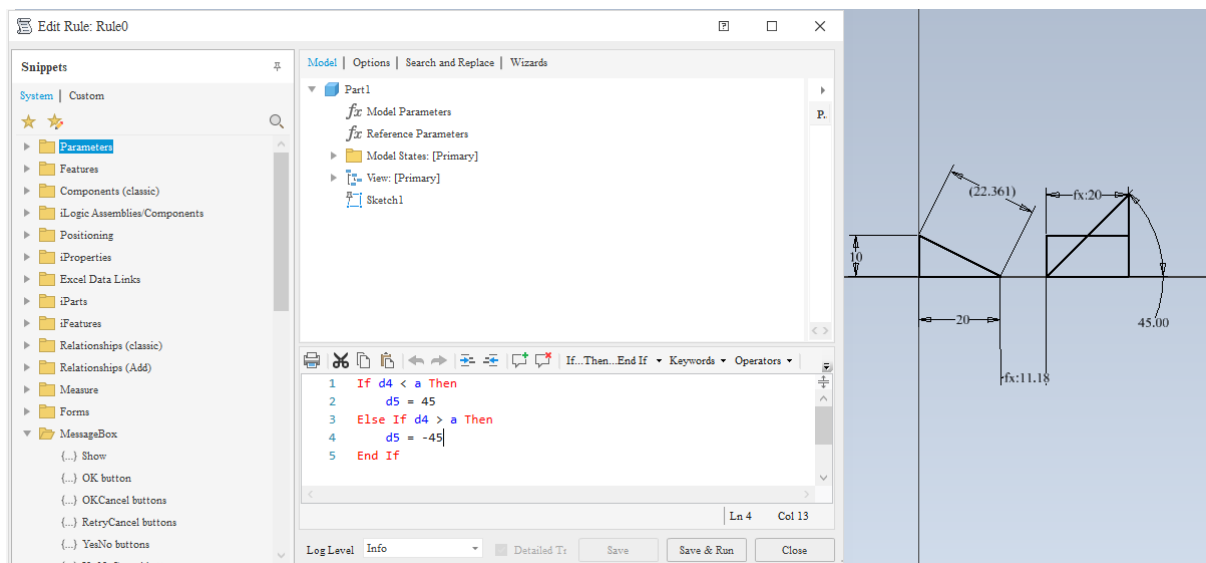


Figure 4. New demo sketch after changing one parameter.

Moreover, logic can be utilised to suppress and un-suppress features on part-level, and parts on assembly-level. Parameters can be linked and shared between different parts, so that one parameter can simultaneously change geometry of multiple parts. In Autodesk Inventor environment, custom parameters can be created either in parameter table, along parameters from sketches and standard features, or in iLogic. Fundamental workflow of iLogic is script writing, also known as rules writing, though it can be expanded further into creation of user-friendly forms or linking spreadsheets like Excel. When the concept is fully understood, it's possible to create more complex models that are limited only by one's imagination and machine's computational restrictions. Example of iLogic script can be seen of Figure 5.

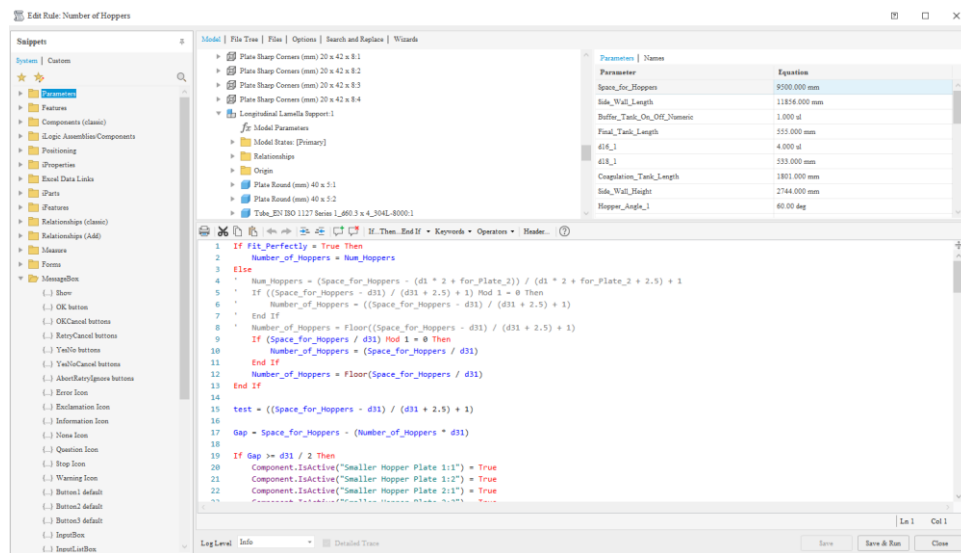


Figure 5. iLogic script example.

To give an example of a possible outcome, parametric model of a containerised lamella clarifier developed by Waterleau can be used. iLogic model can calculate number of hoppers required to fit in the allowed space, which, in turn, is calculated from the user's input of the total length and the length of either of compartments (in front or back of the container). The opposite can also be done – specified geometry (length, depth, angle) of the hoppers and number of them will define length of compartments according to manufacturing preferences. Other parts like stiffeners, frame members, gutters, piping, etc., follow similar rules, while it's also possible to adjust other dimensions such as height and width. Boundary conditions or model limits can also be applied, for example, if in the abovementioned model number of hoppers is so high that the length of either compartment becomes negative, message is displayed that such configuration cannot be created, and new user input is asked, or model is recalculated with the properties being closest to the “impossible” ones. Another possibility

is to swap parts for different manufacturing approaches, as changing sheet parts' arrangement for butt- or corner-welding.

Initially, 40-foot-long configuration with eight hoppers is presented. Then, number of hoppers is reduced to four. After that, total length is halved to 20 feet. Later, number of hoppers is decreased to two. Finally, height is increased by 30%. These configurations are represented on Figure 6, Figure 7, Figure 8, Figure 9 and Figure 10 respectively.

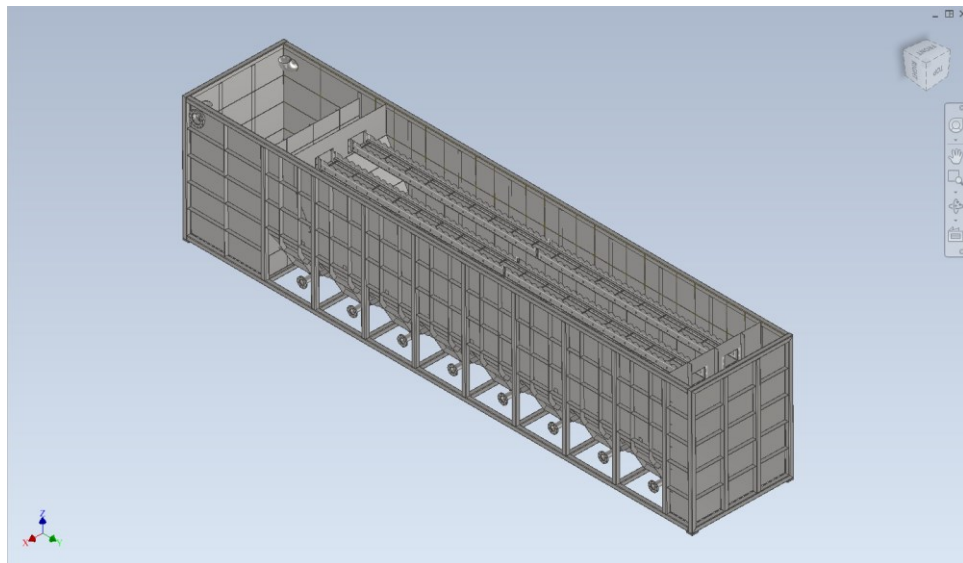


Figure 6. 40-foot-long lamella with eight hoppers.

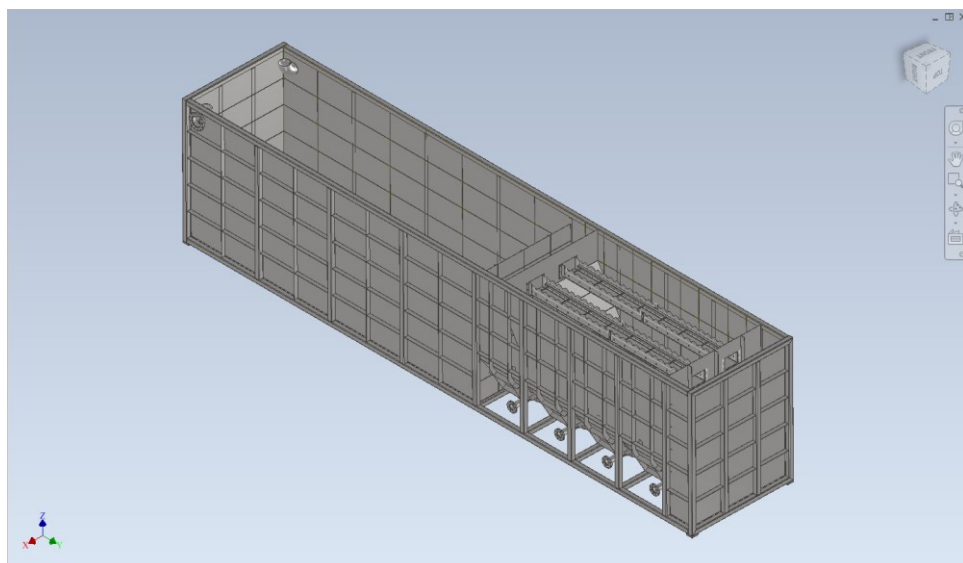


Figure 7. 40-foot-long lamella with four hoppers.

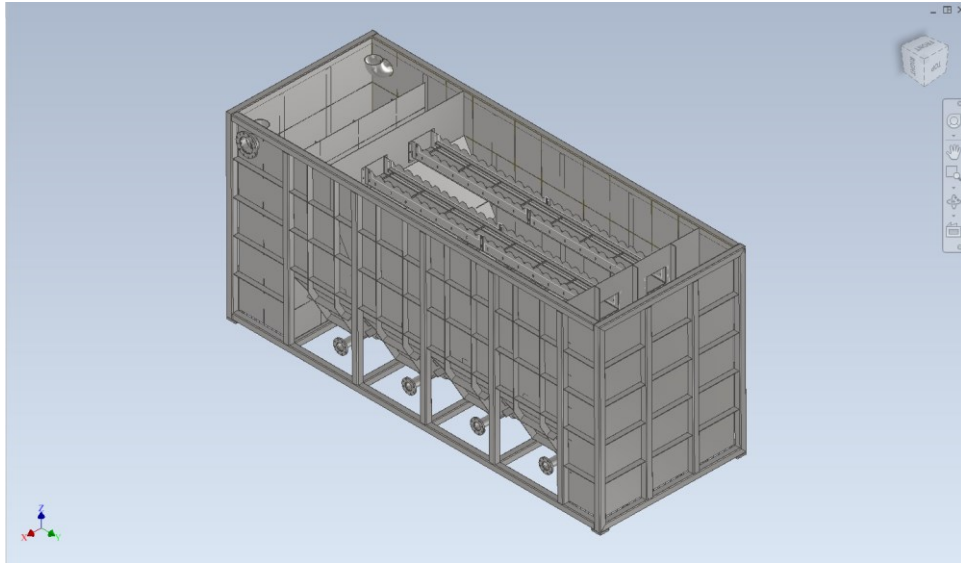


Figure 8. 20-foot-long lamella with four hoppers.

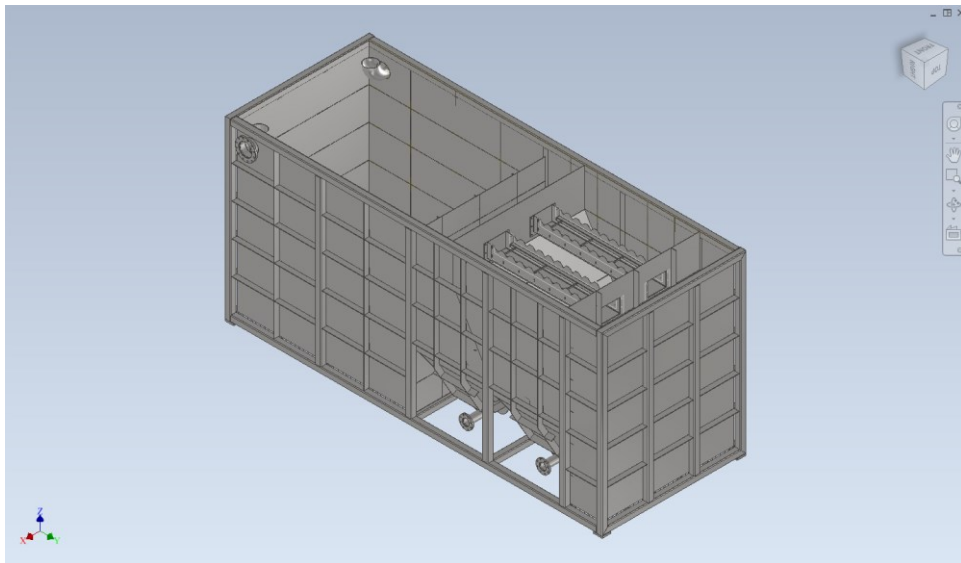


Figure 9. 20-foot-long lamella with two hoppers.

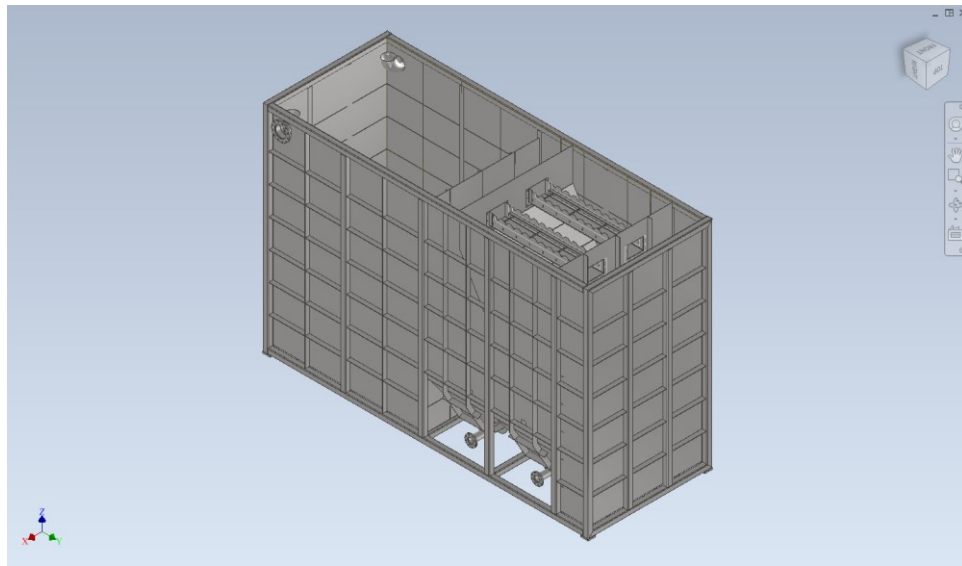


Figure 10. 20-foot-long lamella with 30% increased height.

Note that these five configurations were created in a span of five minutes, considering computational time. Actually, none of the versions were ever directly modelled. Instead, generalised and parametrised model was created, which allows the use of arbitrary length, height, width, number of hoppers, hopper geometry, stiffeners configuration, etc. Overall, iLogic model's complexity with respect to the given dimension heavily depends on the product's topology and geometry. In other words, containerised lamella is relatively easy to "scale" in vertical direction but requires many computations and considerations to "scale" in longitudinal direction, while an axis-symmetric assembly, like a cylindrical tower, can be easily parametrised in the axis direction (e.g. height), but is tricky to do so in radial direction. In any case, parametric approach in 3D (three-dimensional) modelling requires dedication, patience, forward-thinking and complete understanding of the model to be developed from the designer's side. In terms of the software, there are commercially available packages for the most popular CAD programmes developed by third parties, while iLogic is an integrated part of Autodesk Inventor.

It's important to understand that despite many applications – from modularisation to optimisation – parametric modelling is not an ultimate solution. Developing such models takes much longer, especially in the beginning, when a lot of time is spent on creating parameters and establishing associations, however in the long-run time savings will be higher, if the product to be designed is not unique. For instance, if a replacement part is

needed to be designed and fabricated quickly, parametric approach will be a waste of time, while in iterative design parametric modelling is a truly powerful tool. In addition, parametric modelling, as other programmatic solutions, is prone to bugs and some logic errors can have devastating effects on the models, such as breaking all model constraints, or even worse, corrupting files. That's why it's recommended to test any experimental scripts (no matter created by the designer or found elsewhere) on a dummy assembly to avoid costly mistakes, especially if script concerns file management, renaming or properties overwriting.

## 3 Methods

This chapter covers methods being utilised, gives their background and compares different approaches. First, computer aided design (CAD) is discussed, then FEM is investigated, followed by analytical solutions subchapter. The chapter is constructed in a way that the subsequent chapter reports only results.

### 3.1 CAD

CAD tools greatly enhance and speed up development phase in engineering field. Modern CAD allows designers to communicate with manufacturers or constructors in an efficient way. LUT, as many other universities, uses mainly SolidWorks from Dassault Systems for study purposes, while Waterleau uses Inventor from Autodesk. Both are similar in terms of sketching and modelling with some minor differences – one can easily transfer their skills from SolidWorks to Inventor and vice versa. However, there are some bigger differences like application programming interface (API), for example iLogic, and design/analysis add-ons. Software choice is justified because LUT has license for Femap and Ansys for more flexible FEA, while Waterleau uses AutoCAD and Revit for plant layout design and civil engineering, with latter two being also Autodesk products (AutoCAD + Revit + Inventor is a popular package in the industry).

#### 3.1.1 3D Model

Inventor Professional 2024.2 was used for this work. Whatever the configuration is chosen (generic model is on Figure 11), assembly has base as a separate subassembly, which is fixed to the ground via anchoring and connected to the top structure via Lindapters (Figure 12). Lindapter is a beam clamp which has an advantage of higher adjustability over bolted or weld connection. Put differently, clamp allows to change span easily by sliding base along top structure (or vice versa) and tightening clamp when needed. According to the manufacturer of the adapter, static slip resistance is 70 kN or 250 kN tensile (LinDapter, n.d.), so connection is considered to be rigid, which will be important later.

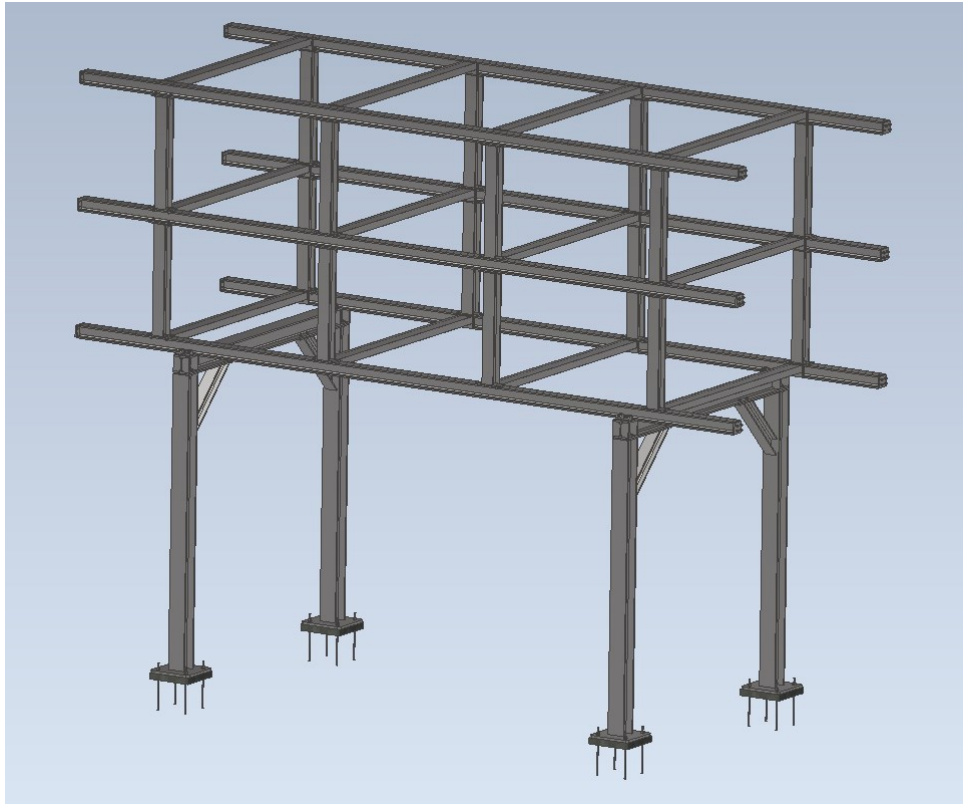


Figure 11. Generic pipe rack section (module).

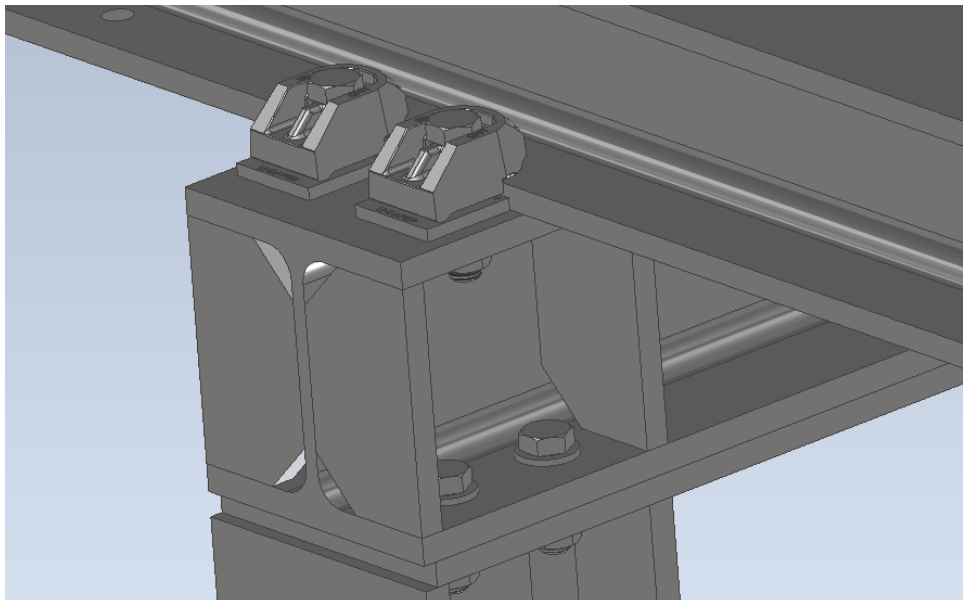


Figure 12. Lindapters clamp orthogonal beams.



Base consists of two columns, beam and bracing between them (Figure 13). Bracing is welded to the columns (highlighted in blue on Figure 14) and then beam is bolted to the columns and the bracing. Beam is stiffened at the connections with columns to avoid undesired torsion and warping of beam flanges and local buckling of a web. Lindapters are located between beam stiffeners. Intermediate plate that connects bracing and column into one piece makes structure more robust and makes installation simpler thanks to easier alignment of parts.

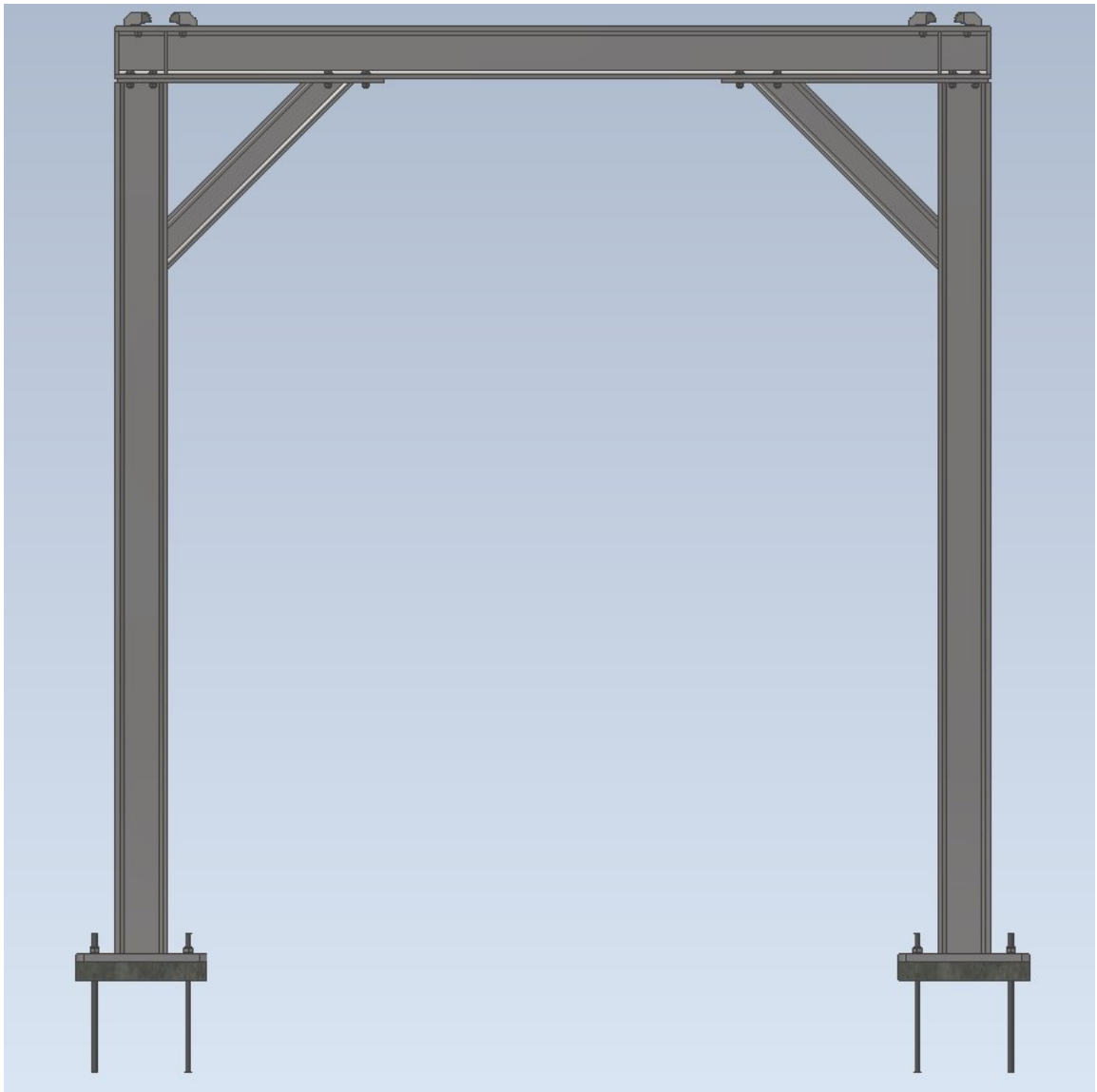


Figure 13. Base subassembly.

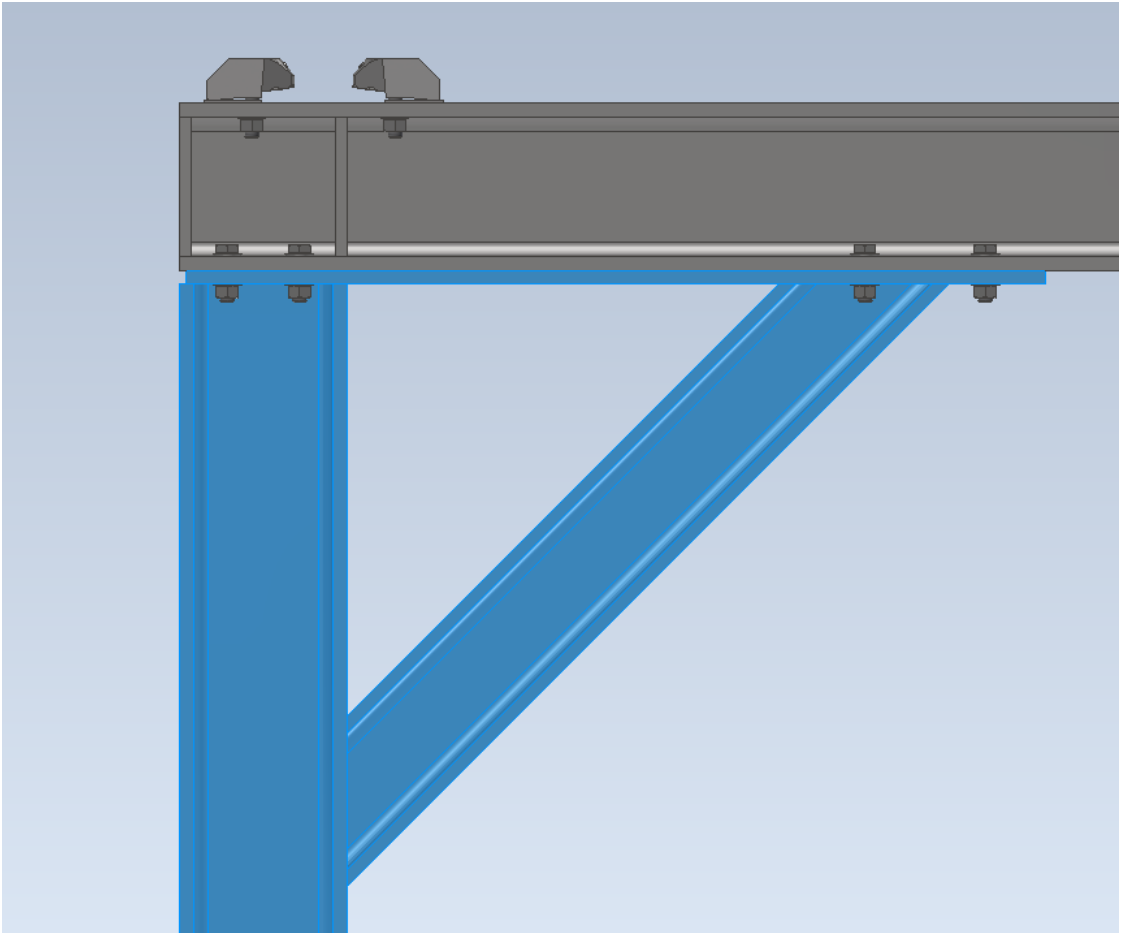


Figure 14. Bracing of a column.

Top frame is a bolted structure (Figure 15). It's important to mention that bolted connections (Figure 16 and Figure 17) between beams require welding of end or side plates, as well as drilling holes in the plates for the bolts, though all these operations can be performed in a workshop, ensuring sufficient quality control, e.g. on a special beam cutting machine with computer numeric control (CNC). Therefore, separate subassemblies can be shipped, and on-site installation will be mostly fastening beams together.

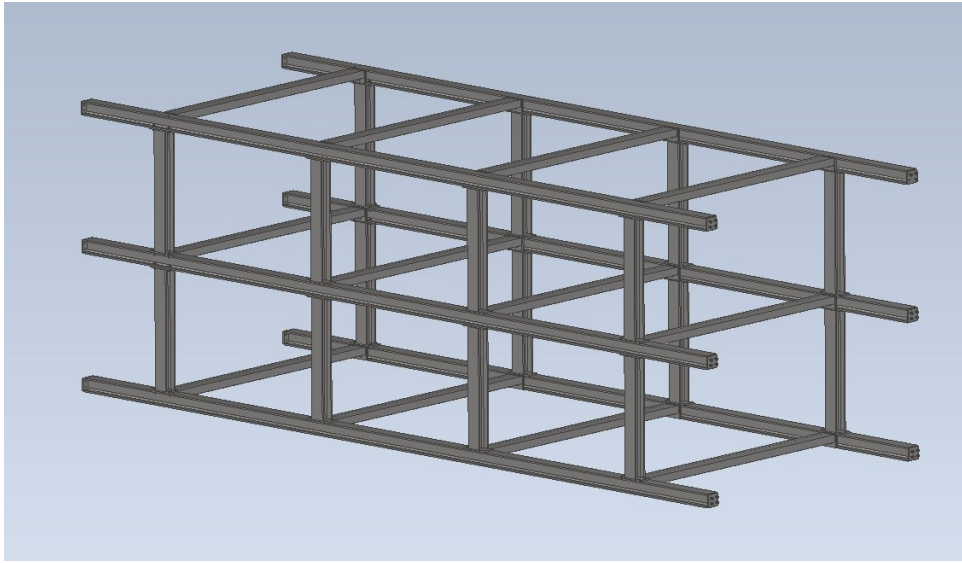


Figure 15. Top frame.

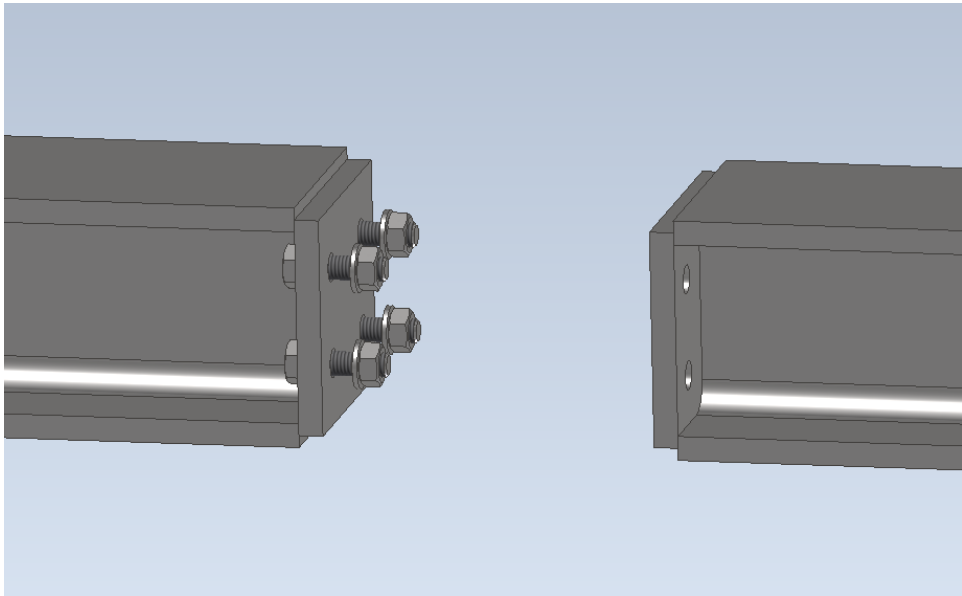


Figure 16. Bolted connection disassembled.

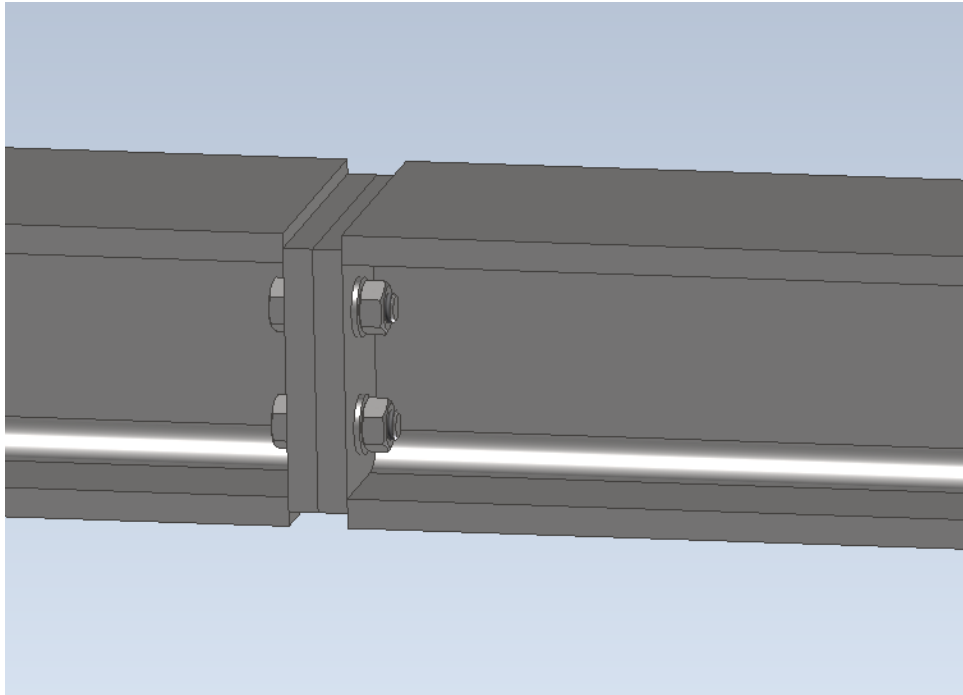


Figure 17. Bolted connection assembled.

Such connection doesn't eliminate on-site welding completely (piping will require additional welding), but greatly reduces it, which has both cost and quality control advantage – on-site welding is usually stick welding (SMAW/MMAW), which requires high level of skill from the welder and takes more time to perform due to clean up operation and electrode change. Spacers, transverse beams and longitudinal beams are all connected in a similar manner (Figure 18).

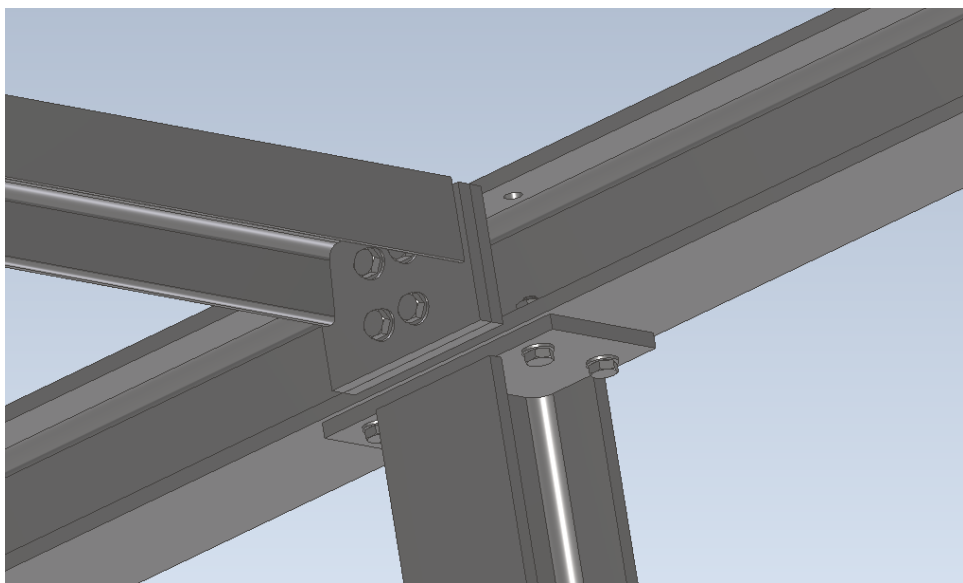


Figure 18. Spacer, transverse beam and longitudinal beam connection.

### 3.1.2 iLogic and pipe rack configurations

As can be seen, modularity of the pipe rack dictates it to be a bolted structure. If it was a weldment, a Frame Generator Inventor environment would be used, where skeletal model (3D sketch) is created, with solid structural members being modelled around 1D (one-dimensional) entities of the sketch. Due to lack of mitre, notch, trim and corner joint operations, as well as presence of only right-angle connections, beam subassemblies with plates are assembled in a more classic CAD approach, in the default environment. Note that all beams and plates are from Content Centre library, not custom parts, which will be important later.

Parametrising of the pipe rack is done similarly to the example from previous chapter, which allows the user to change main dimensions and structural profiles. User-friendly form has been created with iLogic for sizing the pipe rack and selecting required configuration (Figure 19).

The screenshot shows a software interface titled "Piperack Sizing" with a close button (X) in the top right corner. The interface contains several input fields and sliders:

- Piperack\_Setup:** A dropdown menu showing "3B-S".
- Module Length:** A slider set to "6000 mm".
- Piperack Width:** A section with a sub-header "Piperack Width" and a "Width" slider set to "2200 mm". Below the slider, it says "Max 2200 mm".
- Levels:** A dropdown menu showing "3".
- Spacing between Layers:** A slider set to "1000 mm".
- Height Base Frame:** A text input field containing "2450 mm".
- Maximum Load Per Layer:** A dropdown menu showing "250 kg/m".

At the bottom of the form, there are three buttons: "Update Sizes", "Update Bolts", and "Done".

Figure 19. iLogic form for the pipe rack configurator.

Excel sheet can be linked to the 3D model in Inventor. In terms of main dimensions, four standard configurations are used by Waterleau, noted as A, B, C and D (Table 1).

Table 1. Pipe rack configurations (all dimensions are in millimetres)

Config.	Width	Base Height	Spacing	Layer Height	Layers	Free Overhang
A	2200	3600	5000	1000	3	2500
B	1500	3600	4000	750	3	2000
C	1200	2600	5000	750	2	2500
D	2200	6000	8000	1000	3	2500

However, D configuration is currently not available in Inventor. For every dimensional configuration there are three load cases and a modification for seismic region (seismic analysis falls beyond the scope of this work because of its complexity and software limitations that can't simulate earthquakes). In total 24 configurations, but load cases affect only beam profile selection (see Appendix 1).

## 3.2 FEM

FEM is a numeric method that uses discretisation of space into small parts called elements to solve many engineering problems. FEM is mostly used in structural analysis, but can be used for thermal analysis, computational fluid dynamics and other fields of engineering as well. Essentially, FEM solves system of equations to approximate functions between points of interest (functions can be displacements, stresses, strains, etc.).

### 3.2.1 Theoretical background of FEM

In general, many complex physical phenomena can be expressed by partial differential equations (PDE) that are usually impossible to solve explicitly, so integral form (also known as weak form) is used, that can be solved by summation approximation, e.g. solved numerically (Polyanin, et al., 2008). Discretised parts of the problem are known as elements, while their points of interest (located at element bounds) are called nodes (Harish, 2024). PDE are solved at nodes and then interpolated between them via shape functions, linear or polynomial. System of equations in matrix form is:

$$[K]\{\vec{u}\} = \{\vec{f}\} \quad (8)$$

where  $K$  is stiffness matrix, that depends on material's properties and object's geometry,  $\vec{u}$  is a nodal vector (displacement vector), and  $\vec{f}$  is a load (force) vector. Note that stiffness matrix is a scalar, so it doesn't have vector notation. We are trying to find displacement field, so after multiplying both sides by inverse stiffness matrix:

$$\{\vec{u}\} = [K]^{-1}\{\vec{f}\} \quad (9)$$

There are much deeper mathematical explanations with calculus and matrix transformations, but basically majority of academic and commercial FEM solvers try to compute inverse of the stiffness matrix (though some use iterative approach), but for that to happen, boundary conditions – loads and constraints – should be applied, to eliminate some equations, otherwise stiffness matrix is singular and thus cannot be inverted. That is, if structure doesn't resist any loads and is absolutely free to move, then no meaningful results can be obtained from FEA, because system of equations has an infinite number of solutions, since system is linearly dependent.

### 3.2.2 Practical aspects of FEM

There are many pre- and post-processors available for different solvers. For example, NASTRAN solver can be used in both Femap and Inventor NASTRAN, though their pre- and post-processing capabilities are different. Femap has wider selection of element types, material properties and mesh control settings, but Inventor NASTRAN can be embedded in Inventor Professional, thus eliminating the need for CAD model export-import, which greatly simplifies workflow for modular and iterative designs.

Workflow is similar across different pre- and post-processors:

1. Geometry import/creation/modification
2. Assigning simulation properties: material, type of simulation, failure theory, etc.
3. Boundary conditions, e.g. loads and constraints
4. Mesh generation and control
5. Analysis and post-processing

Mesh generation is arguably the most difficult part of FEA for multiple reasons: software doesn't always allow precise control, or is not user-friendly; appropriate element type should be chosen, preferably linear for optimisation, though second order elements became standard in most software packages; less dimensions of the elements is better since less mesh control will be required (e.g. mesh of solid elements is more difficult to control than mesh of shell elements); correct element size is needed not to lose accuracy in areas of interest, but also to be computationally adequate; mesh refinement should be performed to check results convergence. In other words, though solid ten-node tetrahedron element (standard in in-build Inventor FEA environment) might sound like an ultimate one – it's not always the best choice, not only because number of elements can exceed few millions for a relatively big assembly, but also because mesh quality control becomes harder, since one needs to keep an eye on mesh density, aspect ratio of the elements, their skewness, etc. Such approach gets even more complicated when multiple models should be analysed. Consequently, optimisation to some extent is required. It's preferable to reduce the number of dimensions in analysis (for the element), rather than interpolation type – it's important to keep in mind that linear shape functions tend to underestimate displacements in bending problems by excessive linearisation due to phenomenon known as shear locking, when strain, derivative of displacement, becomes constant across the model which underestimates strain energy and skews results, since derivative of a linear function is a constant (Harish, 2023).

Pipe rack is built from beams that typically have their length much greater than cross-section dimensions (e.g. high slenderness ratio), thus such structure can be approximated with 1D beam elements. This way, mesh creation is greatly simplified – user needs to define only number of nodes per beam, which also allows convergence check. However, approximation doesn't take into account details like bolted connections, assuming fixed connections (that's why beam clamp should produce enough clamping force). Geometry discontinuities like endplates are also neglected. As a consequence, stress analysis becomes difficult to perform due to approximations eliminating stress concentrations, that are located at geometry discontinuities. At the same time, overall displacement analysis should remain valid and identify the most loaded members, while separate analysis of connections can be performed separately with shell or solid element mesh with NASTRAN solver in the future.

Structure can be approximated by 1D elements safely if slenderness ratio is more than ten (Duffin, 2023). Moreover, case study by Ryan Dark (2018) suggests that slenderness ratio



of over four can already produce accurate enough results. It's important to note that Dark's case study compares simulation results with analytical solution, not experimental data, and analytical formula that has been used was derived from Euler-Bernoulli beam theory, that also has some assumptions regarding slenderness ratio. In other words, most likely, in practice, both analytical solution and FEA will have a compelling error for low slenderness ratios ( $< 5$ ).

Using Appendix 1, it's possible to find slenderness ratios for worst scenarios – smallest main dimensions with highest loads (and thus bigger profiles). Worst scenario for base column is 1C: HEA120 with column height of 2600 mm, which gives slenderness ratio of 21.67 – acceptable. Worst scenario for longitudinal beam is 1B: HEA120 with span of 4000 mm, which gives slenderness ratio of 33.33 – acceptable. Worst scenario for transverse beam is 1C: UPN100 with width of 1200 mm, which gives slenderness ratio of 12 – acceptable. Worst scenario for spacer beam is 1B: HEA120 with spacing of 750 mm, which gives slenderness ratio of 6.25 – questionable.

It can be observed that almost all members satisfy conservative requirement of slenderness ratio of ten, except spacers. According to the previous research, slenderness ratio of 6.25 will still yield acceptable results, but high accuracy is not expected. Spacers can be meshed with beam elements also due to the fact that there are multiple spacers on every span, so they are naturally less stressed, and load is transferred more evenly through spacers than, for example, through columns, so no sharp gradients are expected there. Bracing, being secondary structure, can also be meshed with beam elements, despite low slenderness ratio.

Taking abovementioned information in consideration, Frame Analysis environment can be used in Inventor Professional, which requires assembly to be either modelled in Frame Generator environment or constructed from Content Centre parts. Though Frame Analysis doesn't use a traditional FEM solver, according to Autodesk linear, two-node beam elements with six DOF (degrees of freedom) at each node are used for meshing and solver type can be chosen by the user, Gaussian elimination included (used to compute inverse stiffness matrix directly and it's utilised in this study). Linearity is not a big issue in this case, since h-refinement is simple in 1D analysis by adding custom nodes and creating new elements, but Frame Analysis has a more user-friendly feature where number of calculation points per element can be set (default is 50). However, shortcomings of linearity should be kept in mind.

### 3.2.3 Simulation setup

While setting up the simulation, it's important to mention that symmetry will not be utilised since some asymmetric loads are expected in the future, and computational time will be insignificant anyway because of 1D analysis. The same material is used for all structural members – S235JR structural steel with the properties from Waterleau material library, as shown on Table 2.

Table 2. Material properties

Density, kg/m <sup>3</sup>	7850
Young's modulus, GPa	220
Poisson's ratio	0.275
Yield strength, MPa	207
Tensile strength, MPa	345
Shear modulus, GPa	81.7

Young's modulus depends on the temperature, and the used value is slightly higher than standard 210 GPa for most steels, so it was probably defined for below room temperature. Another thing to note is that yield strength depends on the thickness of the product. Designation of the steel implies yield strength of 235 MPa, but it's true only for thinner plates (less than 16 mm), and starts to decrease with thickness increase. Value that was used is conservative, but such details must be discussed with particular suppliers, since different manufacturers use different techniques and equipment. S235JR also has good weldability (Metinvest, n.d.) and, as for other metals, isotropic behaviour is simulated. Galvanised steel was chosen over stainless due to its lower price and sufficient strength properties for a structure like pipe rack. Economic analysis of the pipe rack falls beyond the scope of this thesis, but from Waterleau's experience, stainless steel can be four and more times expensive per mass unit than galvanised steel. Nevertheless, stainless steel can be used for base subassembly fabrication in case it's used separately as a quick solution for pipes support. In addition, number of beam points is set to 50.

Mesh generation and applying boundary conditions are shown on a generic pipe rack (Figure 20) with arbitrary dimensions, all other simulations follow the exact same pattern. First, existing solid model of the pipe rack is converted into skeleton model. Note that it's the opposite workflow to Frame Generator, where solid model is created from a user-defined

skeletal model. Essentially, the result is a 3D sketch, but members are now 1D elements (in green), connected by nodes (in dark blue), previously solid members are displayed as transparent, so that conversion imperfections can be seen.

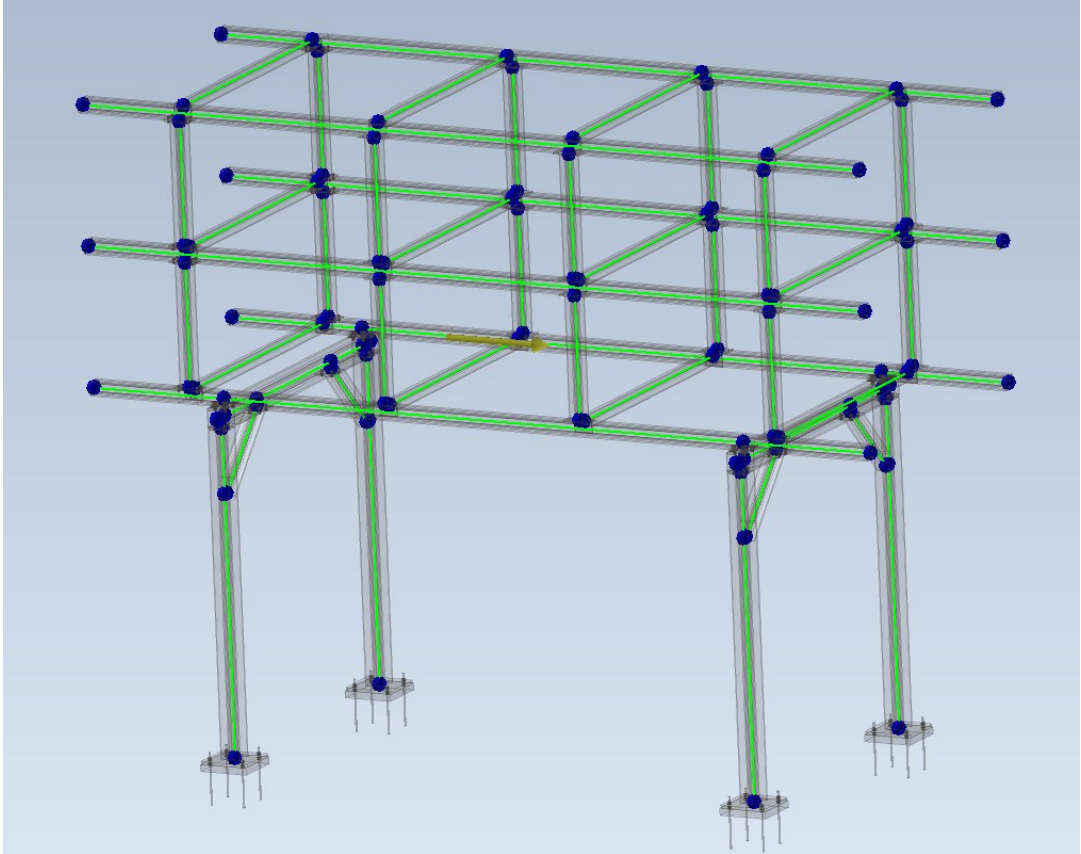


Figure 20. Skeletal model of a generic pipe rack.

Geometry investigation and manual adjustments are required, since conversion algorithm is not universal, the user might want to increase or decrease number of rigid links (in orange). For example, with standard settings, base subassembly is poorly connected, with column being joined to the base beam only at one point (Figure 21), near the bracing, while spacers and transverse beams are not attached to longitudinal beams at all (Figure 22). From the previously discussed theory, we can deduce that absence of any type of connections/bonds between members will result in a singular stiffness matrix, the inverse of which can't be computed, so no useful results can be produced. The physical interpretation is that if transverse beams are not connected to the rest of the structure, then any load applied to them (even gravity) will not be transferred to the other structural members – in reality unsupported beam would fall off indeed. Consequently, additional rigid links must be added or created.

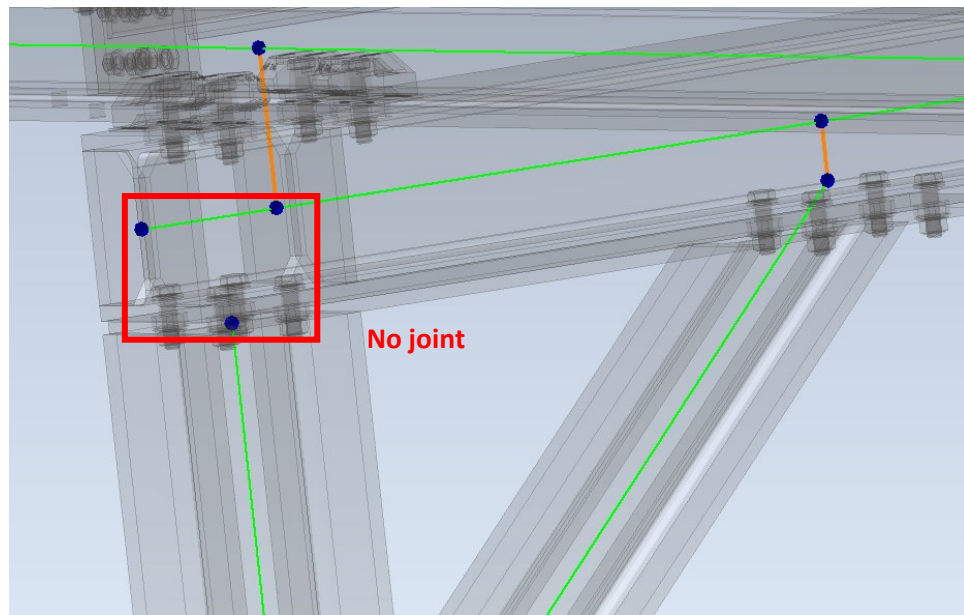


Figure 21. Inaccurate column connection.

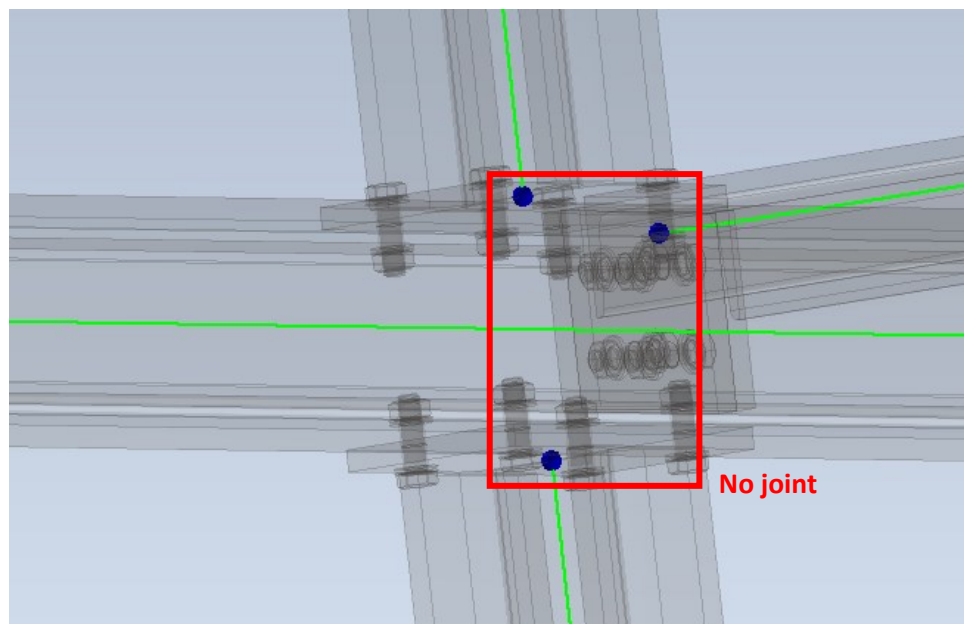


Figure 22. Inaccurate spacers and transverse beam connection.

Then tolerance of rigid link creation can be adjusted, not absolutely, but as a percentage. Thus, iteration is required. Default value is two percent, increasing it to ten partially solves the issue, after updating the model. (Younis, 2010)

For instance, now spacers are attached to the longitudinal beam, but not the transverse beam (Figure 23). Consequently, tolerance is further increased to 20%.

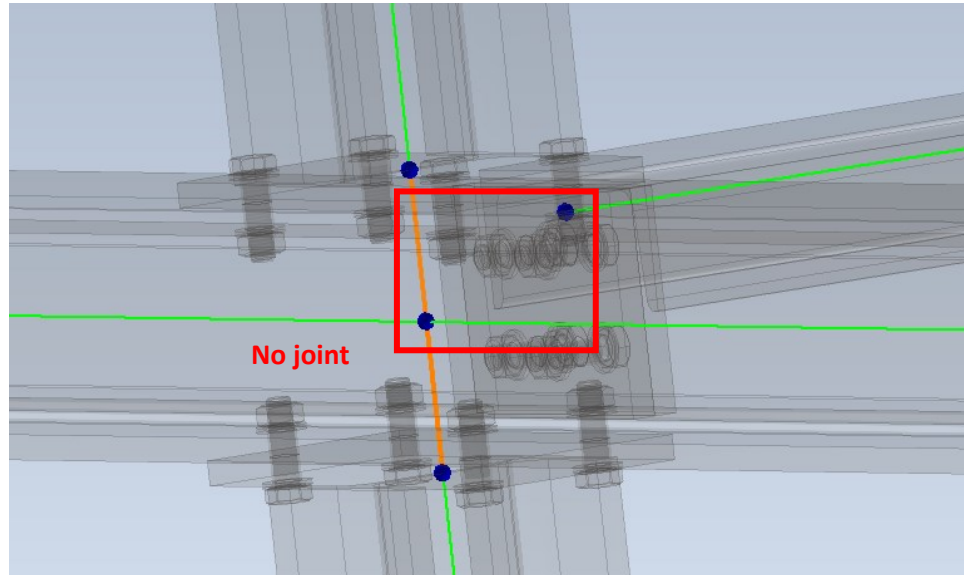


Figure 23. Still incomplete connection.

This time all geometry discontinuities are cured with additional rigid links, so that each column attaches to two points on the base beam, thanks to bracing (Figure 24), and all spacers and transverse beams are connected to longitudinal beams (Figure 25). It is also possible to create custom rigid links and nodes. Members can be converted to rigid links as well, to represent, for example, anchoring.

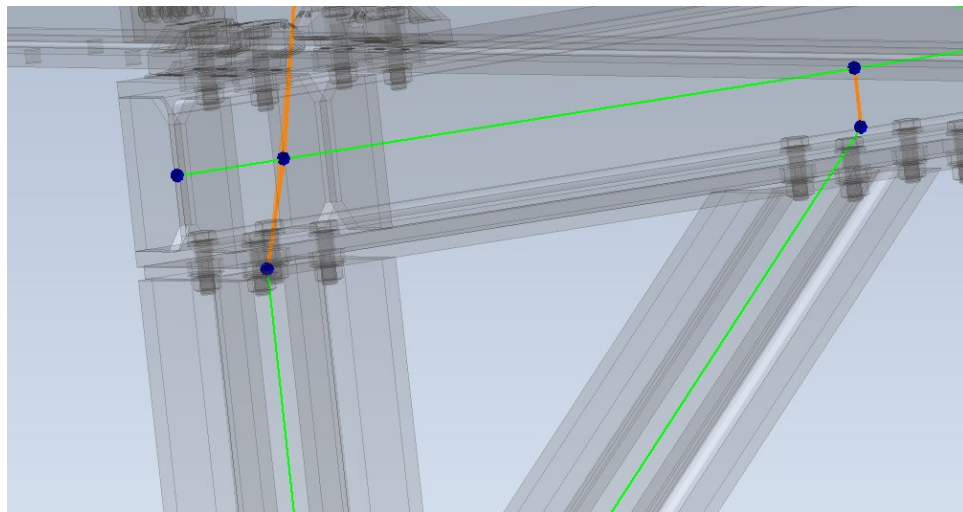


Figure 24. Accurate column connection.

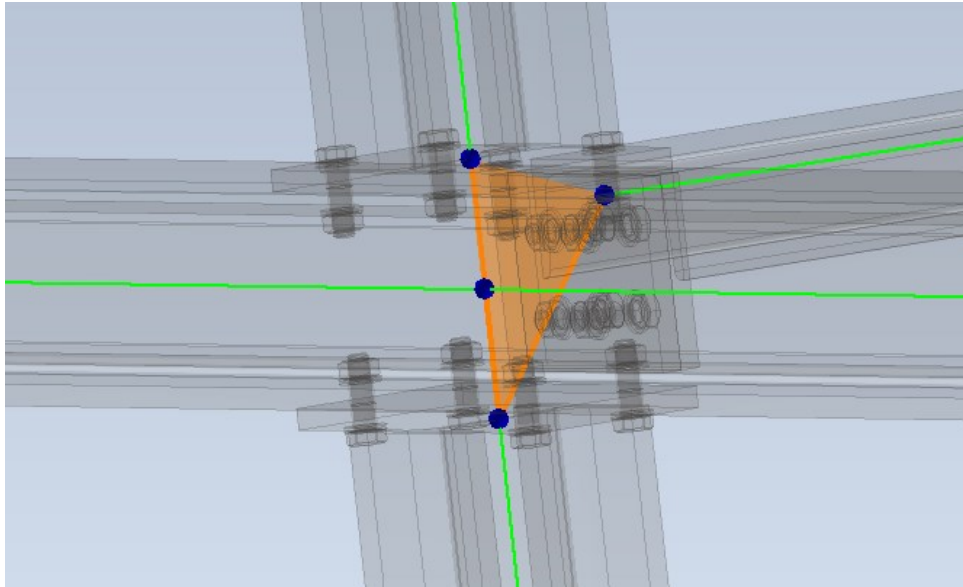


Figure 25. Accurate connection.

After geometry modifications, previously solid members can be made invisible and boundary conditions should be applied. It makes sense to start with constraints first, because they will be consistent throughout all simulations – either pinned or fixed at the bottom of the structure, unlike loads, that can be continuous in nature, having different magnitudes and directions, applied to different nodes/elements. Initially, pipe rack is considered to be anchored at the ground, so fixed constraints are applied at the bottom (Figure 26).

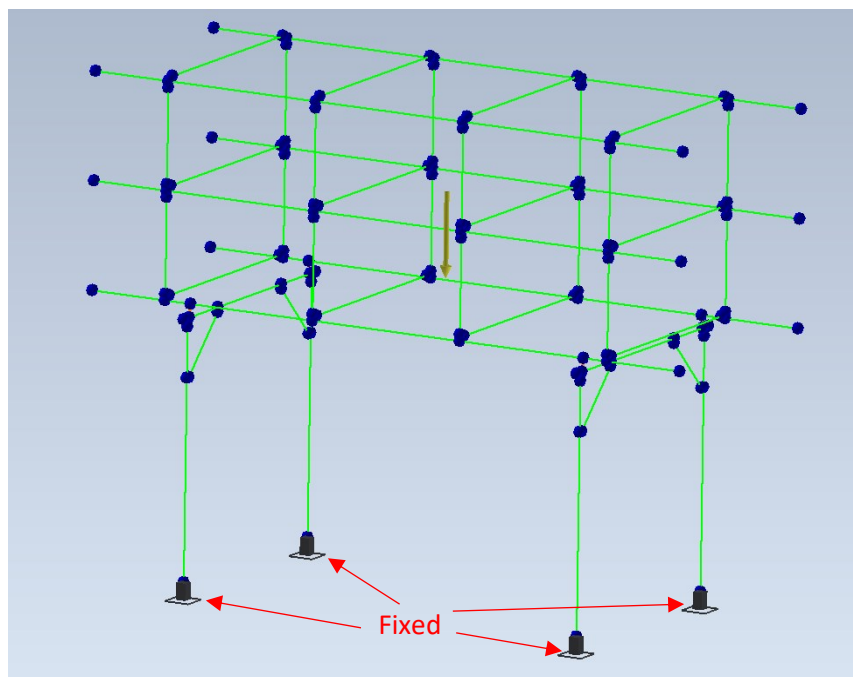


Figure 26. Constraints.

Reader can also notice that now the yellow arrow points downwards – it's a gravity vector, so self-weight is taken into account in the simulations. Load from piping can be considered continuous for now and is applied only to transverse beams, wind load can be applied also continuously from lateral directions, while snow load can be neglected due to its small effect in comparison to other loads. Load from piping, set to 0.5 N/mm, but is rounded to 1 visually when showed on the model (Figure 27).

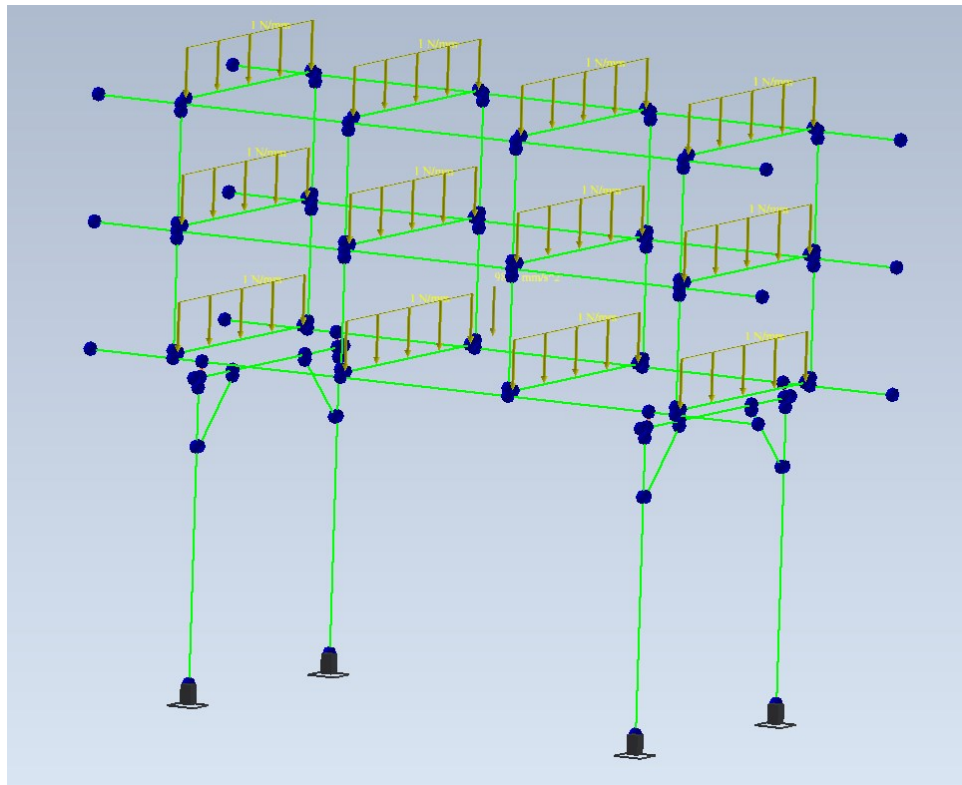


Figure 27. Boundary conditions.

Load from piping and wind – latter acts in  $x$ -direction, set to 0.3 N/mm, but rounded to 0 visually when showed on the model (Figure 28).

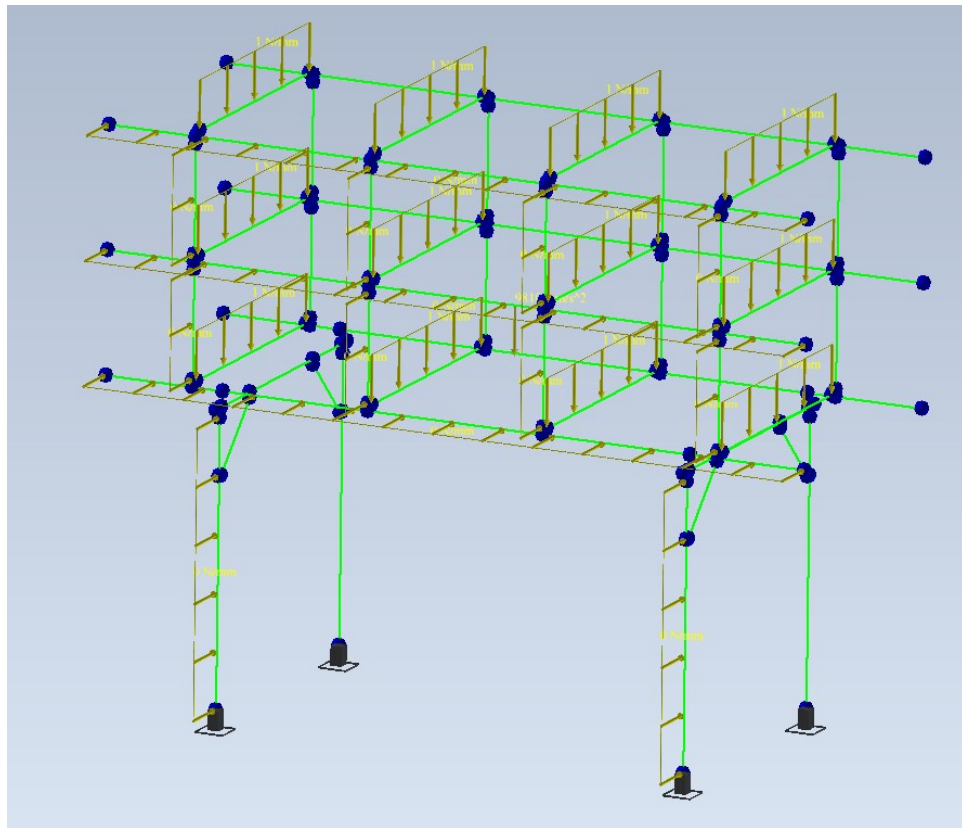


Figure 28. Wind load added.

When all the boundary conditions are set, linear static analysis can be performed. Displacement colour map is showed on the actual deformation model (Figure 29) and adjusted deformation model (Figure 30). As expected, top part has higher displacement because the whole structure is bent in the wind direction, similar bending angle yields bigger displacement for the point that is further away from the point of rotation (fixed constraint). At the same time, the middle of the longitudinal beam has higher deflection than its sides – can be confirmed with engineering judgement. Note that, unfortunately, software shows only magnitude of a displacement vector, e.g. no separate displacements along given axis can be seen. This is why later, when comparing with analytical solutions, loads in only one direction will be considered to eliminate uncertainty of vector projection.



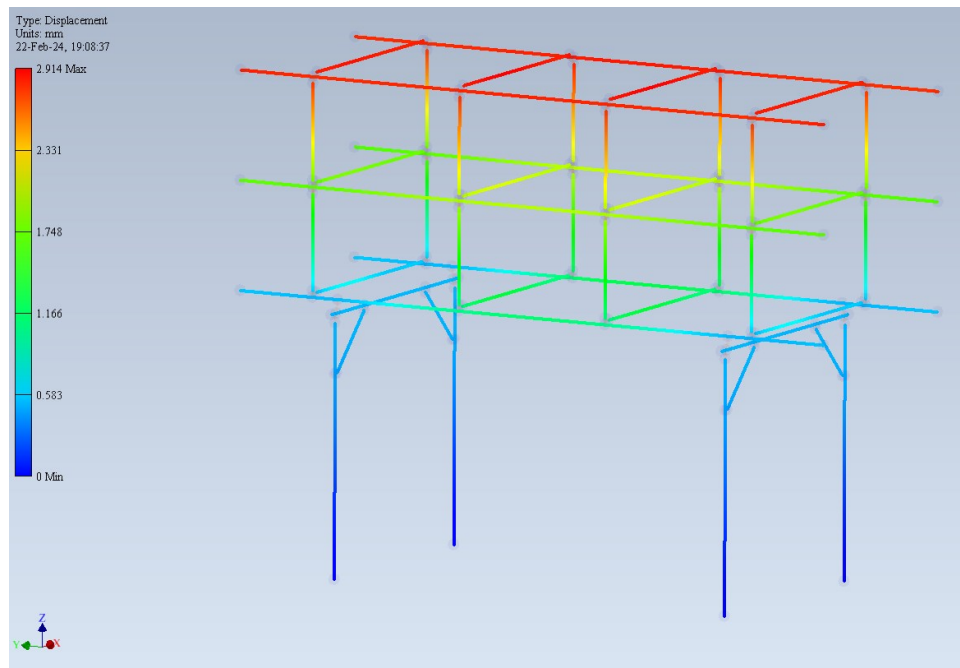


Figure 29. Displacement colour map.

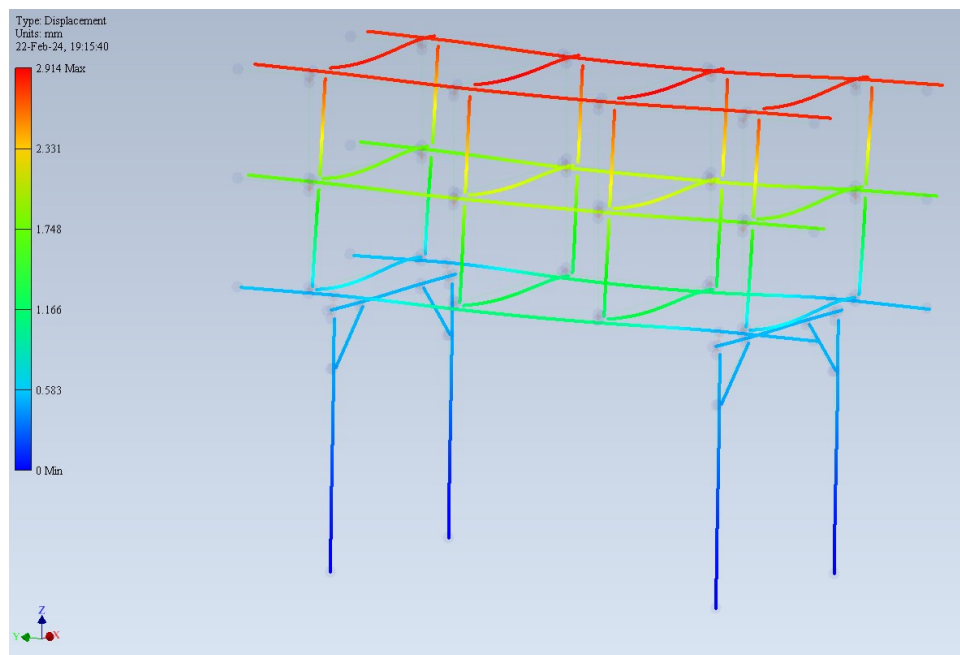


Figure 30. Adjusted (exaggerated) deformation.

Forces in vertical direction distribution is shown on Figure 31. Higher loading of farther columns is due to the moment created by wind load.

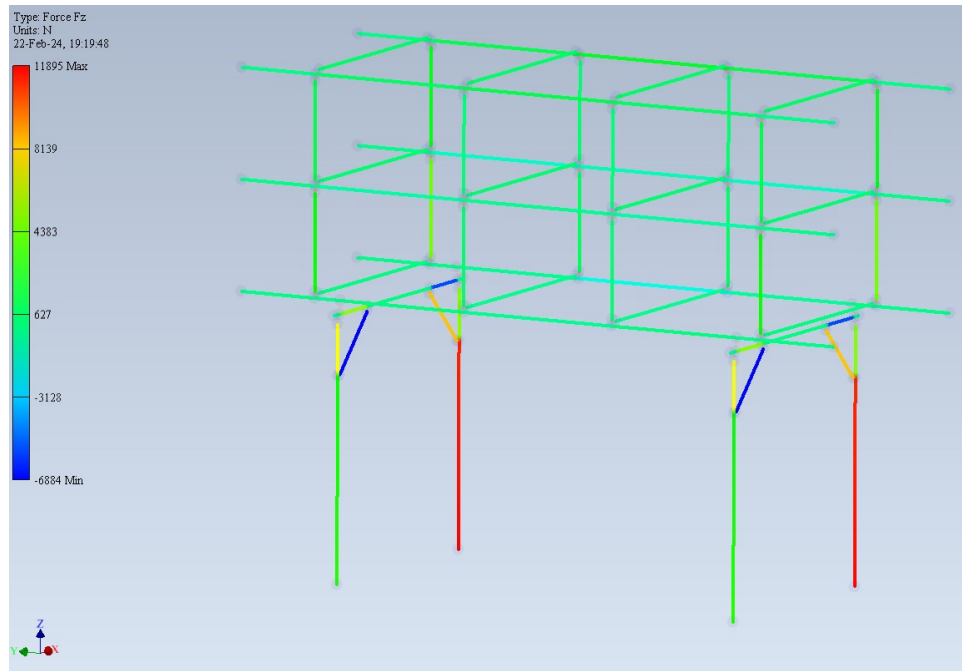


Figure 31. Vertical forces distribution.

Useful feature of Frame Analysis is the ability to plot internal force and moments diagrams directly on the model, as depicted on Figure 32.

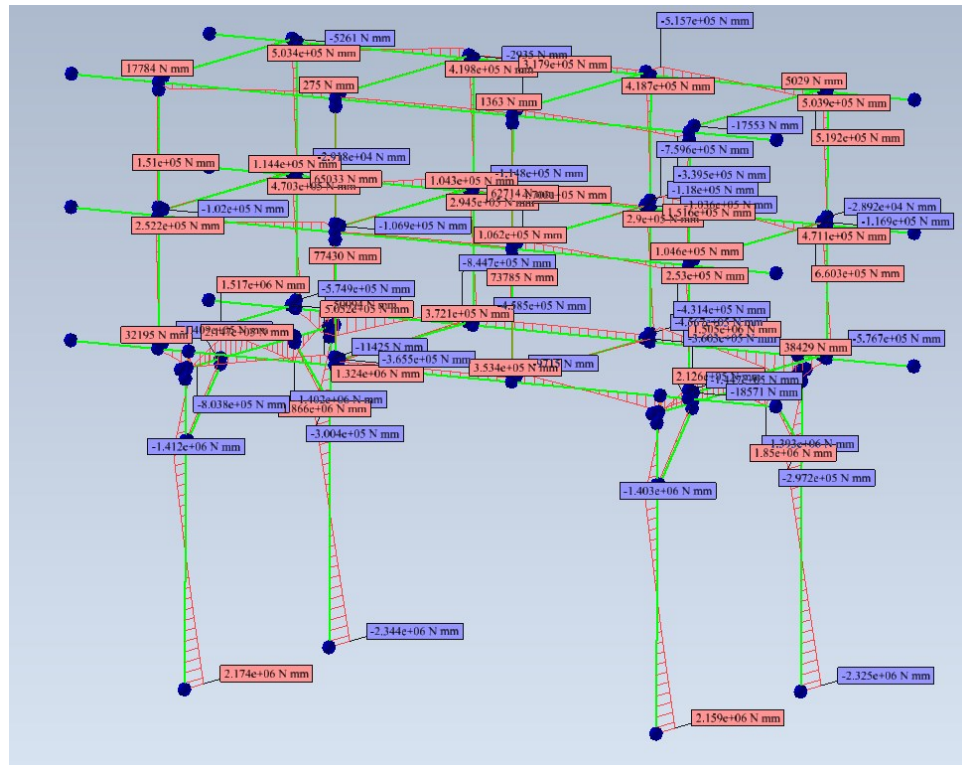


Figure 32. Beam diagrams.

Though big assemblies like pipe rack look messy and crowded when diagrams for all the members are shown, it's possible to evaluate beams separately. Reaction and internal forces and moments can be compared with hand calculations to verify FEA results. Lastly, there is a tool called probe to find the exact value of the output field. For example, let's place probe at the most loaded segment from combined normal stress (Figure 33).

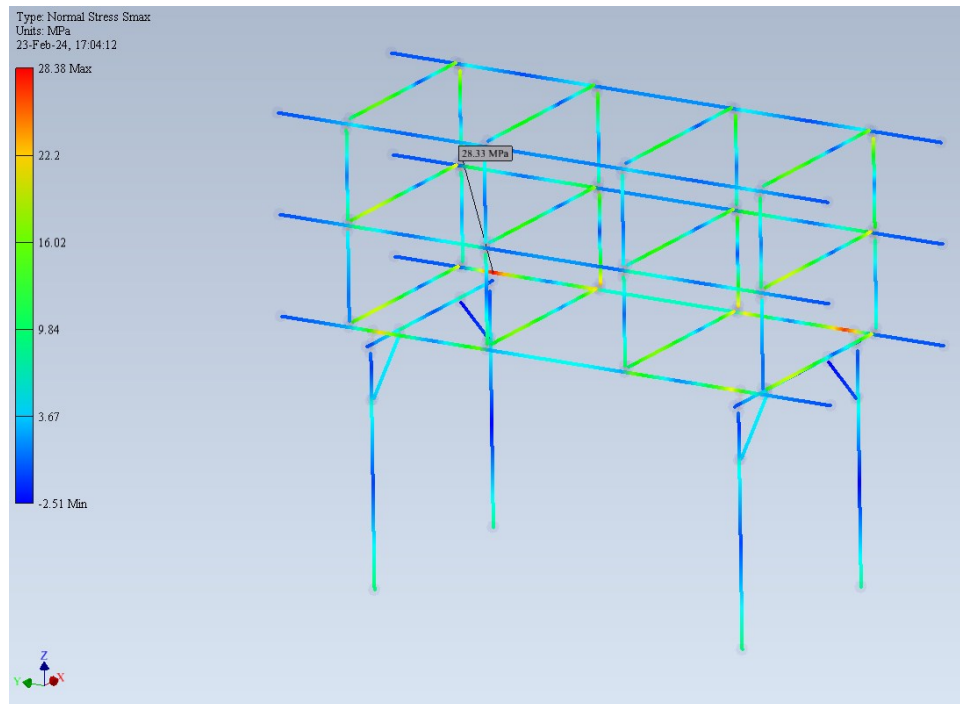


Figure 33. Combined normal stress colour map with a probe.

It's known that normal stress can be caused by bending moment (in two different planes, as on Figure 34 and Figure 35) and by axial forces (Figure 36). There are separate outputs for each of them, so it's possible to double check the combined stress result. Please note that local axes are used, not global.

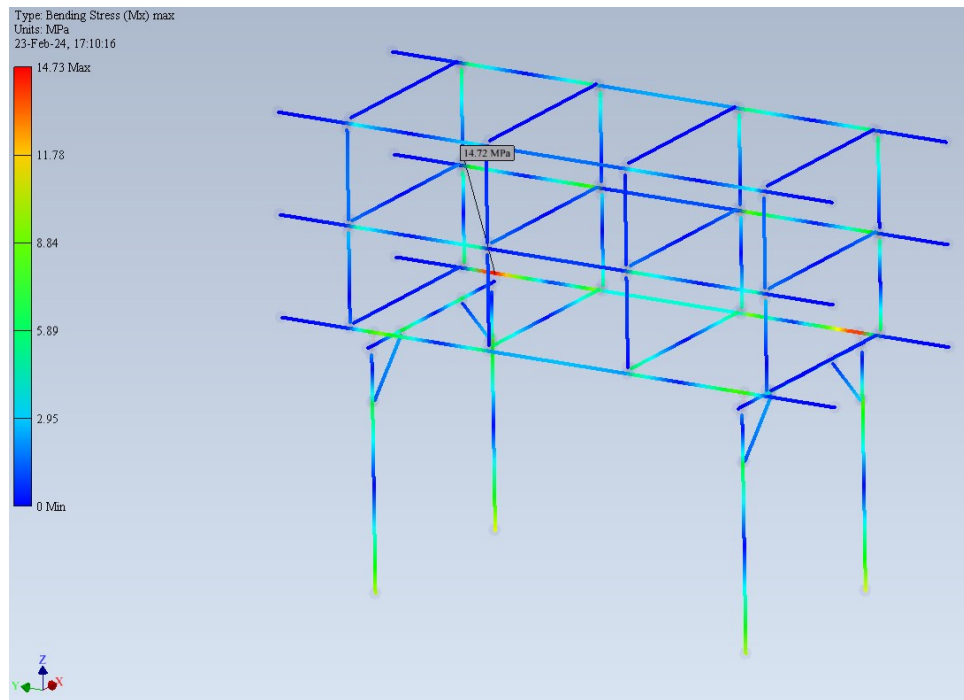


Figure 34. Normal stress from bending moment around  $x$ -axis.

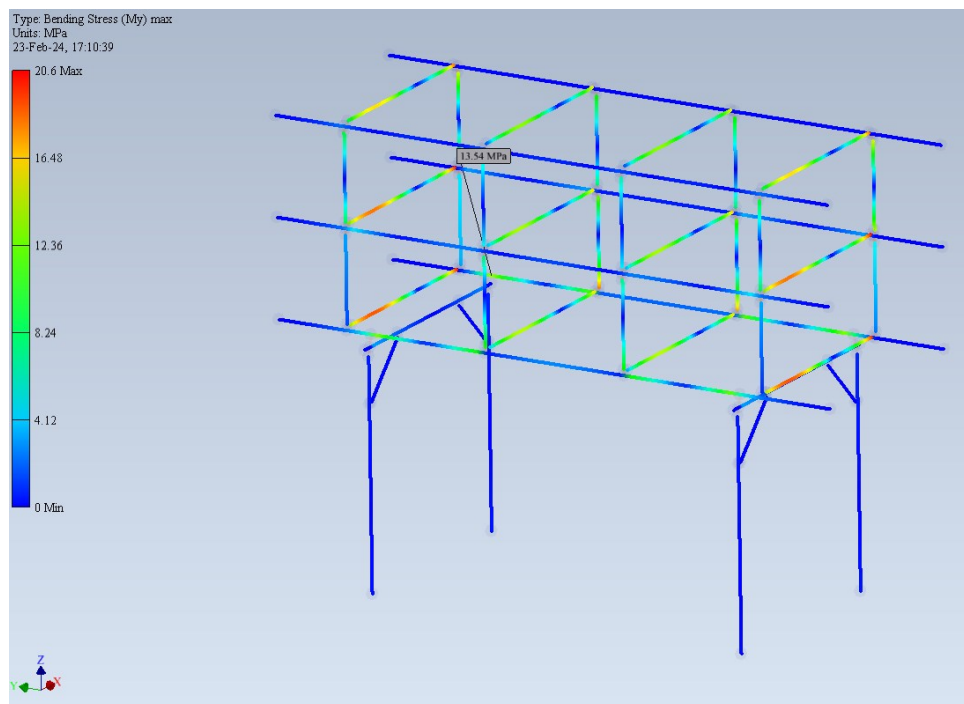


Figure 35. Normal stress from bending moment around local  $y$ -axis.

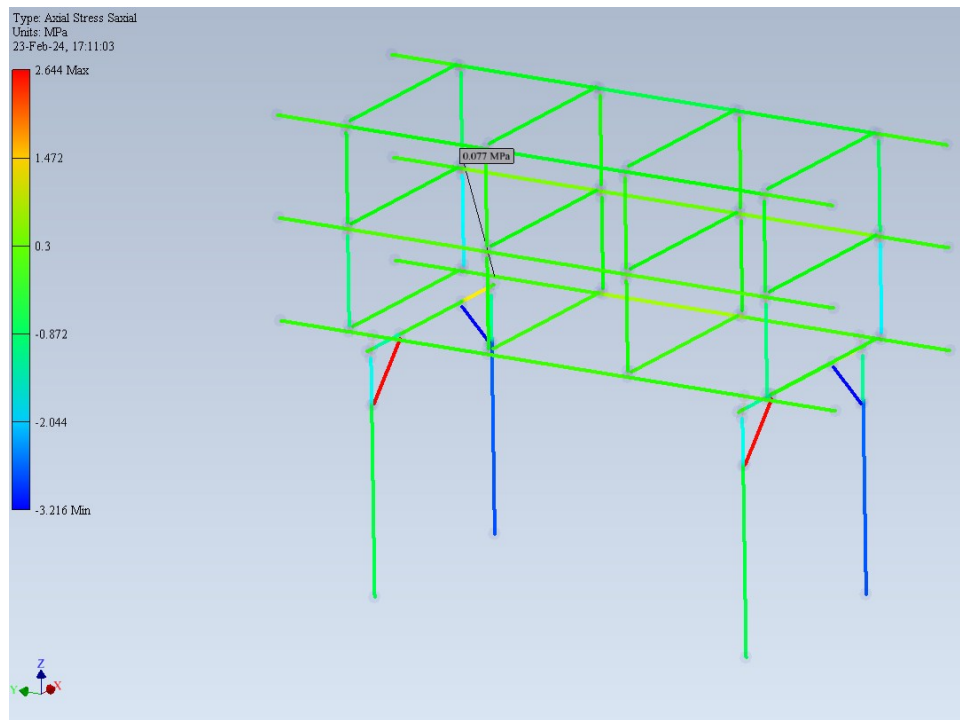


Figure 36. Normal stress from axial force.

Now we can simply sum up values from separate bending and axial stresses to find out that combined normal stress is correct indeed:  $14.77 + 13.54 + 0.077 = 28.337$ , considering visual rounding. There are no combined shear stresses, however. As a conclusion, software seems to produce adequate results and combine them correctly.

### 3.3 Analytical solution

The idea of analytical solutions (hand calculations) is to support and validate FEA, not to get accurate results. Thus, some rough approximations are allowed, such as rounding and assumptions.

#### 3.3.1 Reactions

The first thing to do with such structures is to calculate reaction forces. When only vertical load is present, sum of reaction forces equals to the applied load and self-weight of the pipe rack. It's viable to assume that load is distributed equally through four columns due to high

level of symmetry in this case, consequently, all four reaction forces are roughly the same and due to lack of lateral load, vertical component is dominant. Of course, weight can also be calculated by hand, but the process is long, monotonous and prone to errors, so properties from Inventor can be used, which are very accurate. Assembly used in this section has a mass of little bit less than 1846 kg.

Then, according to Newton's third law, sum of all forces in vertical direction is zero, so:

$$\sum_{i=1}^4 F_R = mg + nwl \quad (10)$$

$$F_R = \frac{mg + nwl}{4} \quad (11)$$

where  $F_R$  is reaction force (four in total),  $m$  is mass of the pipe rack,  $g$  is gravitational acceleration,  $n$  is number of transverse beams that support load from piping,  $w$  is uniform load from piping,  $l$  is length of transverse beams and  $i$  is a summation variable which designates in turn each of the integers 1, 2, 3 and 4, also called index due to its variation, unlike parameter. Mass is taken from Inventor property and rounded. In general, uniform load from piping/wind can be converted to a point force (that is located in the midpoint of the applied load) as follows:

$$F = wl \quad (12)$$

Later in formulae: numbers will be used immediately instead of  $n$ ; uniform load magnitude will be mentioned only when it changes; length will be reported as length of the structural member of interest.

In this example there are 12 transverse beams, with load of 500 N/m and length of the transverse beam (excluding end plate's thickness) is 1960 mm. Substituting numbers yields:

$$F_R = \frac{1846 \cdot 9.81 + 12 \cdot 500 \cdot 1.96}{4} = 7467.315 \text{ N} \quad (13)$$

which deviates from the simulation by 6.3%, as can be seen on Figure 37.

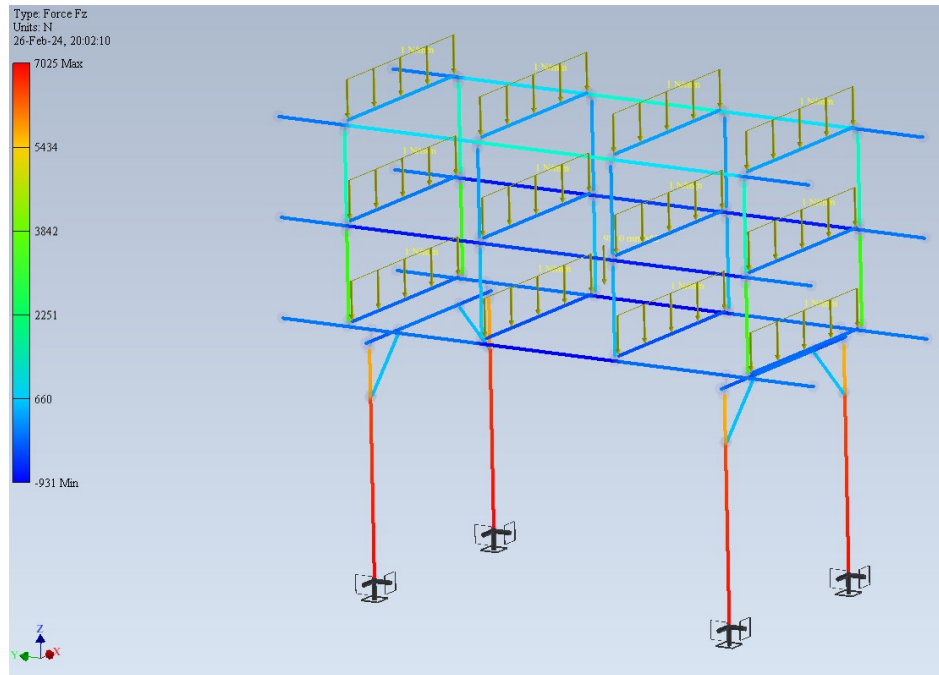


Figure 37. Vertical forces distribution with piping and gravity (dead load).

Depending on the complexity of the model, acceptable error between FEA and analytical solution can range from 5 to more than 20%. Reaction forces calculations are trivial and such deviation should be understood better. To understand limitations of the software, we need to try a different combination of loads. It's possible to remove gravity from the simulation and compare results with hand calculations again.

$$F_R = \frac{nwl}{4} = \frac{12 \cdot 500 \cdot 1.96}{4} = 2940 \text{ N} \quad (14)$$

It's important to remember that a slight asymmetry exists in the model (though it can be avoided if needed), so reaction forces on the left and on the right are not entirely equal, as can be seen on Table 3. Figure 38 demonstrates distribution of vertical forces.

Table 3. Reactions

Reactions	Left side	Right side
Force X	64 N	-63 N
Force Y	-11 N	12 N
Force Z	2954 N	2926 N
Moment X	10.105 Nm	-8.749 Nm
Moment Y	48.3 Nm	-46.976 Nm
Moment Z	-0.027 Nm	-0.029 Nm

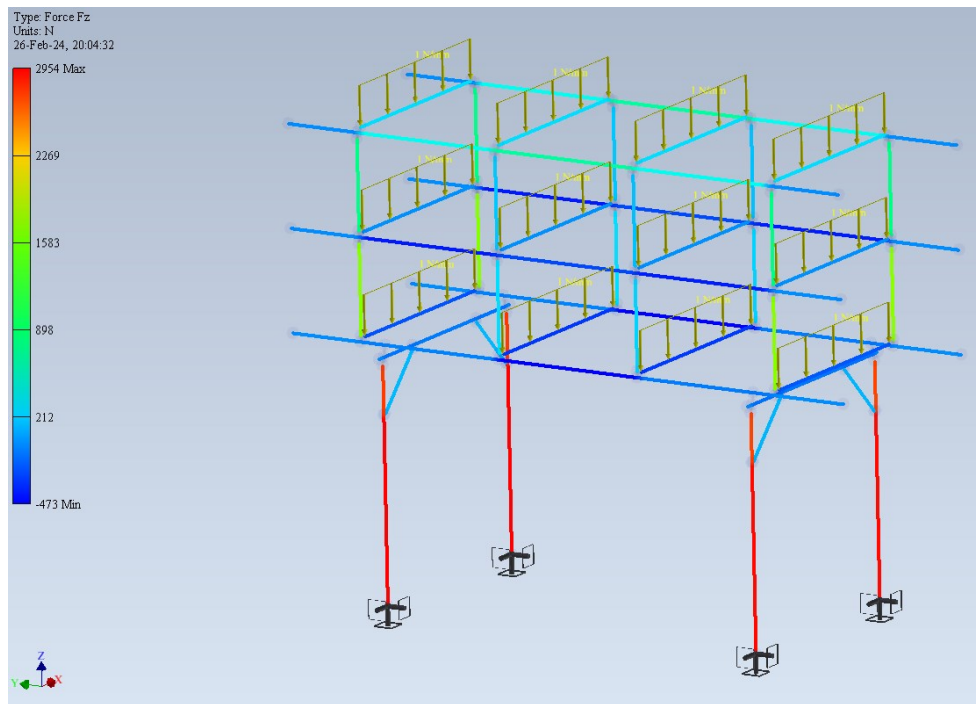


Figure 38. Vertical forces from piping only.

If an average of 2954 and 2926 is taken, then 2940 is obtained for forces in  $z$ -direction – same value as the analytical answer, meaning that direct loads (at least vertical ones) are calculated correctly. Also, notice how FEM assigns non-zero reaction forces in other two directions at one support, and the same values at the other, but with the opposite sign, so that they balance each other out and produce no resultant force, while analytically there are no horizontal forces predicted. This is a well-known phenomenon that is acceptable here but should always be treated with care – in some cases “non-existent” reactions can reach high values, still producing no resultant force, but at the same time loading member unrealistically, overestimating stresses and strains.

Then we can do the opposite – remove piping load and keep only gravity.

$$F_R = \frac{mg}{4} = \frac{1846 \cdot 9.81}{4} = 4527.315 \text{ N} \quad (15)$$

while simulation predicts ten percent lower value again (Figure 39). It’s also observed that relative error has increased, thus deviation between methods occurs indeed in self-weight calculation.



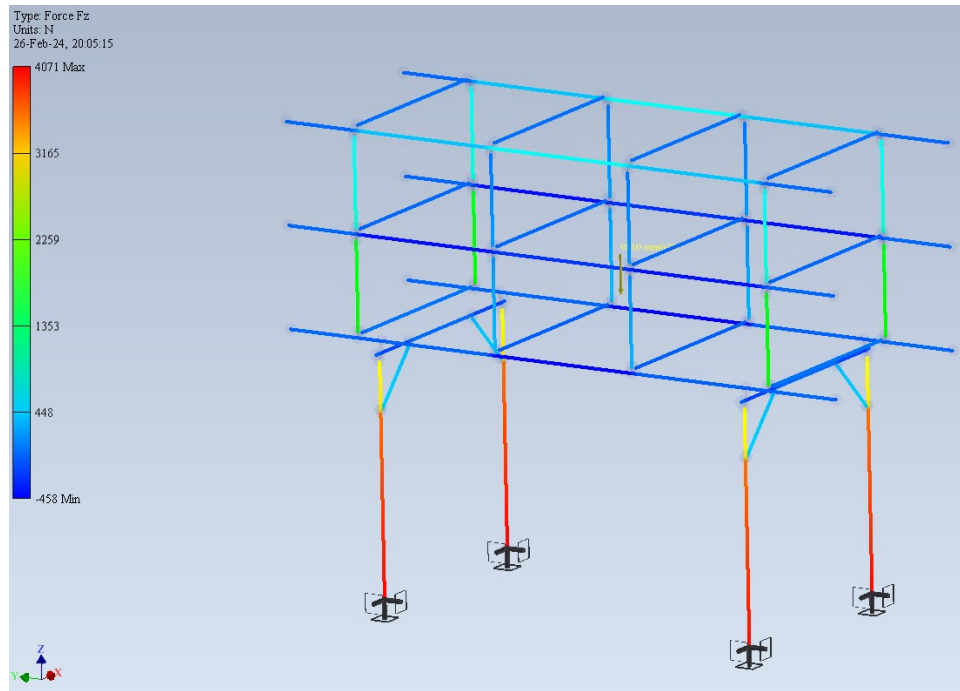


Figure 39. Vertical forces from gravity only.

It's known that gravity's acceleration magnitude and direction are correct, which leads to an assumption that mass is underestimated in the simulation. Using predicted force, we can calculate that Frame Analysis estimates self-weight of the pipe rack at 1660 kg. Note that subscript “*sim*” will be used forward on for variables from simulation.

$$F_{R, sim} = 0.25 \cdot m_{sim} g \rightarrow m_{sim} = \frac{4F_{R, sim}}{g} = \frac{4 \cdot 4071}{9.81} \approx 1660 \text{ kg} \quad (16)$$

It can be explained by approximation of the pipe rack as a pure frame, e.g. not accounting for end plates, side plates and bolted connections. To verify our assumption, we need to calculate mass of these components and see if it makes for this 186 kg difference. Table 4 lists number of used plates and miscellaneous with their respective masses (masses are extracted from Inventor properties).

Table 4. Plates and their weight

Name	Mass, kg	Number
End plate	0.671	12
Transverse beam plate	0.6	48
Spacer plate	1.377	32
Strutting of base beam	0.405	16
Bracing plate	6.384	4
Footing plate	7.217	4
Footing	7.523	4

In addition, 64 four-bolt connections with mass of 0.2 kg each (four-bolt connection) are present. In total, these additional parts equate to 184.692 kg (another kilogram comes from anchoring studs). This confirms our assumption. Note that mass of added material during welding of plates is not considered either in simulation, or in analytical solution, so load from gravity is conservative in any case.

There are two options available. First, mass difference can be ignored, since its effect is relatively small. We can also deduce that a relative error decreases with an increasing load and increases with a pipe rack size increase. Second, mass deviation can be accounted for in simulation by adjusting gravity vector's magnitude:

$$F_R = F_{R, sim} \quad (17)$$

$$mg = m_{sim}g_{sim} \rightarrow g_{sim} = \frac{mg}{m_{sim}} = \frac{mg^2}{4F_{r, sim}} \quad (18)$$

$$g_{sim} = \frac{1846 \cdot 9.81}{1660} \approx 10.91 \frac{m}{s^2} \quad (19)$$

If we substitute new gravitational constant into simulation, then more realistic results are achieved (Figure 40).

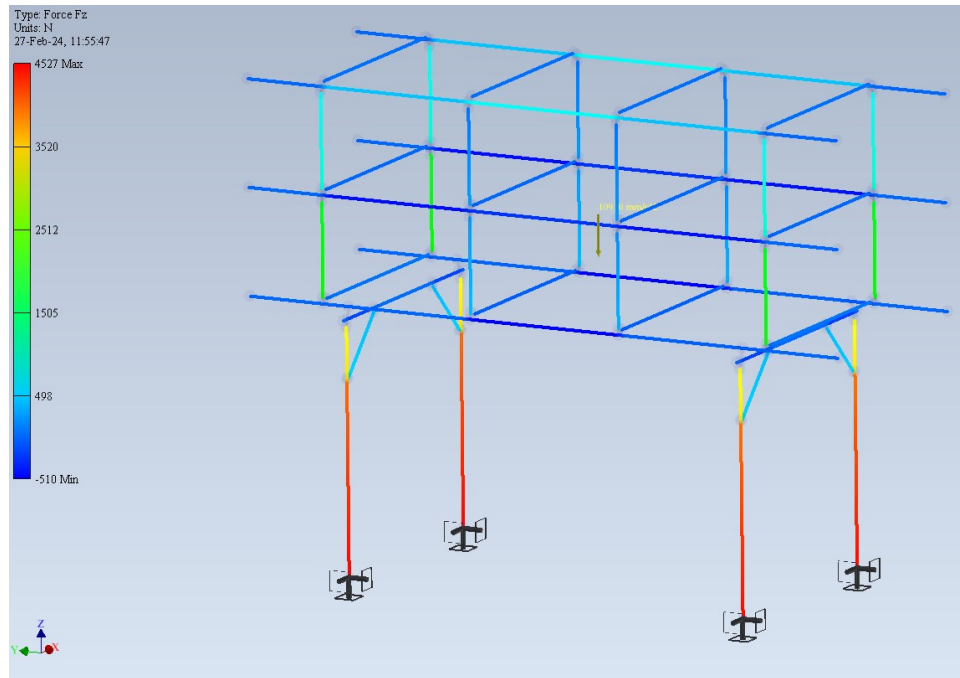


Figure 40. Vertical forces with new gravitational constant and gravity only.

Similarly, initial problem is solved with the acceptable deviation from analytical solution (Figure 41).

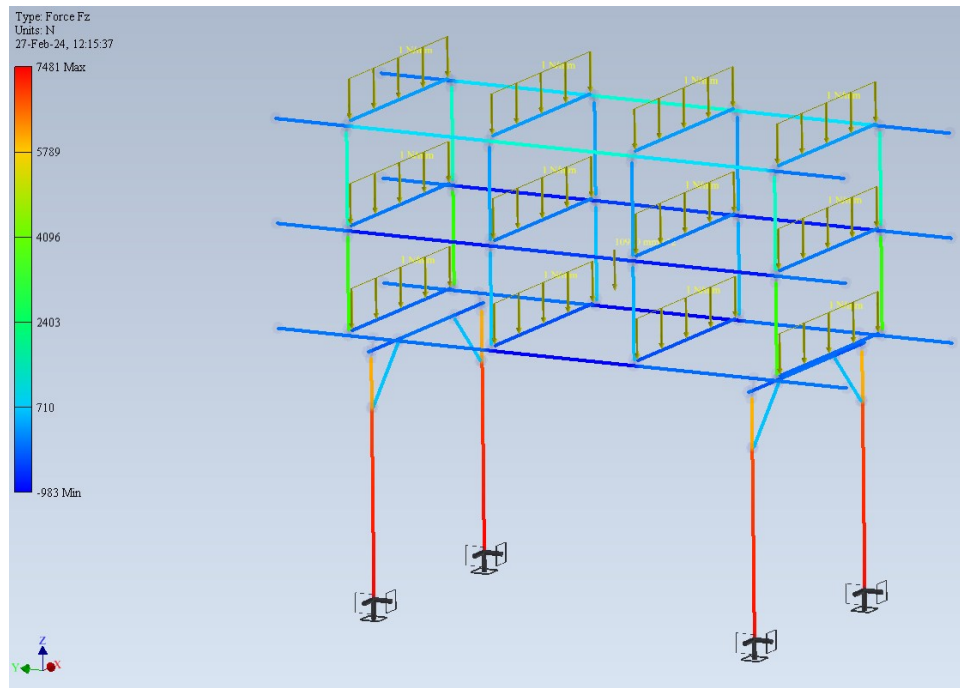


Figure 41. Vertical forces with dead load and new gravitational acceleration.

Now, if needed, it's always possible to compensate for the mass difference using following dependency:

$$g_{sim} = 24.059025 \frac{m}{F_{R,sim}} \quad (20)$$

If lateral load from wind is present, it gets more complicated. To simplify this case, all vertical loads are omitted and only wind load is kept. Calculations are simplified further into 2D, and the pipe rack is cut in half in the middle for that, so only half of the wind load is considered, e.g. only one column, four spacers, and half load from each longitudinal beam. Side view from the software can be used as a reference for a free body diagram. Local  $xy$ -frame is introduced, forces are in red, moments are in yellow, as shown on Figure 42.

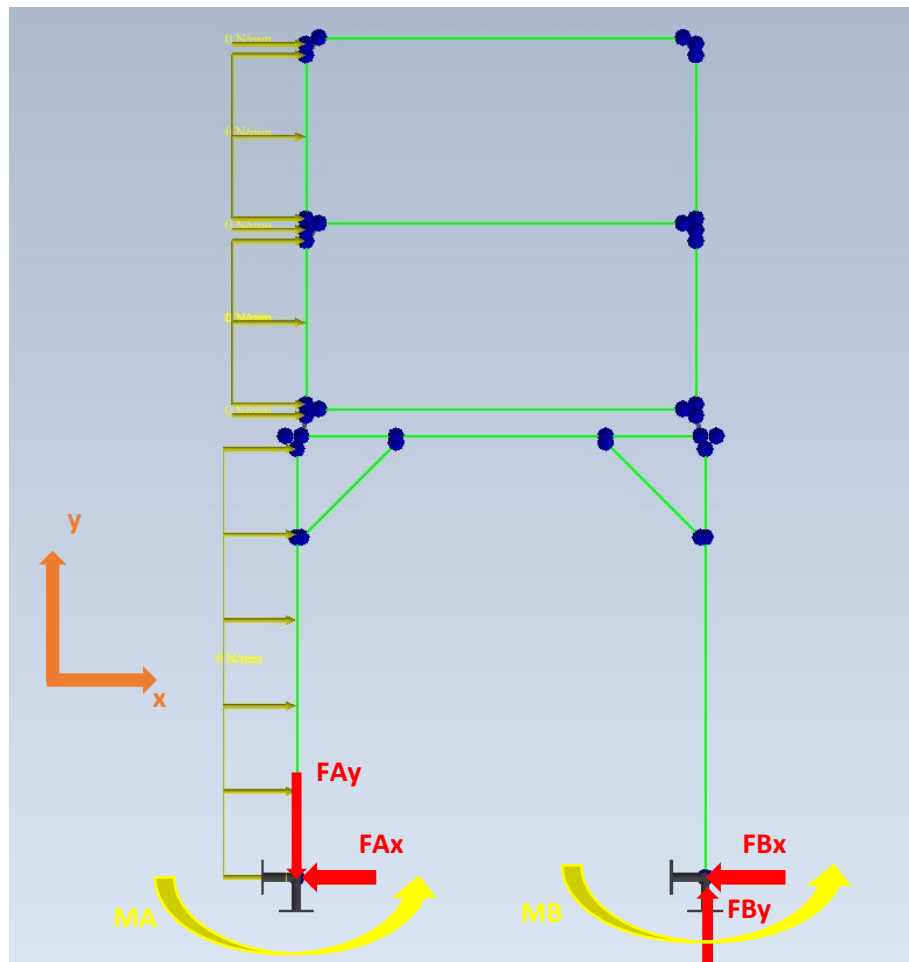


Figure 42. 2D sketch for wind load analysis.

Sum of forces in  $y$ -direction is zero, thus:

$$F_{Ay} = F_{By} \quad (21)$$

Sum of forces in  $x$ -direction is zero, thus:

$$F_{Ax} + F_{Bx} = F_{column} + \frac{F_{long}}{2} + \frac{F_{long}}{2} + \frac{F_{long}}{2} + 2F_{spacer} + 2F_{spacer} \quad (22)$$

where  $F_{column}$  is wind force on a column,  $F_{long}$  is wind force on a longitudinal beam,  $F_{spacer}$  is wind force on a spacer. These forces are calculated as eq. (12). Lengths are 2305 mm, 5980 mm and 880 mm for column, longitudinal beam and spacer respectively.

Sum of moments around point A is zero, thus:

$$M_A + F_{By}W = F_{column}h_{column} + F_{long}\frac{h_{long,1}}{2} + F_{long}\frac{h_{long,2}}{2} + F_{long}\frac{h_{long,3}}{2} + \quad (23)$$

$$+ 2F_{spacer}h_{spacer,1} + + 2F_{spacer}h_{spacer,2}$$

where  $M_A$  is reaction moment at point A and  $W$  is width of a pipe rack, while  $h_{column}$ ,  $h_{long}$  and  $h_{spacer}$  are heights of centres of masses (COM) of column, longitudinal beam and spacer respectively. In other words, these parameters show the distance between COM and the ground for the member in question. It is obvious that for a horizontal member like longitudinal beam, height of COM is just the distance between neutral surface of a beam and the ground, e.g. its length doesn't affect COM height, only its elevation has effect on it. At the same time, for vertically placed members, COM height equals the distance from their midplane (cross-section that is located in the middle of the member) to the ground, e.g. COM height depends not only on the height of the member's support (e.g. elevation), but on its length as well. It is convenient to use these parameters, since loads converted into forces will act on the same height, though not always through the same point, but it's irrelevant in 2D problem, since depth has no effect here. Subscripts after comma represent subsequent member. For example,  $h_{long,1}$  means COM height of the bottom longitudinal beam, while  $h_{long,2}$  means COM height of the middle longitudinal beam and  $h_{long,3}$  means COM height of the top longitudinal beam, same concept is applied to spacers. One can verify later that difference between these values will be equal to the layer height – 1000 mm in this case.

There are six unknowns – four reaction forces and two reaction moments, while there are only three equilibrium equations. To reduce redundancy degree, supports can be

approximated as pinned, thereby removing reaction moments and decreasing number of unknowns by two. Consequently, force equilibriums remain the same, but new moment equation is:

$$F_{By}W = F_{column}h_{column} + F_{long} \left( \frac{h_{long,1} + h_{long,2} + h_{long,3}}{2} \right) + \quad (24)$$

$$+ 2F_{spacer}(h_{spacer,1} + h_{spacer,2})$$

from where we can express and solve vertical reaction forces:

$$F_{By} = -F_{Ay} = \quad (25)$$

$$= \frac{F_{column}h_{column} + F_{long} \left( \frac{h_{long,1} + h_{long,2} + h_{long,3}}{2} \right) + 2F_{spacer}(h_{spacer,1} + h_{spacer,2})}{W}$$

Since uniform load is the same everywhere, we can rewrite and substitute:

$$F_{By} = -F_{Ay} = \quad (26)$$

$$= \frac{300 \left( 2.305 \frac{2.305}{2} + 5.98 \left( \frac{2.485 + 3.485 + 4.485}{2} \right) + 2 \cdot 0.88(2.985 + 3.985) \right)}{2.2} =$$

$$= 6297.840341 \text{ N}$$

Please remember that linear analysis is performed. In reality, deformation would result in the centre of gravity shift closer to the B support, thus making vertical reaction at B higher than at A, but it's reasonable that large deformations are not expected in this study, so it can be safely said that linear analysis is sufficient. Distribution of horizontal reactions is not trivial to compute (though it was cross-checked and confirmed by another employee in Robot Structural Analysis Professional), but it can be easily verified that total wind load equals to the sum of horizontal reactions.

$$F_{Ax} + F_{Bx} = 300 \cdot 2.305 + \frac{3 \cdot 300 \cdot 5.98}{2} + 4 \cdot 300 \cdot 0.88 = 4438.5 \text{ N} \quad (27)$$

Simulation with remodelled supports as pinned predicts similar reactions (note that moments are zero now), as depicted on Table 5.

Table 5. Reactions for A and B

Reaction	A	B
Force X	-2376 N	-2079 N
Force Y	1 N	-1 N
Force Z	-6321 N	6321 N
Moment X	0 Nm	0 Nm
Moment Y	0 Nm	0 Nm
Moment Z	0 Nm	0 Nm

Deviation for both vertical and horizontal reactions is less than one percent, which is a good result.

### 3.3.2 Base frame

Base frame can also be analysed separately, with only wind load being present. Pre- and post-processing of the subassembly is the same as for the pipe rack. Structure is statically indeterminate with third degree of redundancy, but because base of the pipe rack is a trivial rigid frame, it's reasonable to approximate reactions and internal moments with already derived formulae from a book by A. Kleinlogel (deviations are expected due to bracing).

$$k = \frac{I_{beam}}{I_{column}} \cdot \frac{H}{W} = \frac{8643725 \cdot 2.305}{3175216 \cdot 2.32} = 2.70464132 \quad (28)$$

where  $H$  is height of the pipe rack. Lower moment of inertia is taken for column because column is free to buckle in both directions and will do it around weaker axis, due to superposition. Coefficients:

$$N_1 = k + 2 = 4.7046132 \quad (29)$$

$$N_2 = 6k + 2 = 17.22788279 \quad (30)$$

Forces:

$$F_{Bx} = \frac{wH(2k + 3)}{8N_1} = \frac{300 \cdot 2.305(2 \cdot 2.7046 + 3)}{8 \cdot 4.7046} = 154.5022087 \text{ N} \quad (31)$$

$$F_{Ax} = -(wH - F_{Bx}) = -(300 \cdot 2.305 - 154.502) = -536.99779123 \text{ N} \quad (32)$$

$$F_{By} = -F_{Ay} = \frac{wH^2k}{lN_2} = \frac{300 \cdot 2.305^2 \cdot 2.7046}{2.32 \cdot 17.22788} = 107.858365 \text{ N} \quad (33)$$

Moments:

$$M_B = \frac{wH^2}{4} \left( -\frac{k+3}{6N_1} + \frac{4k+1}{N_2} \right) = \frac{300 \cdot 2.305^2}{4} \left( -\frac{2.704+3}{6 \cdot 4.704} + \frac{4 \cdot 2.704+1}{17.227} \right) = \quad (34)$$

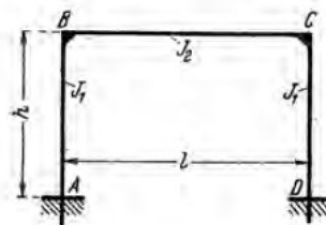
$$= 192.83193 \text{ N} \cdot \text{m}$$

$$M_A = \frac{wH^2}{4} \left( -\frac{k+3}{6N_1} - \frac{4k+1}{N_2} \right) = \frac{300 \cdot 2.305^2}{4} \left( -\frac{2.704+3}{6 \cdot 4.704} - \frac{4 \cdot 2.704+1}{17.227} \right) = \quad (35)$$

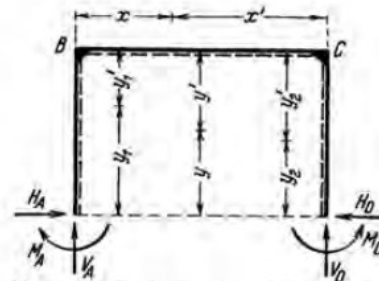
$$= -353.8904121 \text{ N} \cdot \text{m}$$

Note that formulae derivations assume reaction directions as shown on Figure 43 and Figure 44, consequently, minus sign represents that reaction is in the opposite direction to the one depicted on the pictures.

### Fully fixed symmetrical rectangular frame



Shape of Frame  
Dimensions and Notations



This sketch shows the positive direction of the reactions and the coordinates assigned to any point. For symmetrical loading of the frame use  $y$  and  $y'$ . Positive bending moments cause tension at the face marked by a dashed line.

### Coefficients:

$$k = \frac{J_2}{J_1} \cdot \frac{h}{l}$$

$$N_1 = k + 2$$

$$N_2 = 6k + 1.$$

Figure 43. Kleinlogel, A. 1952, p. 147.



**Case 41/7: Uniformly distributed load acting on the left leg**

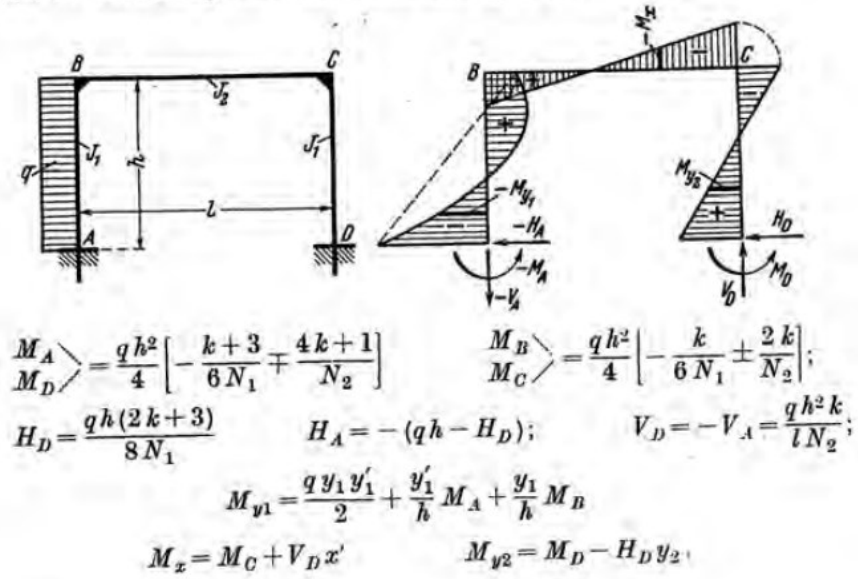


Figure 44. Kleinlogel, A. 1952, p. 150.

Simulation results are seen on Figure 45 and Figure 46.

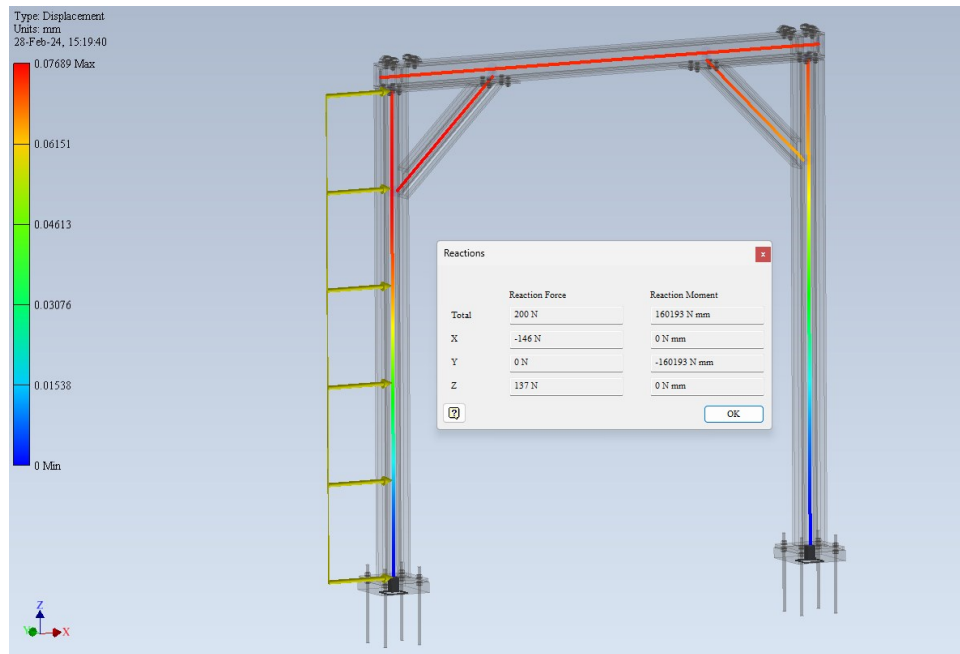


Figure 45. Base displacement field and reactions at the left.

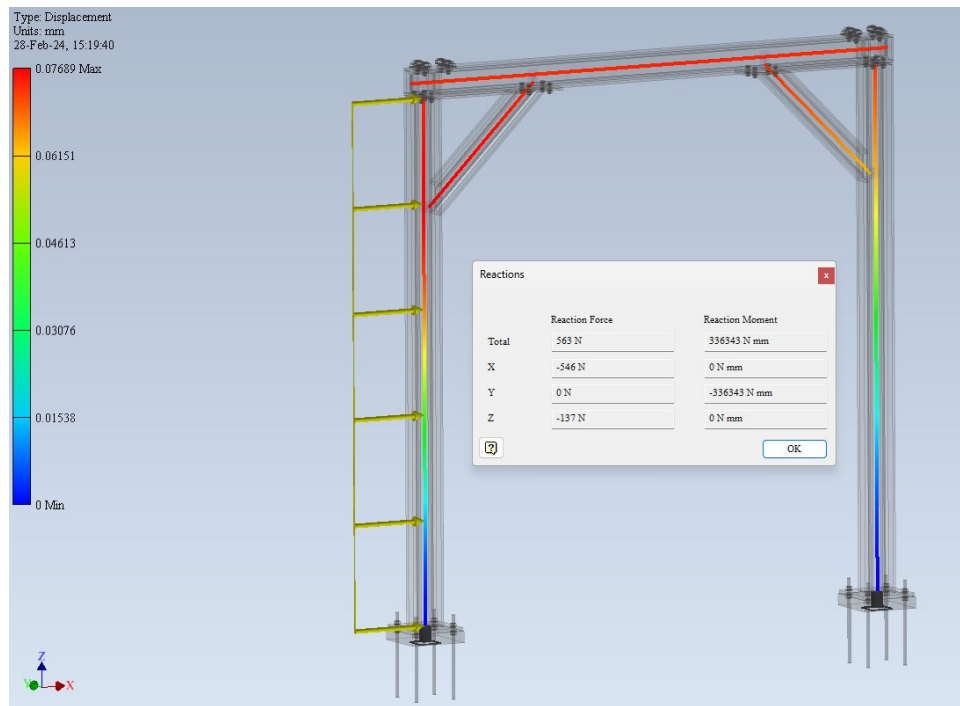


Figure 46. Base displacement field and reactions at the right.

Difference of over 20% in vertical reaction force can be explained by bracing, that reduces loads.

We can also calculate bending moments at the frame corners to see the effect of the bracing:

$$M_l = \frac{wH^2}{4} \left( -\frac{k}{6N_1} + \frac{2k}{N_2} \right) = \frac{300 \cdot 2.305^2}{4} \left( -\frac{2.704}{6 \cdot 4.704} + \frac{2 \cdot 2.704}{17.227} \right) = \quad (36)$$

$$= 86.93574695 \text{ N} \cdot \text{m}$$

$$M_r = \frac{wH^2}{4} \left( -\frac{k}{6N_1} - \frac{2k}{N_2} \right) = \frac{300 \cdot 2.305^2}{4} \left( -\frac{2.704}{6 \cdot 4.704} - \frac{2 \cdot 2.704}{17.227} \right) = \quad (37)$$

$$= -163.29566 \text{ N} \cdot \text{m}$$

where  $M_l$  is moment in the left corner and  $M_r$  is moment in the right corner. It can be observed that bracing decreases moments at the corners, with local peak occurring at the bracing connection (Figure 47).

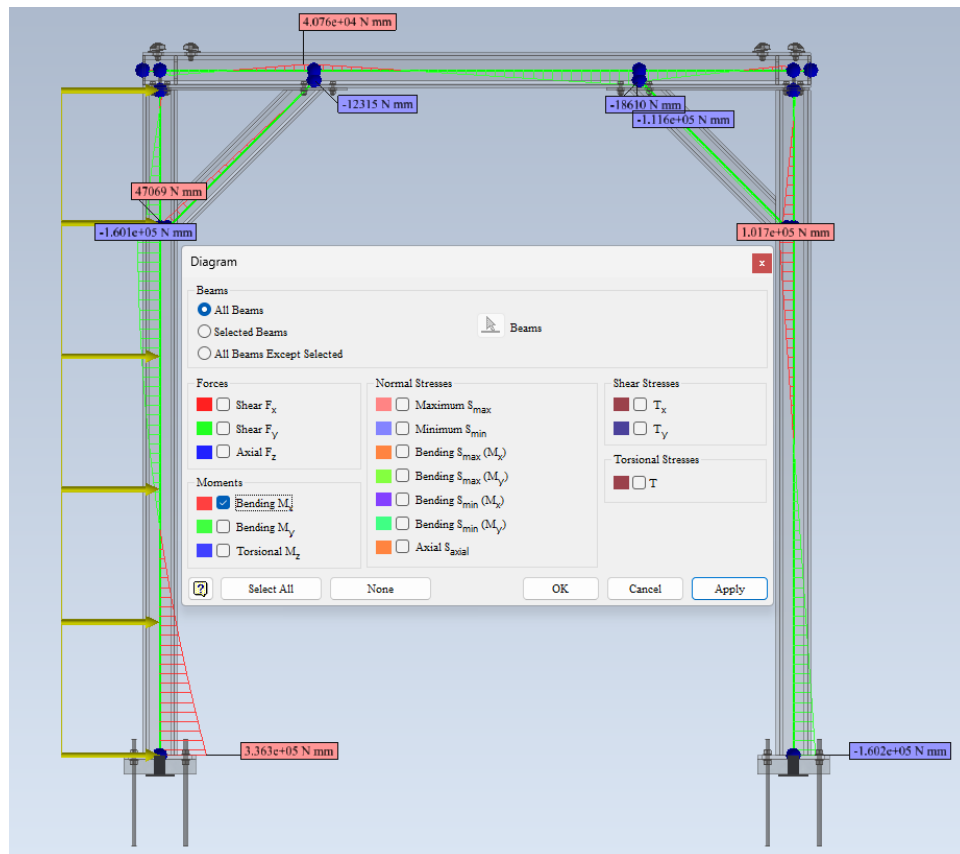


Figure 47. Beam diagrams.

### 3.3.3 Beam deflection

We can also estimate displacement field's accuracy. For that, let's consider a transverse beam as a separate structure, more particularly as a beam with uniform load across its entire length, fixed at both ends. It's obvious that maximum deflection is at the midpoint, so by comparing just this value comparison of beam diagrams can be avoided. According to Euler-Bernoulli theory, maximum deflection for such case is given analytically:

$$\delta_{max} = \frac{wl^4}{384EI} = \frac{500 \cdot 1.96^4}{384 \cdot 220 \cdot 10^9 \cdot 193581 \cdot 10^{-12}} = 0.451208898 \text{ mm} \quad (38)$$

where  $\delta_{max}$  is maximum deflection (in the midpoint) and  $E$  is Young's modulus.

Next, it's visible that the ends of the transverse beams under discussion are not fixed in global coordinate system; they are fixed to the longitudinal beams only via rigid links. Due

to longitudinal beams deformation, start and end points of the transverse beams are slightly displaced downwards. This is where it's important to mention the difference between the terms displacement and deflection, that will be important later, to avoid any confusion. In this thesis displacement is defined as a vector that connects initial and final coordinates of a given point in space, whilst deflection is defined as a measure of member sagging only (Risa, 2018). That is, displacement shows deformation in global coordinate system, while deflection demonstrates deformation in local coordinate system of a given member, i.e. displacement captures movement of the entire structure, while deflection encompasses deformation due to load specific to the member in question only and doesn't include effects from neighbouring members. Displacement is a more common variable in FEM because it's a vector, having both magnitude and direction, while deflection is considered to be a scalar in engineering, so it has only magnitude, and is usually computed for different directions separately, though technically a member can deflect, say, vertically in two directions – downwards or upwards, but usually it's highlighted in a different, non-mathematical, way, leaving deflection as a non-vector. There is a good illustration (Figure 48) of the difference between displacement and deflection by Artur Kosakowski (2012).

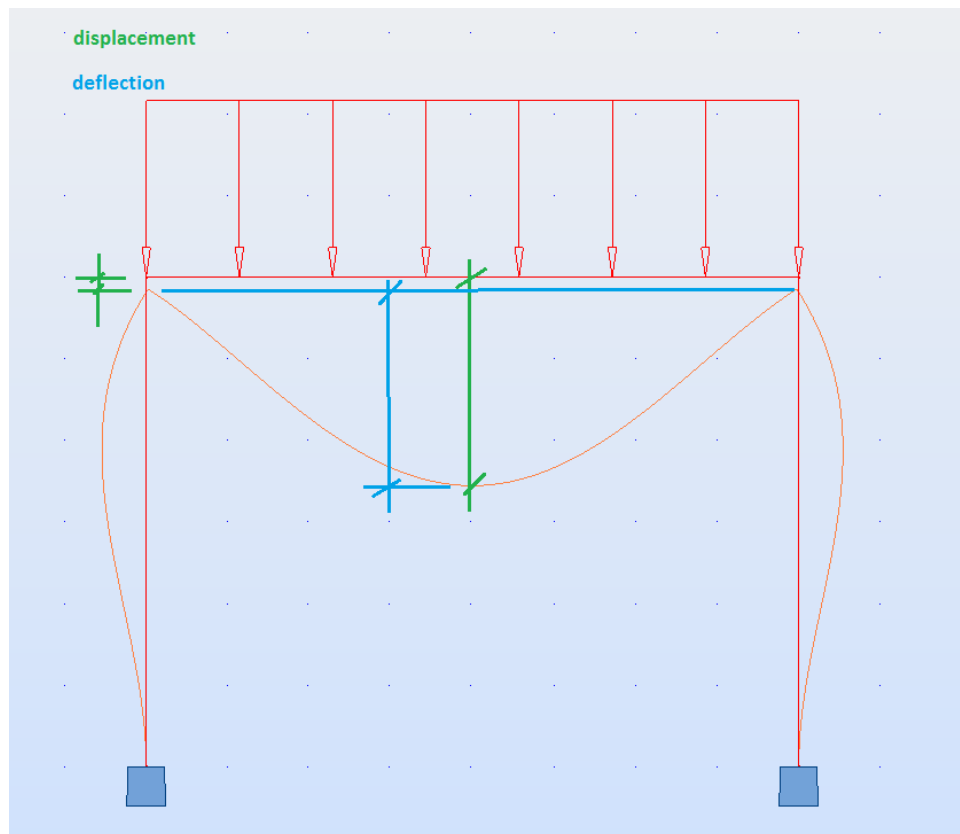


Figure 48. Displacement vs Deflection, Kosakowski (2012).

In global coordinate system columns buckle due to load transferred from the beam, which results in the beam's ends downward movement (denoted by green lines on the left from the left column). However, in local coordinate system, beam deformation due to load is measured with respect to these beam's ends, that remain fixed in this reference frame, since frame moves with them (blue line connects start and end points of the already lowered beam). In trivial problems, displacement is higher than deflection because it is essentially a summation of deflection and deformation from neighbouring members. It's important to understand the difference between displacement and deflection because both concepts are vital in structural analysis – displacement should stay within limits to eliminate possible equipment damage or visual appearance deterioration, while deflection should comply with the deflection ratios defined in engineering standards. Note that different sources use slightly different words for these concepts, for example sometimes displacement is referred to as “absolute deflection” when deflection as it is defined in this work is referred to as “relative deflection”. Lastly, deformation refers to an ambiguous change in geometry of the object due to loading.

Before comparing analytical value to the simulation, both wind and gravity loads need to be turned off (analytical formula derivation neglects self-weight of a beam). Frame Analysis also doesn't report deflections. To compensate for that, probe feature is used to measure exact displacement at the start, the middle and the end of the transverse beam (Figure 49). Then we can calculate deflection in the middle predicted by the software via subtraction of the end's displacement from the displacement in the middle, but before doing it we need to verify that piping load produces just truly vertical displacement, because Frame Analysis reports total magnitude of the displacement, without  $x$ -,  $y$ - and  $z$ -components. This way we can show that the calculated value from different displacements will be vertical deflection that we are interested in, without lateral movement (Figure 50).

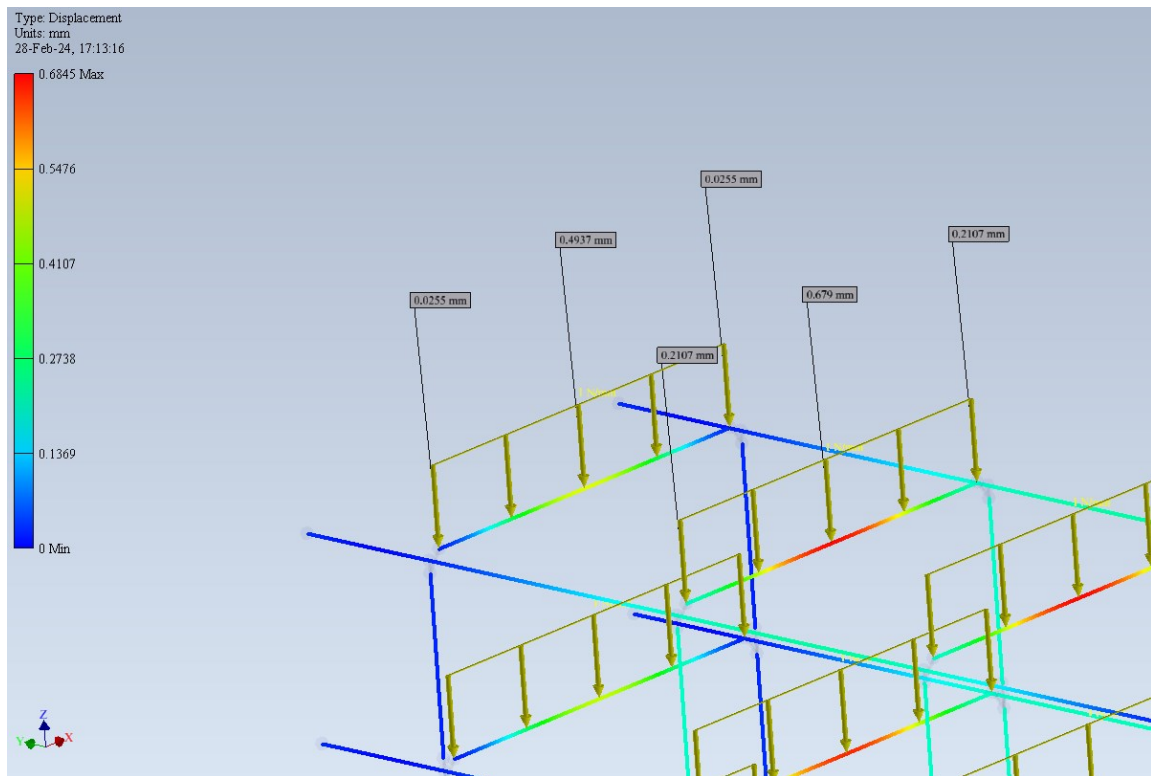


Figure 49. Probe measurements.

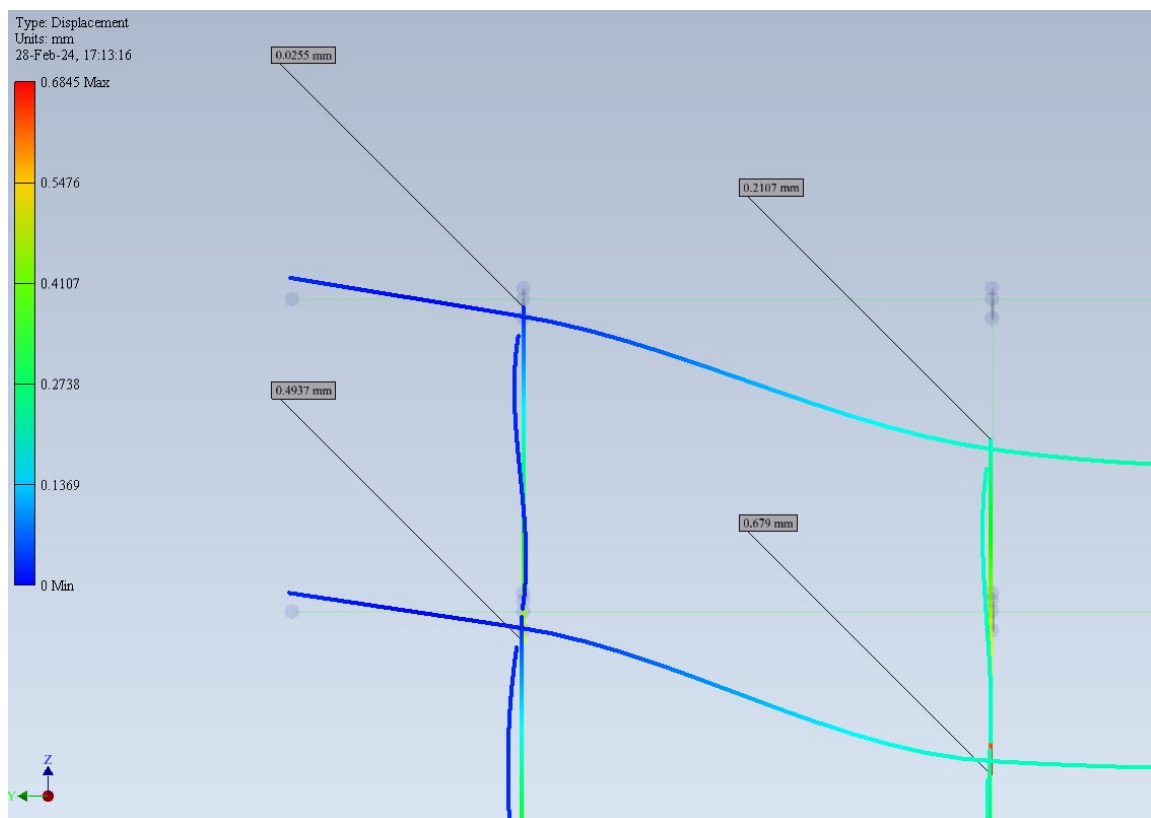


Figure 50. Adjusted deformation.

Deformation is exaggerated visually fivefold on the Figure 50, so that it's observable that while spacers buckle, transverse beams remain in-plane. It essentially confirms that outlined displacements indeed demonstrate purely vertical deformation.

On the farther beam it can be concluded that deflection in the middle is  $0.4937 - 0.0255 = 0.4682$  mm, and displacement is the same at the start and at the end points, meaning that longitudinal beams deflect equally on both sides, as expected. For the closer beam the same can be shown:  $0.679 - 0.2107 = 0.4683$  mm, which means that all transverse beams deflect equally in their local coordinate systems, as predicted. However, displacement on the closer beam is higher because longitudinal beam deflects there more, being further away from the base support.

Ratio of FEA to analytical value is  $\frac{0.4682}{0.4512} \approx 1.038$ , which means that deviation is less than four percent. One can note that the error diminishes as the structure becomes less complex. In other words, while one-beam problems can be approximated accurately with only a few percent deviation, more complex structures, basically consisting of multiple one-beam substructures, can have much higher divergences with analytical solutions, due to rounding error accumulation.

### 3.3.4 Joints

Lastly, forces at the joints can be verified. Top joint has one applied force and two unknown resultant forces – shear force in longitudinal beam and axial force in spacer. In the middle and bottom joints forces are distributed similarly. Actual distributions are not solved (that would require additional equations) but confirmation of the joints equilibrium is done instead. Hand sketch on Figure 51 demonstrates forces at the joints, with their sum being approximately zero (error of few percent is possible due to rounding). Figure 52, Figure 53 and Figure 54 report forces in different axes.

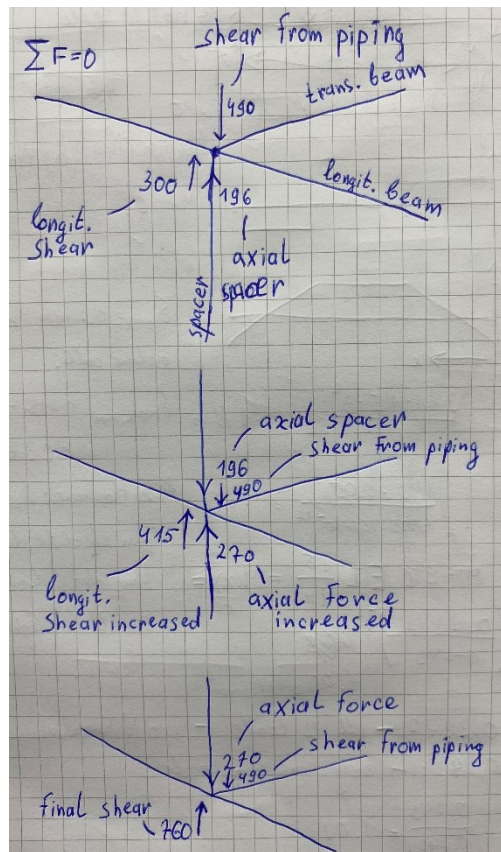


Figure 51. Hand sketch.

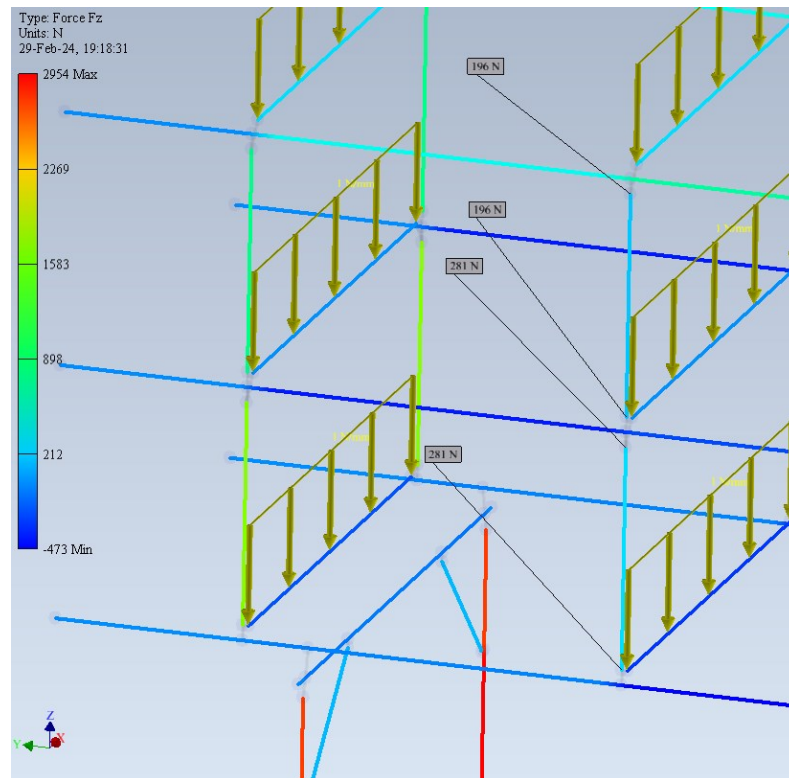


Figure 52. Forces in z-direction.



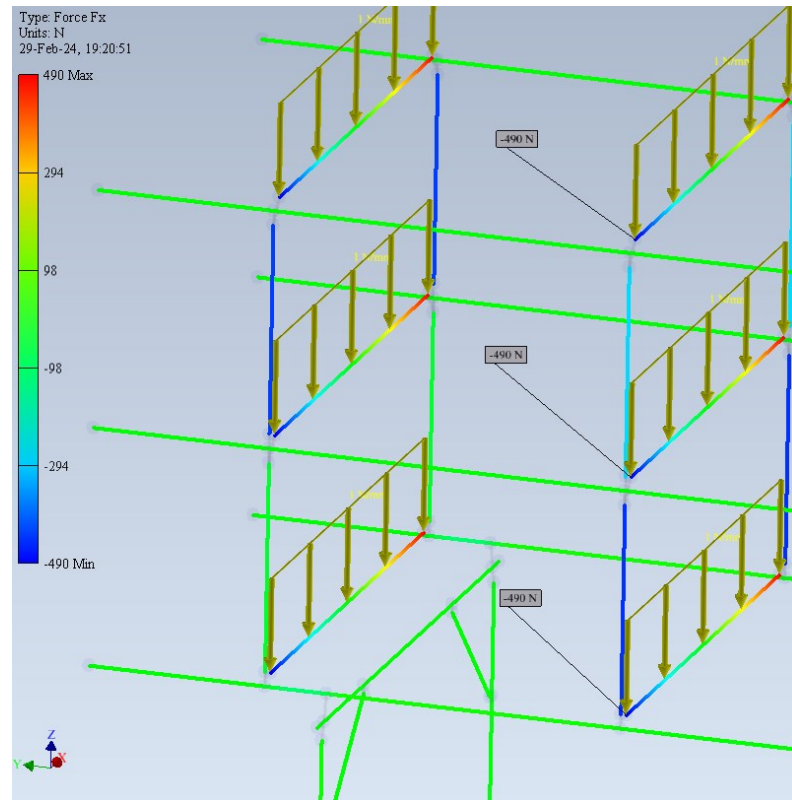


Figure 53. Forces in local  $x$ -direction.

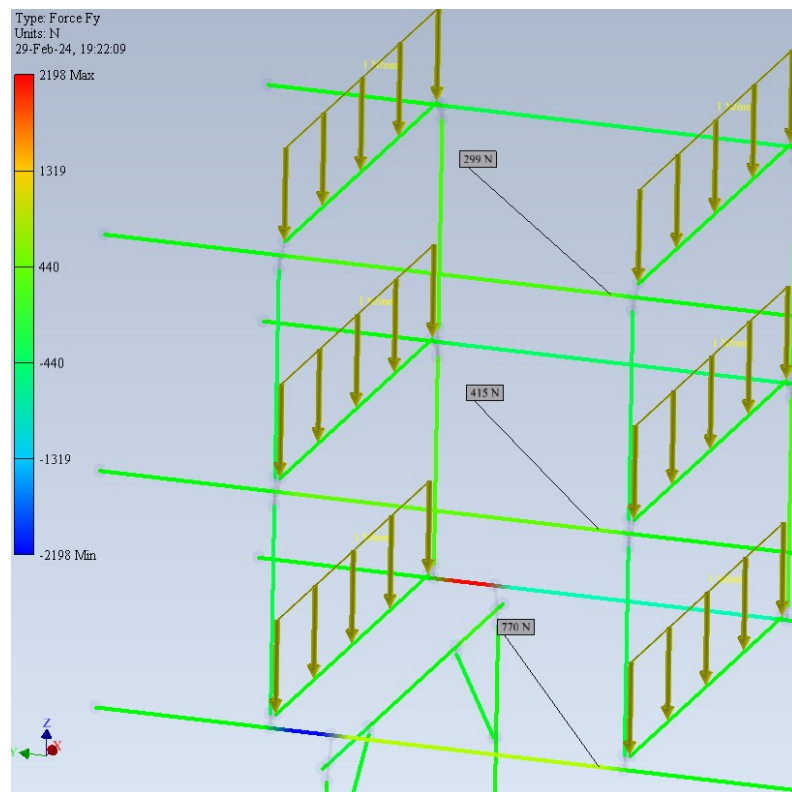


Figure 54. Forces in local  $y$ -direction.

Note that shear forces in longitudinal beams are measured at a small distance from the joints, it's done intentionally to take into account joints' thickness, where shear is not constant. Considering that it deteriorates the accuracy, bringing uncertainty, and rounding, it's plausible that all the joints are indeed in equilibrium.

### 3.3.5 Dead and live loads

Load from piping in kg/m has been specified by Waterleau. However, some practical examples can be shown. For instance, data sheet from Flamco can be used (see Appendix 2). From there it can be seen that a single DM600 pipe full of water will result in  $453 \cdot 1.5 = 679.5$  kg per transverse beam, while ten DN200 pipes full of water will result in roughly the same load. At the same time, fifteen DN80 pipes can result in 255 kg. Note that multiple combinations of pipe layouts are possible, and most likely specified loads took into account heaviest possible combinations or considered weight of supports, valves, equipment, etc. Another aspect to mention is that from structural analysis point of view it's better to place bigger pipes on the sides of the transverse beams, while lighter pipes should be grouped in the middle, so deflection of beams is minimised. However, in real applications this approach is not always feasible, and sometimes heavier pipes are placed in the middle for various reasons, but mostly due to easier installation. As a result, it's difficult to compile all possible pipe layout configurations, so approximation as uniform load is justified.

For further calculations, load in kg/m can be easily converted to N/m by multiplying it by  $9.81 \text{ m/s}^2$  while wind load requires more explanations. Depending on the speed, wind exerts pressure on objects. Since only linear load is applied to beams, pressure should be converted to linear load. Dynamic pressure is given by:

$$p = \frac{1}{2} \rho v^2 C_d \quad (39)$$

where  $p$  is pressure,  $\rho$  is air density,  $v$  is wind speed and  $C_d$  is a drag coefficient. We can also say that  $A$  is cross-section area of an object, thus finding force exerted on the object from wind, by simply multiplying wind pressure by this frontal area. At the same time, area can be divided into two components – beam depth and length, area being a product of these two dimensions. Depth is known and is constant, so we can find load per length unit. If we

define beam depth as  $B$ , we can find linear load from wind by multiplying previous equation by  $A$ , and then dividing by beam length, so the end result is:

$$w = \frac{1}{2} \rho v^2 B C_d \quad (40)$$

Air density can be approximated as  $1.2 \text{ kg/m}^3$  and maximum wind speed considered is  $30 \text{ m/s}$ . The only unknown is a drag coefficient. For I-beam in 2D, drag coefficient can be approximated as  $2.05$  (Aziz, et al., 2008), as seen on Figure 55.

It's important to remember that drag coefficient is a function of Reynolds number, so we can verify that our assumption is acceptable. Characteristic length of a beam is its length when considering flow to be orthogonal (non-axial) to it. Dynamic viscosity of air is  $1.789 \cdot 10^{-5} \text{ Pa} \cdot \text{s}$  at normal conditions.

$$Re = \frac{\rho v l}{\mu} = \frac{1.2 \cdot 30 \cdot 0.86}{1.789 \cdot 10^{-5}} = 1730575.741 \quad (41)$$

which is more than  $10^4$  that is required for our estimation to be acceptable. Note that typically drag coefficient is stabilising at high Reynolds numbers.



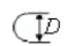


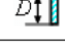





Type of body		Reference area $S$ ( $b = \text{length}$ )	Reynolds number $Re$	Drag coefficient $C_D$
Square rod		$S = b D$	$Re > 10^4$	$\rightarrow 2.00$
		$S = b D$	$Re > 10^4$	$\rightarrow 1.50$
Semicircular shell		$S = b D$	$Re > 10^4$	$\rightarrow 1.20$ $\leftarrow 2.30$
Semicircular cylinder		$S = b D$	$Re > 10^4$	$\rightarrow 1.15$ $\leftarrow 2.15$
Equilateral triangle cylinder		$S = b D$	$Re > 10^4$	$\rightarrow 1.40$ $\leftarrow 2.10$
Flat plate		$S = b D$	$Re > 10^4$	$\rightarrow 1.90$
T-beam		$S = b D$	$Re > 10^4$	$\rightarrow 1.80$ $\leftarrow 1.65$
I-beam		$S = b D$	$Re > 10^4$	$\rightarrow 2.05$
Hexagon		$S = b D$	$Re > 10^4$	$\rightarrow 1.00$
		$S = b D$	$Re > 10^4$	$\rightarrow 0.70$
Circular cylinder		$S = b D$	$Re > 10^4$	$\rightarrow 0.51$

Figure 55. Drag coefficients for different shapes (Aziz et al., 2008).

To give an example, 30 m/s wind is approximated to exert the following linear load on the HE140B:

$$w = \frac{1}{2} 1.2 \cdot 30^2 \cdot 0.14 \cdot 2.05 = 154.98 \frac{\text{N}}{\text{m}} \quad (42)$$

Similarly, load on piping can be calculated. Let's consider pipe with 0.6 m diameter and drag coefficient of 0.51, while characteristic length is similar to the previous example:

$$w = \frac{1}{2} 1.2 \cdot 30^2 \cdot 0.6 \cdot 0.51 = 165.24 \frac{\text{N}}{\text{m}} \quad (43)$$

It's important to keep in mind that in reality wind is not uniform and is typically increasing from the bottom to the top, so realistically load should be triangular or trapezoidal, but it's modelled as uniform for simplicity. It's also difficult to analytically take into account wakes, so instead it is assumed that wind acts only on the first surface that it encounters. Wind load acting on the side of the pipe rack considered only because in this case its effect is greater.

However, according to Eurocode 1: EN 1991-1-4 (Cook, 2007), predicted wind load is two times higher for the piping. Advise Mechanical Solutions calculations according to the standard are shown on Figure 56.

<u>Wind loads (WLX and WLY) (acc. to [03])</u>			
Max structure height, z	5.6 m		
Basic ref. wind velocity, $v_{b,0}$	30 m/s	(Specified by Waterleau)	
Wind direction factor, $C_{dir}$	1 -		
Season factor, $C_{season}$	1 -		
Basic wind velocity, $v_b$	30 m/s	$(v_{b,0} * C_{dir} * C_{season})$	
Roughness category, $z_0$	0.05 -	Terrain category II (Specified by Waterleau)	
Max height, z	5.6 m		
Terrain factor, $k_r$	0.19 -	$(0.19 * (z_0/z_{0,II})^{0.07})$	
Roughness coefficient, $c_r(z)$	0.9 -	$(k_r * \ln(z/z_0))$	
Orography factor, $c_o(z)$	1 -	$(\Phi < 0.05)$	
Mean wind velocity, $v_m$	26.9 m/s	$(c_r(z) * c_o(z) * v_b)$	
Turbulence factor, $k_t$	1 -		
Air density, $\rho$	1.25 kg/m <sup>3</sup>		
Peak velocity pressure, $q_p(z)$	1123 N/m <sup>2</sup>	$\left[ 1 + \frac{7 * k_t}{c_o(z) * \ln(z/z_0)} \right] * 0.5 * \rho * v_m^2(z)$	
Force coefficient piping	0.5	GEP	
Pressure on piping	562 N/m <sup>2</sup>		
 <u>Wind load on piping</u>			
	Max. pipe height		
Layer 1 (bottom)	0,60 m	=	<b>0.34 kN/m</b> (Pressure on piping * height)
Layer 2 (middle)	0,60 m	=	<b>0.34 kN/m</b> (Pressure on piping * height)
Layer 3 (top)	0,60 m	=	<b>0.34 kN/m</b> (Pressure on piping * height)

Figure 56. Advise Mechanical Solutions calculations.

The difference can be explained by more conservative approach in civil engineering standards, while previous calculations are more academic. However, same results for wind load on beams are obtained from both approaches.

## 4 Results

This chapter was shortened due to publication requirements. Complete record of simulation results can be found in Appendix 3. After all results have been reported, it's time to perform reliability and objectivity analyses. Next chapter will address these issues, comparing results with the previously reported results from Advise Mechanical Solutions. Here, examples of displacement colour maps for 1A, 1B and 1C only are present.

### 4.1 Configuration A

Displacement colour map of 1A is depicted on Figure 57.

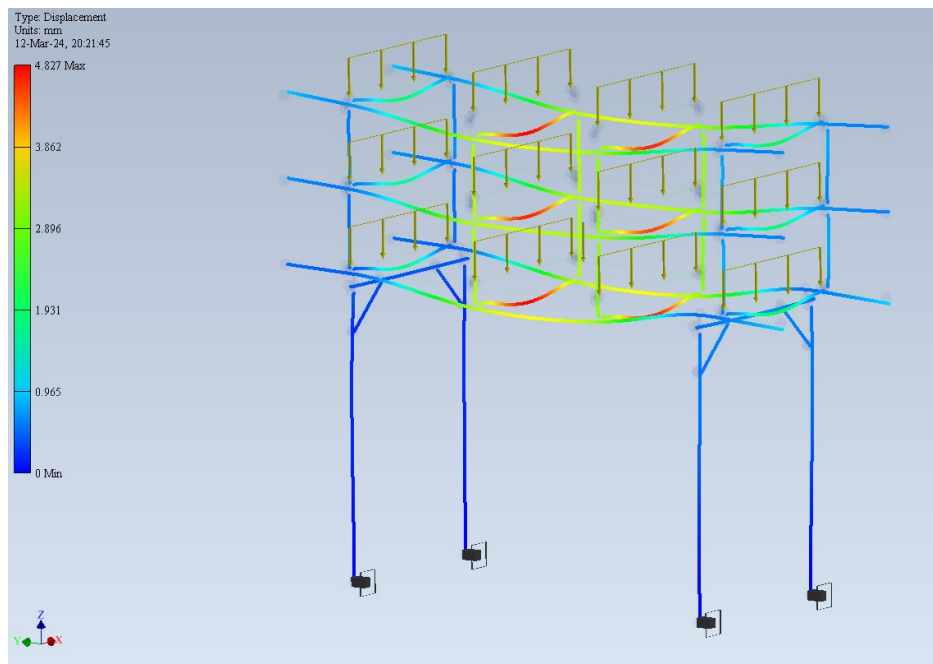


Figure 57. 1A, displacements from dead load only.

### 4.2 Configuration B

Displacement colour map of 1B is depicted on Figure 58.

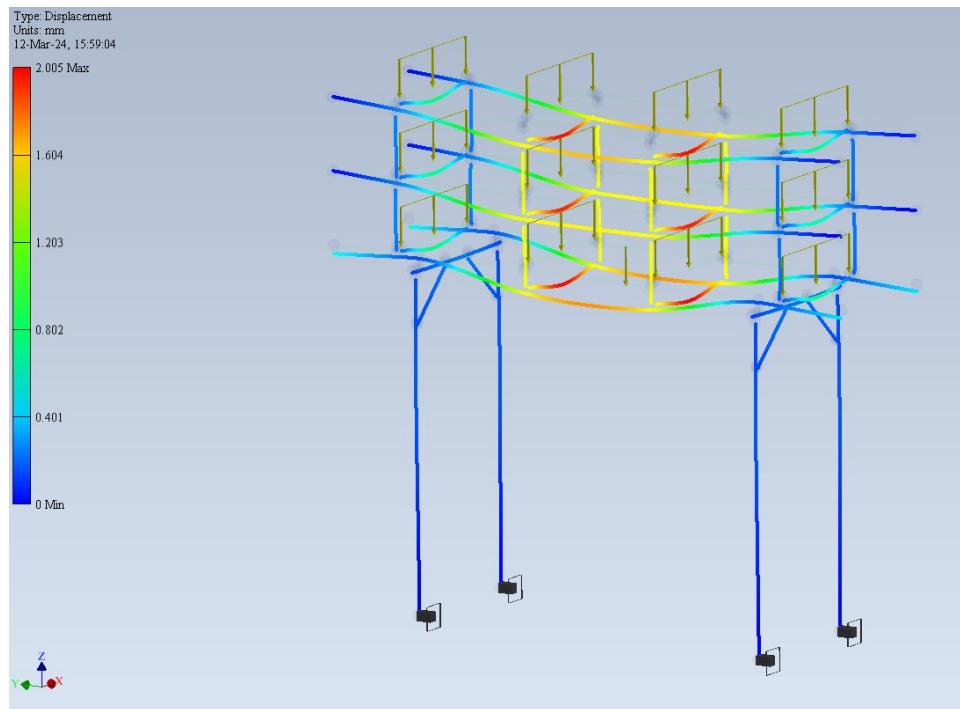


Figure 58. 1B, displacements from dead load only.

### 4.3 Configuration C

Displacement colour map of 1C is depicted on Figure 59.

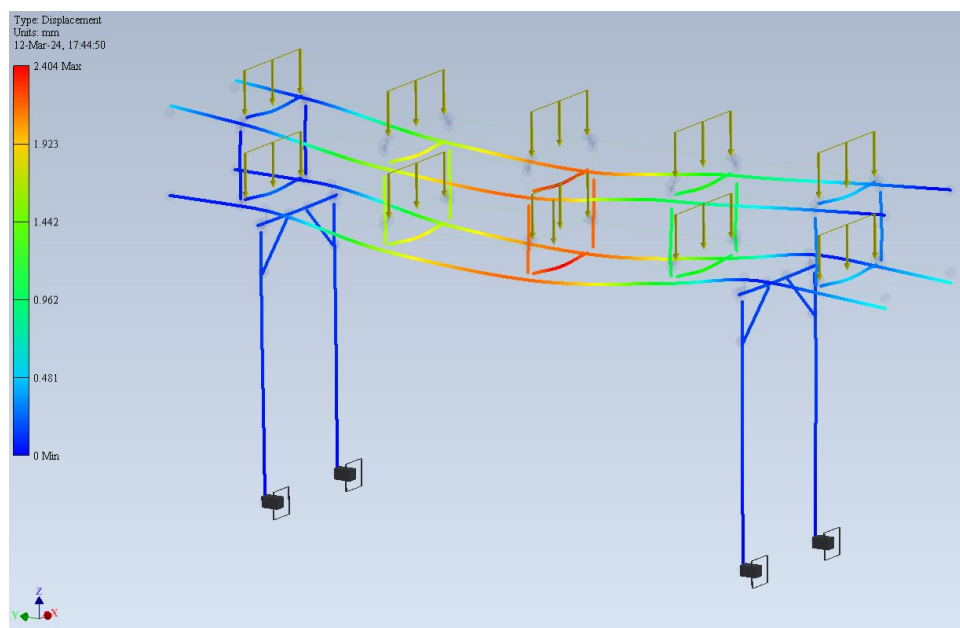


Figure 59. 1C, displacements from dead load only.

## 5 Discussion

Combining design automation iLogic with the embedded Frame Analysis environment allowed fast and smooth analysis of nine different pipe rack configurations. Otherwise, more time would have been spent on either 3D remodelling of the pipe rack every time, or export/import operations of the assembly. Consequently, new configurations can be created and evaluated in a similar, time-efficient way. Analytical solutions were performed in detail for multiple load cases to validate FEA adequacy, thus confirming simulation results being acceptably accurate and precise. However, it is vital to understand that all engineering calculations and simulations are just approximations of the reality, and their rationality depends on the particular phenomenon under consideration. What this means is that all the results should be treated in a critical and professional manner.

### 5.1 Reliability and objectivity

Reliability of the methods is confirmed by the fact that simulations were performed in several runs (reader can see date and time of simulation output in the top left corner of the pictures), every time starting from the geometry conversion. Nonetheless, same results were obtained each time, confirming that method is well-established. Thesis is also highly objective since no bias or personal opinion has affected it, and active voice is used only to engage the reader. Instead, engineering judgement and analytical reasoning were utilised. Next subchapters discuss results sensitivity and compare them with previous findings, ensuring soundness of the achieved results. Further, future improvements are proposed, highlighting the current limitations.

### 5.2 Comparison with previous results, example 3A

Achieved results can be compared with the report from Advise Mechanical Solutions. Full comparison is difficult to perform because of fundamental differences. For example, in Frame Analysis a colour map is produced, with no ability to export tabulated displacements/stresses for every point. On the contrary, Advise Mechanical Solutions used



RISA-3D, and their report doesn't contain colour maps, but only tables of numeric results. In addition, as discussed earlier, Frame Analysis outputs only absolute magnitude of a displacement value, while RISA-3D reports displacements in all three directions separately and can output deflections similarly. Combining it with the fact that the report contains only maximum and minimum values for the given pipe rack configuration, it can be concluded that it's impossible to precisely compare results due to them being in different dimensions sometimes. For example, consider a case with piping load only: we can't compare accurately displacement at the transverse beam midpoint, since Frame Analysis predicts magnitude of the displacement (there is still lateral displacement, though sometimes negligible), while RISA-3D reports vertical displacement from piping only and lateral displacement from combined wind load (because wind produces higher lateral displacement, and only minimum and maximum values are reported for the given configuration). Thus, it's possible to estimate and discuss the difference between vertical deflection, but not measure it precisely and accurately – either intermediate values from RISA-3D are needed, or per-axis results from Frame Analysis, which is hardly achievable in the time frame of this thesis and completely impossible respectively. First, 3A can be investigated (Figure 60).

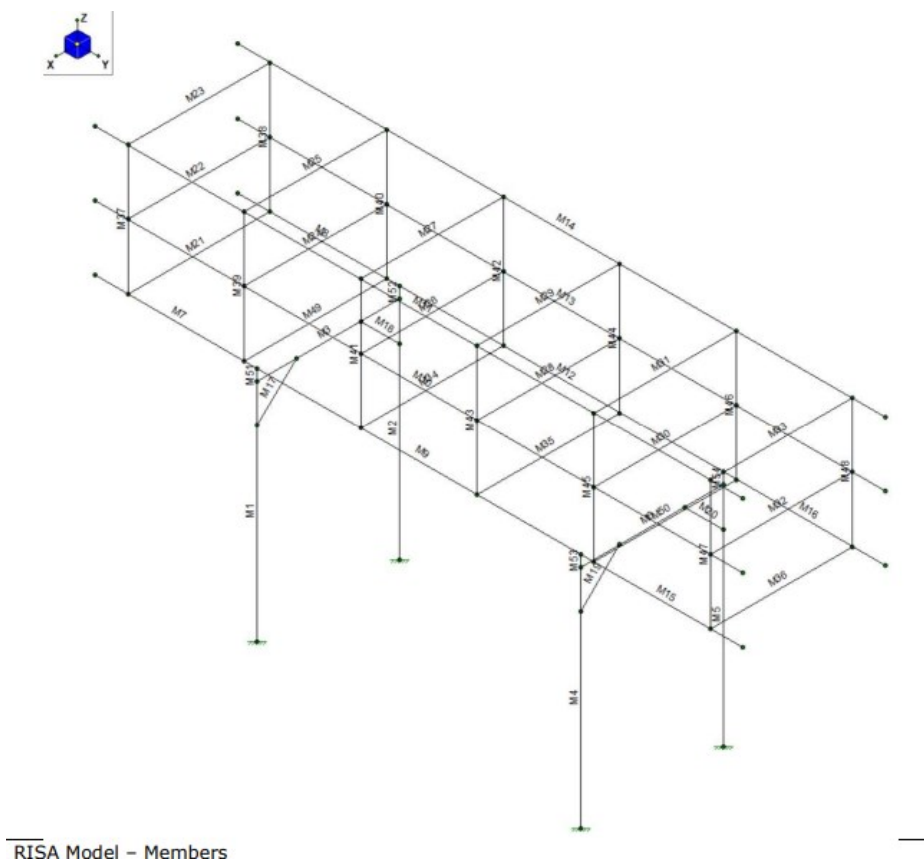


Figure 60. Risa-3D model of 3A (Advise Mechanical solutions).

As can be seen, the model is different in a way that it has longer overhangs – there are six more transverse beams (and eight more spacers) in the model and longitudinal beams are roughly two metres longer than in Inventor. It has a significant impact on total weight, COM, reaction forces and loads carried by columns, but a small effect on local displacements and stresses, that can be neglected if volume between the columns is considered, according to Saint-Venant's principle. Supports are fixed, with overhang ends being free, same as in Inventor. Overall, RISA-3D model is more realistic if analysis was focused on a separate module, but considering the repetitiveness of the pipe rack, Inventor model is also realistic enough because the structure between the columns remains relatively similar.

Simulation setup from the report is also slightly different – Young's modulus is set to 210 GPa, Poisson's ratio to 0.3, yield strength to 235 MPa and ultimate strength to 360 MPa, though density is the same as in Frame Analysis. There is also a negligible difference in second moments of area of different profiles – due to small fillet radii variance. Similar meshing approach is utilised as well.

The most important difference between the simulations are boundary conditions, more particularly loads. Advise Mechanical Solutions report contains a non-uniform load from piping on some transverse beams, mostly on the lower level. According to RISA-3D, these non-uniform loads are most likely the result of converting an area distributed load to a linear distributed load, thus they are listed as Transient Area Loads. Snow load was also considered, but it's no more than 70 N/m, which is dozens of times less than piping load, so it has virtually no effect on the results. But the most significant deviation in simulations is members dimensioning, especially pipe rack width. Width specified by Waterleau refers to the outer dimension, while in structural analysis distance between centre axes is measured. Consequently, to find a transverse beam length, a profile width of longitudinal beams and side plates thicknesses should be deducted from the pipe rack width, for both sides. For example, 3A is 2200 mm wide (top structure), but transverse beam length is only 1960 mm, as seen on Figure 61.

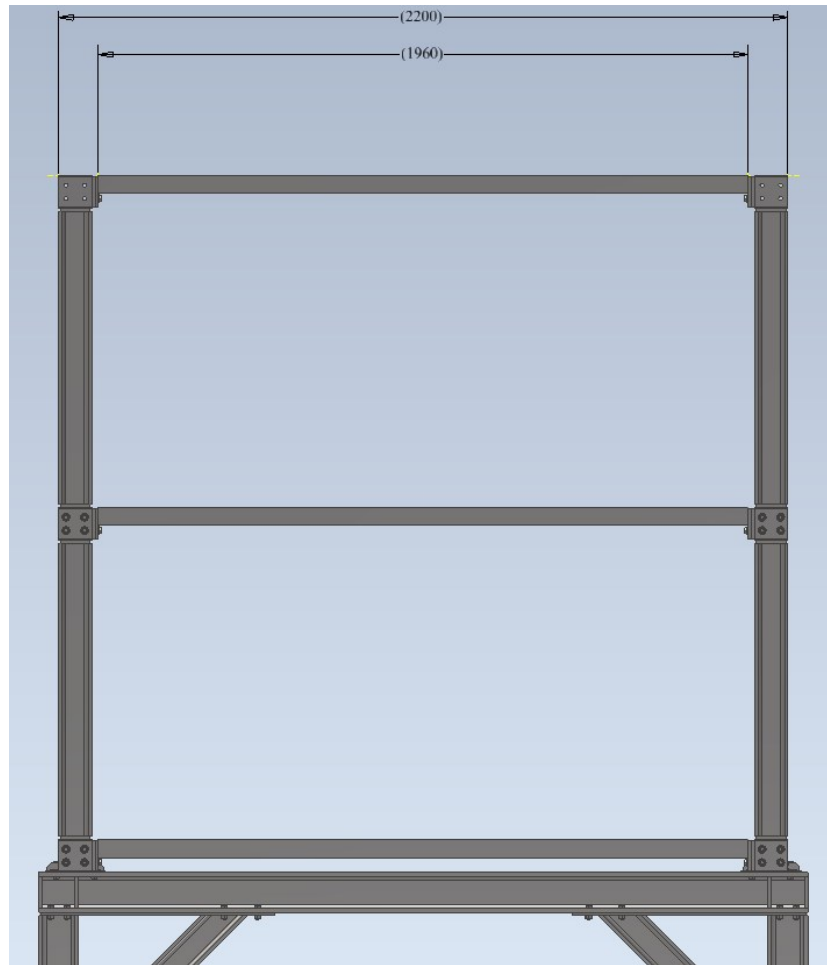


Figure 61. Difference in dimensions.

Difference of 12% might look insignificant, but it becomes bigger in B configuration and even bigger in C configuration, because pipe rack width decreases more in relative terms than longitudinal beam profile width. Furthermore, when applying a uniform load, the maximum deflection is proportional to the beam length in fourth power, and 12% difference becomes 57%. Basically, the report applies loads to the over dimensioned structure (true for all simulations), skewing the results. Pay attention to the most right column on Figure 62, value of 2.2 instead of 1.96 is used.

**Member Distributed Loads (BLC 16 : BLC 5 Transient Area Loads) (Continued)**

	Member Label	Direction	Start Magnitude[kN/m.C.kg/m <sup>2</sup> ]	End Magnitude[kN/m.C.kg/m <sup>2</sup> ]	Start Location[m,%]	End Location[m,%]
35	M30	X	.272	.272	0	2.2
36	M32	X	.209	.209	0	2.2
37	M23	X	.209	.209	0	2.2
38	M25	X	.272	.272	0	2.2
39	M27	X	.27	.27	0	2.2
40	M29	X	.27	.27	0	2.2
41	M31	X	.272	.272	0	2.2
42	M33	X	.209	.209	0	2.2

Figure 62. Transient Area Loads (Advise Mechanical Solutions).

Most likely it happened due to either incorrect conversion of solid model to skeletal one, or due to direct modelling in RISA-3D, when dimensions were overestimated. It's important to note that this mistake took place due to confusion between engineering and structural dimensions and doesn't question Advise Mechanical Solutions expertise.

Wind load on beams is similar to Frame Analysis, except for some additional beams having wind load applied and consideration of another wind direction, along the pipe rack length. Reported reactions are shown on the sixth column (from left to right) in kN on Figure 63.

19	10	N1	.055	-.14	25.604	.174	.061	0
20	10	N2	-.055	-.14	25.604	.174	-.061	0
21	10	N17	.055	.14	25.604	-.174	.061	0
22	10	N18	-.055	.14	25.604	-.174	-.061	0
23	10	Totals:	0	0	102.417			
24	10	COG (m):	X: 1.1	Y: 5	Z: 4.536			

Figure 63. Reactions from RISA-3D (Advise Mechanical Solutions).

Difference with Frame Analysis is around 25% but is expected due to RISA-3D model being heavier and with more transverse beams.

Let's compare M27 and M31 from Figure 60 and their analogues in Inventor. Before comparing results, we can estimate expected error with eq. (38). Then, ratio of deflections should be:

$$\frac{RISA - 3D}{Frame Analysis} = \frac{\frac{2450 \cdot 2.2^4}{384 \cdot 210 \cdot 10^9 \cdot 430621 \cdot 10^{-12}}}{\frac{2450 \cdot 1.96^4}{384 \cdot 220 \cdot 10^9 \cdot 430621 \cdot 10^{-12}}} = \left(\frac{2.2}{1.96}\right)^4 \cdot \frac{220}{210} = \quad (44)$$

$$= 1.662914131$$

Due to different geometry and material properties, 66% higher value is expected. However, as mentioned earlier, analytical formula doesn't take self-weight into account, and gravity load is considered in both simulations: RISA-3D report includes gravity in all scenarios automatically.

Note that the abovementioned calculation (numerator) shows that RISA-3D prediction of the deflection from a uniform load is also close to analytical solution, e.g. roughly 1.6 mm. Figure 64, Figure 65 and Figure 66 show results for M27, M31 and M9 respectively – they will be used extensively in the next pages, while Figure 67 shows colour map from Frame Analysis. All numeric calculations till subchapter 5.3 are based on these figures.

Member	Sec		x [mm]	LC	y [mm]	LC	z [mm]	LC	x Rotate [rad]	LC	(n) L/y' Ratio	LC	(n) L/z' Ratio	LC
39		max	.005	12	12.988	12	.515	11	-5.876e-4	12	NC	12	NC	12
40		min	-8.931	11	-.016	10	.361	10	-1.297e-3	11	NC	10	NC	10
41	M27	max	.007	12	13.662	12	3.923	11	1.098e-3	11	NC	12	NC	12
42		min	-15.404	11	-.005	11	2.074	10	5.873e-4	10	NC	10	NC	10
43		max	.004	12	13.668	12	5.397	12	1.062e-3	12	NC	12	2400.269	10
44		min	-15.407	11	-.008	11	2.99	10	5.873e-4	10	NC	10	1302.072	12
45		max	0	12	13.672	12	6.625	12	1.062e-3	12	NC	12	1390.286	10
46		min	-15.411	11	-.004	11	3.656	10	5.873e-4	10	NC	10	754.196	11
47		max	-.002	10	13.668	12	5.476	11	1.062e-3	12	NC	12	2400.274	10
48		min	-15.414	11	-.002	10	2.99	10	5.873e-4	10	NC	10	1061.184	11
49		max	-.004	10	13.662	12	3.708	12	1.062e-3	12	NC	12	NC	12
50		min	-15.418	11	-.004	11	2.074	10	5.873e-4	10	NC	10	NC	10

Figure 64. M27 results (Advise Mechanical Solutions).

11	M31	1	max	.007	12	13.689	12	.902	12	5.209e-4	12	NC	12	NC	12
12			min	-15.478	11	.013	10	.404	10	1.093e-4	10	NC	10	NC	10
13		2	max	.004	12	13.695	12	2.6	12	5.209e-4	12	NC	12	2387.889	10
14			min	-15.481	11	.013	10	1.325	10	1.094e-4	10	NC	10	1295.408	12
15		3	max	0	10	13.698	12	3.834	12	5.209e-4	12	NC	12	1383.191	10
16			min	-15.485	11	.013	10	1.995	10	1.094e-4	10	NC	10	750.336	11
17		4	max	-.002	10	13.695	12	2.883	11	5.21e-4	12	NC	12	2387.881	10
18			min	-15.489	11	.013	10	1.325	10	1.094e-4	10	NC	10	979.33	11
19		5	max	-.004	10	13.689	12	.902	12	5.21e-4	12	NC	12	NC	12
20			min	-15.492	11	.013	10	.404	10	1.094e-4	10	NC	10	NC	10

Figure 65. M31 results (Advise Mechanical Solutions).

201	M9	1	max	12.985	12	-.123	10	8.899	11	6.807e-4	11	NC	12	NC	12
202			min	.015	10	-.264	11	-.002	10	-1.561e-5	10	NC	10	NC	10
203		2	max	12.973	12	-1.607	10	10.365	11	1.581e-3	11	3368.168	10	NC	12
204			min	.005	10	-3.045	11	0	10	-3.508e-4	12	1798.104	11	3412.109	11
205		3	max	12.965	12	-2.474	10	10.878	11	1.833e-3	11	2126.162	10	NC	12
206			min	0	11	-4.672	11	.007	10	-4.478e-4	12	1134.347	11	2527.137	11
207		4	max	12.955	12	-1.607	10	10.365	11	1.581e-3	11	3368.172	10	NC	12
208			min	-.012	11	-3.046	11	0	10	-3.547e-4	12	1797.618	11	3412.143	11
209		5	max	12.936	12	-.123	10	8.899	11	6.807e-4	11	NC	12	NC	12
210			min	-.032	11	-.264	11	-.003	12	-2.269e-5	12	NC	10	NC	10

Figure 66. M9 results (Advise Mechanical Solutions).

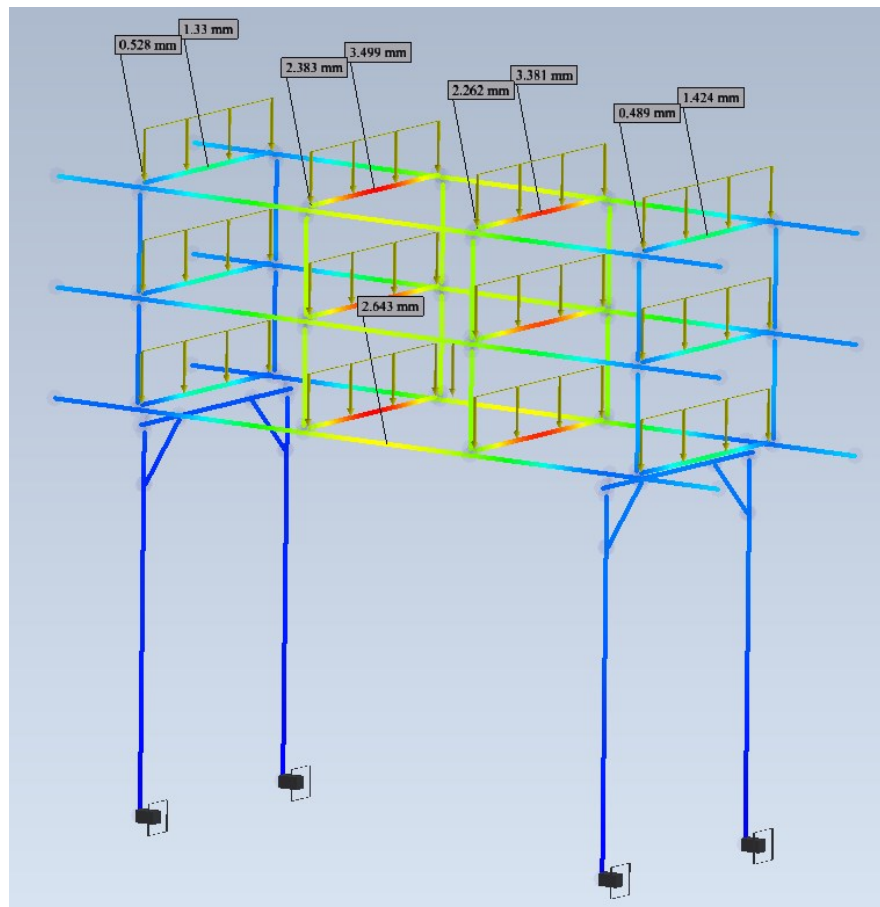


Figure 67. Frame Analysis results with probe measurements.

In RISA-3D, five calculated points per beam are reported, but only maximum and minimum values. For load from piping only we consider LC (Load Combination) 10 which outputs minimum. It can be seen that symmetry exists, e.g. points 1 and 5, or 2 and 4 have the same displacements in  $z$ -direction in M27 and M31. To find deflection in the midpoint due to uniform load, we need to subtract value of point 5 from point 3:  $3.656 - 2.074 = 1.582$  mm and  $1.995 - 0.404 = 1.591$  mm for M27 and M31 respectively. For Frame Analysis similar calculations are:  $3.499 - 2.383 = 1.116$  mm and  $1.424 - 0.489 = 0.935$  mm. An important thing to mention is that RISA-3D calculates deflection ratios (last four columns, NC is displayed when ratio is more than 10000) using beam deflections that are not reported, i.e. values from left-hand columns are not used for deflection ratios because they report displacements. We can verify that by using deflections that were just calculated. Note that since RISA-3D refers to the standards, where allowable ratio is defined, it calculates ratios for different members and if the ratio is higher than denominator of the ratio in the standard, it passes the code check. For example, if allowable deflection ratio is  $\frac{L}{360}$  then all calculated ratios should be more than 360. For hand calculations usually the opposite is done – maximum allowable deflection is derived from the given ratio and compared with the results. For M27:

$$\delta_{max} = \frac{L}{ratio} \rightarrow ratio = \frac{L}{\delta_{max}} = \frac{2200}{1.582} = 1390.64 \quad (45)$$

which is almost exactly the value from the report. And Frame Analysis yields higher safety factor for the structure:

$$ratio = \frac{L}{\delta_{max}} = \frac{1960}{0.935} = 2096.26 \quad (46)$$

Difference for M31 is totally justified as previously stated:  $0.935 \cdot 1.66 = 1.5521$  mm, which is close to RISA-3D prediction. But M27 has higher deviation in results than expected.

### 5.2.1 Sensitivity and buckling analyses

Higher deviation for M27 is caused by main drawback of Frame Analysis – displacement magnitude value has been used. It can be demonstrated on fivefold exaggerated deformation from Figure 68.

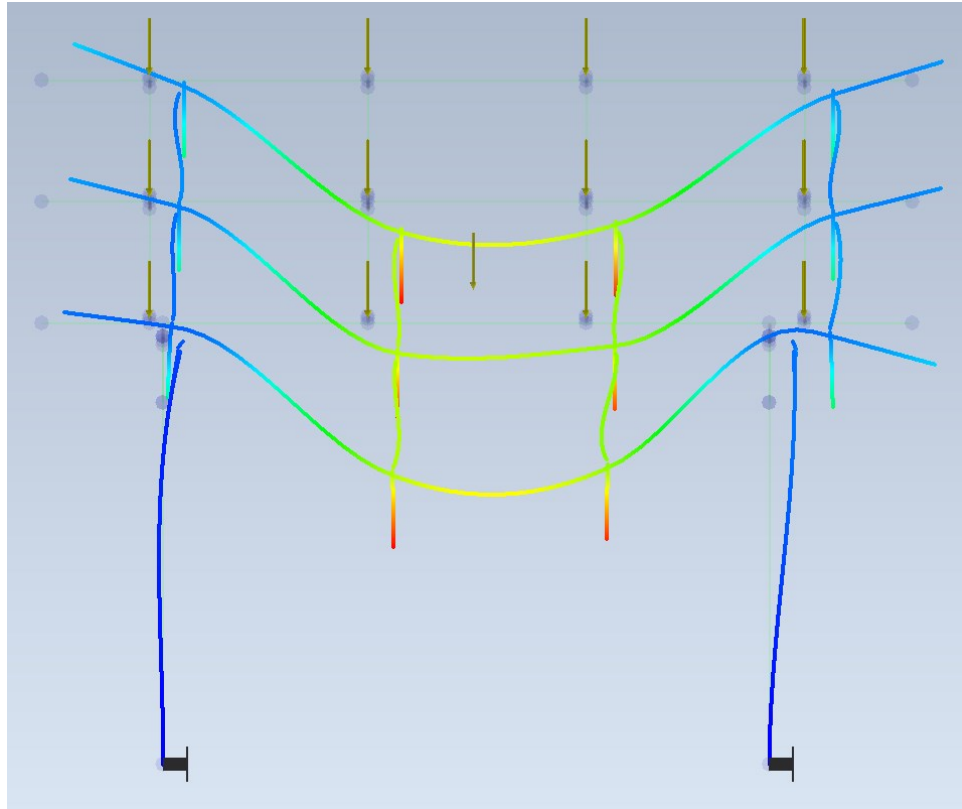


Figure 68. Adjusted deformation with free overhangs.

Compare it with Figure 50. Buckling of columns induces lateral displacement, so vertical deflection is actually smaller for M27 in Frame Analysis, we just can't directly measure it, since displacement is reported. Instead, we know how displacement magnitude is calculated (assuming lateral displacement in only one direction), squaring two known displacements and taking square root of their sum. Consequently, we can iterate and estimate this lateral translation to be:

$$\sqrt{0.935^2 + 0.61^2} = 1.116389269 \quad (47)$$

which means that column buckling results in 0.61 mm shift to the right. Reasons behind column buckling in this case are unclear. Furthermore, the buckling mode of columns is not as expected – columns behave not as braced, but as sway members, left column buckles like its top is free to move and bottom is fixed, while right column buckles like its top is roller supported and bottom is fixed. Such behaviour can be compared with the known modes of buckling (Herbert, 2006) from Figure 69.




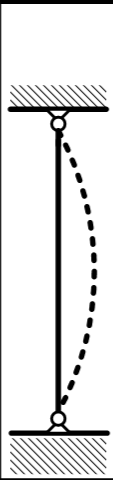
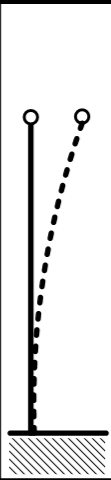
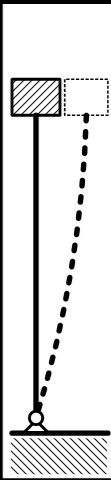
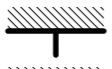

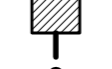
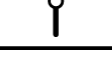
Buckled shape of column shown by dashed line						
Theoretical K value	0.5	0.7	1.0	1.0	2.0	2.0
Recommended design value K	0.65	0.80	1.2	1.0	2.10	2.0
End condition key	   	Rotation fixed and translation fixed Rotation free and translation fixed Rotation fixed and translation free Rotation free and translation free				

Figure 69. Column buckling modes (Herbert, 2006).

We can use Euler's critical load for column to make a quick analytical buckling analysis:

$$P_{cr} = \frac{\pi^2 EI}{(K_{ef} l)^2} \quad (48)$$

where  $K_{ef}$  is a column effective length factor and  $\pi$  is a well-known constant. Flexural buckling of first order (single wave) is considered only, since the bracing is only at the ends.

For 3A:

$$P_{cr} = \frac{\pi^2 \cdot 220 \cdot 10^9 \cdot 3180000 \cdot 10^{-12}}{(2 \cdot 3.6)^2} = 133193.9668 \text{ N} \quad (49)$$

Even when worst scenario is considered (free end), critical load is much higher than any of the simulated forces. Keep in mind that assembled pipe rack is expected to experience higher forces in columns because in Frame Analysis simplified module was analysed, as discussed



previously. However, as can be seen from Figure 63, more realistic values of axial force are not estimated to approach calculated critical load either. It means that columns are not expected to fail due to buckling. Note that Euler's formula has few idealisations that can't be met in reality – for example perfectly axial load or ideal column symmetry. Thus, predicted capacity is overestimated, but it's still much bigger than our loads. In theory, both columns should behave similarly – top frame is not restricted in longitudinal movement by boundary conditions, i.e. overhang ends are free. If overhang ends are fixed, then slightly different results can be observed, as on Figure 70 and Figure 71.

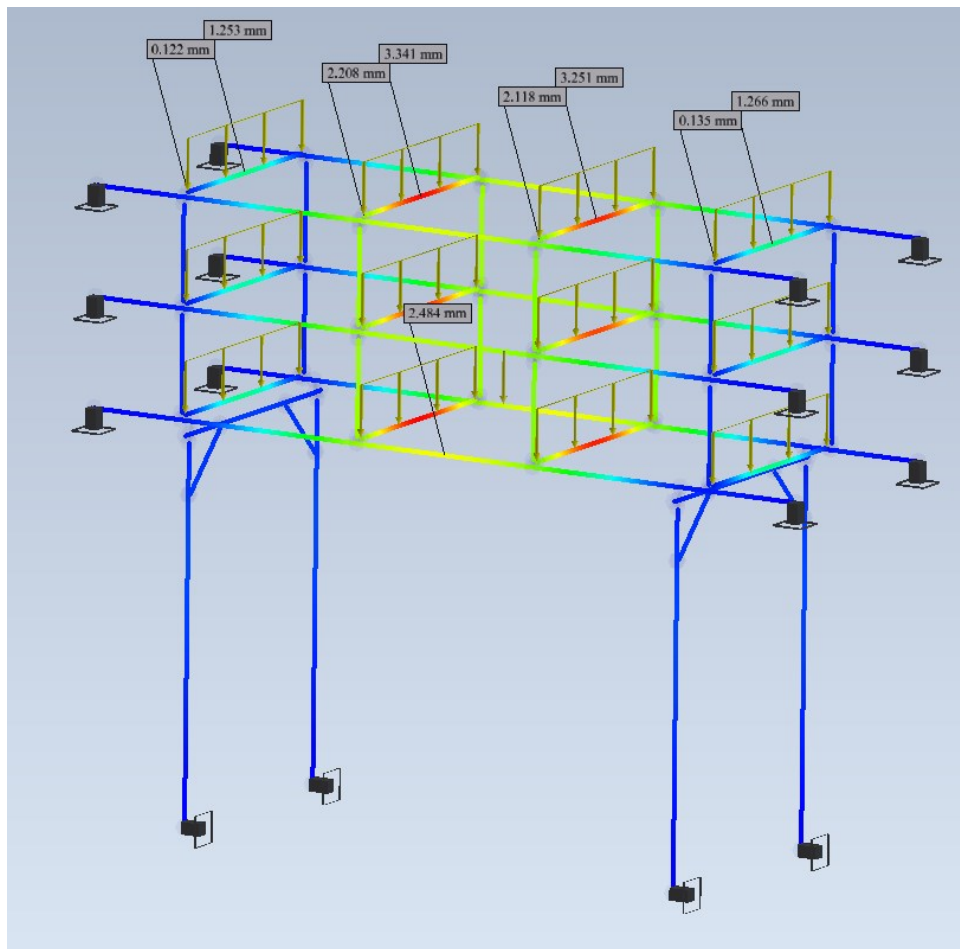


Figure 70. Fixed free overhangs with probe measurements.

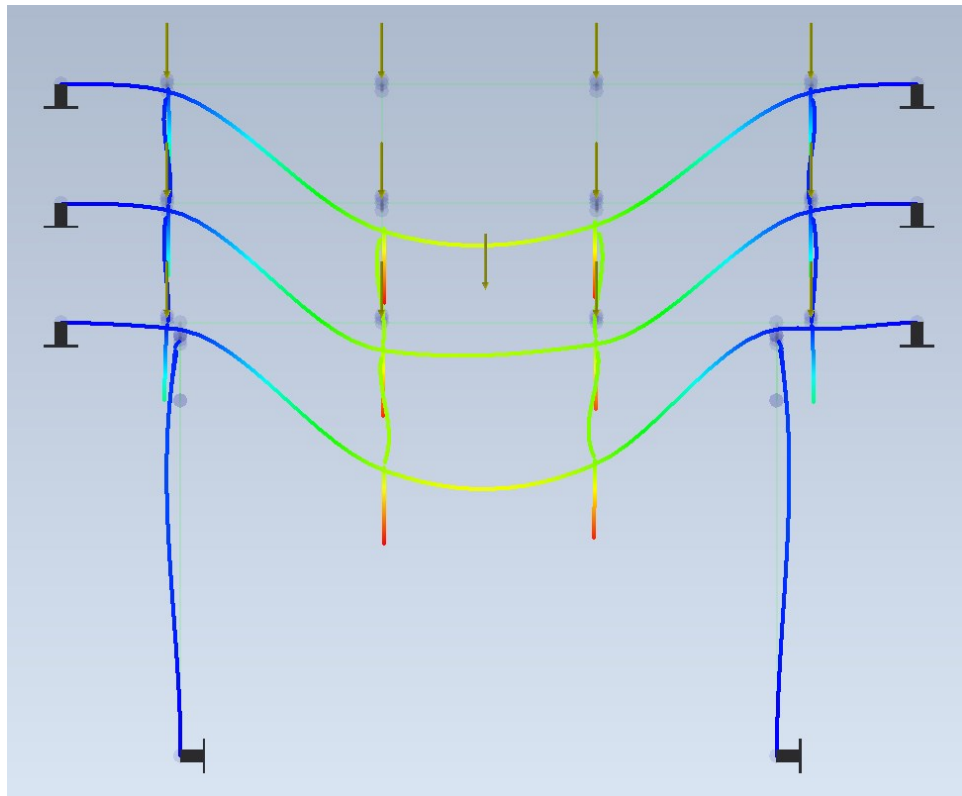


Figure 71. Adjusted deformation with fixed overhangs.

While displacements got a little bit more consistent (previously there was a small difference between midpoint deflections for different transverse beams), columns now buckle more realistically. When constraining overhang ends with pinned or roller supports, similar results are achieved.

For M9 reported displacements are inverted – to see displacement in global  $z$ -direction we need to take value from  $y$ -axis column (same for deflection ratios). Reader can verify it by closely comparing values from different columns – typically  $x$ - and  $y$ -axis displacements are the largest and are over 10 mm, like for M27 and M31, while for M9 it's  $x$ - and  $z$ -axis displacements that are caused by a wind load, making  $y$ -axis displacements those from piping. In addition, symmetry is observed in  $y$ -axis column, as mentioned earlier. Now we need to take maximum value, because it will be the smallest by magnitude – all values in the column are negative. We can see that 2.474 mm is 6% smaller than 2.643 mm predicted by the model with unrestricted overhangs. With fixed overhang ends, 2.484 mm is predicted by Frame Analysis, so error is reduced to less than half percent. This greatly supports our buckling assumption but doesn't completely explain it. It's still ambiguous why this buckling

didn't affect previous calculations like on Figure 50. It means that model has certain degree of sensitivity regarding buckling modes, since values of different magnitudes result in different buckling modes.

As previously, we can confirm deflection ratio at the longitudinal beam. Deflection from the report is  $2.474 - 0.123 = 2.351$  mm, so the deflection ratio is:

$$ratio = \frac{5000}{2.351} = 2126.75 \quad (50)$$

Which is again almost the same as the reported value. It's obvious that Frame Analysis would predict very similar ratio, since difference between simulated displacements is less than half per cent. It can also be now confirmed that transverse beam not only has the highest displacement, but also has the highest deflection with respect to its length, since it was demonstrated that longitudinal beam has a higher deflection ratio, although values are close.

### 5.3 Comparison with previous results, example 1C

The same process can be performed for 1C (Figure 72) to find out that the deviation is higher than expected (Figure 73).

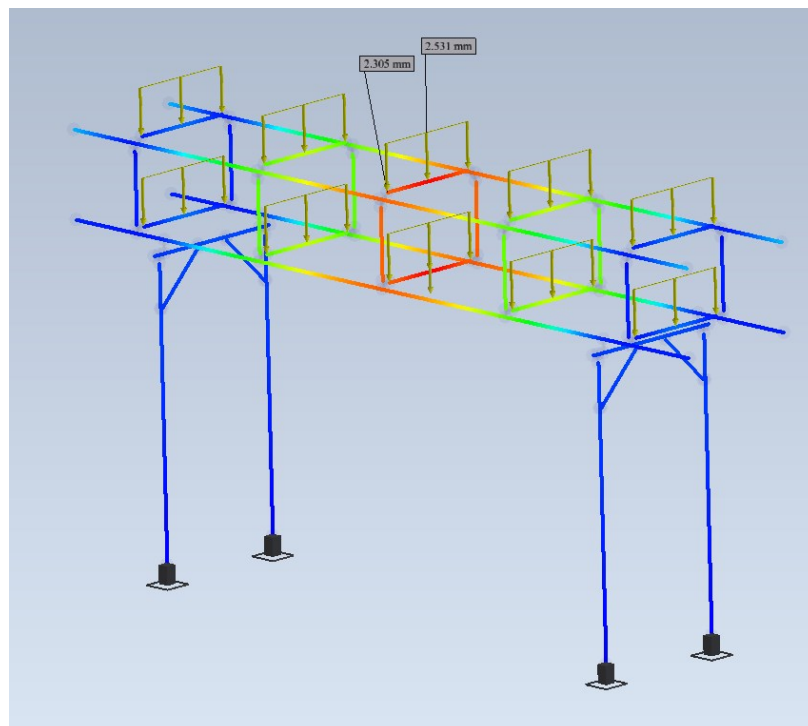


Figure 72. 1C probes.

221	M23	1	max	.007	12	3.282	12	4.467	11	0	11	NC	12	NC	12
222			min	-4.429	11	0	10	3.877	10	-3.642e-5	12	NC	10	NC	10
223		2	max	.004	12	3.283	12	4.892	11	0	11	NC	12	2381.157	10
224			min	-4.433	11	0	10	4.381	10	-3.638e-5	12	NC	10	2183.159	12
225		3	max	0	12	3.285	12	5.231	12	0	11	NC	12	1369.782	10
226			min	-4.436	11	0	10	4.753	10	-3.635e-5	12	NC	10	1255.803	11
227		4	max	-.003	12	3.285	12	4.825	12	0	11	NC	12	2381.146	10
228			min	-4.439	11	0	10	4.381	10	-3.632e-5	12	NC	10	2079.787	11
229		5	max	-.006	10	3.285	12	4.276	12	0	11	NC	12	NC	12
230			min	-4.443	11	0	10	3.877	10	-3.629e-5	12	NC	10	NC	10

Figure 73. Results M23 (Advise Mechanical Solutions).

Frame Analysis predicts 0.226 mm of deflection, RISA-3D reports 0.876 mm, which is 3.876 times higher, when  $\left(\frac{1.2}{0.92}\right)^4 \cdot \frac{220}{210} = 3.032334178$  bigger value was expected. It's essential to understand that the calculated values are applicable only in the considered cases, i.e. there is no linear dependency, such as “if deflection is three times bigger, then displacement is also three times higher”. Analytical solution converges with Frame Analysis, but not with the report. Consequently, there is a variance in boundary conditions, more precisely loads. A closer look at the report reveals that almost 30% higher load was used with sudden jumps in values indeed (Figure 74).

Member Distributed Loads (BLC 15 : BLC 2 Transient Area Loads)						
Member Label	Direction	Start Magnitude(N/m.C.kg/m*2)	End Magnitude(N/m.C.kg/m*2)	Start Location(m.%)	End Location(m.%)	
1	M19	-7.661	-7.661	0	1.2	
2	M26	-9.261	-9.261	1.3e-5	1.2	
3	M27	-9.194	-9.194	0	1.2	
4	M40	-7.662	-7.662	1e-5	1.2	
5	M43	-8.937	-8.937	0	.3	
6	M43	-9.156	-9.265	.3	.6	
7	M43	-9.265	-9.153	.6	.9	
8	M43	-9.153	-8.939	.9	1.2	
9	M45	-9.262	-9.262	8.1e-5	1.2	
10	M48	-265.483	-87.505	.144	.159	
11	M48	-87.505	1.483	.159	.175	
12	M48	1.483	1.483	.175	.19	
13	M48	1.483	1.483	.19	.205	
14	M48	1.483	1.483	.205	.22	
15	M48	1.483	1.483	.22	.235	
16	M48	1.483	1.483	.235	.251	
17	M48	1.483	1.483	.251	.266	
18	M48	1.483	1.483	.266	.281	
19	M48	1.483	1.483	.281	.296	
20	M48	1.483	1.483	.296	.311	
21	M48	1.483	1.483	.311	.326	
22	M48	1.483	1.483	.326	.342	
23	M48	1.483	1.483	.342	.357	
24	M48	1.483	1.483	.357	.372	
25	M48	1.483	1.483	.372	.387	
26	M48	1.483	1.483	.387	.402	
27	M48	1.483	1.483	.402	.418	
28	M48	1.483	-29.202	.418	.433	

Figure 74. Uneven load distribution (Advise Mechanical Solutions).

This difference compensates for the error. Moreover, this difference coincides with the load combination factor of 1.35 applied to dead loads (omitted in this study). Also, magnitude of the displacement – that is mostly affected by longitudinal beam deflection, which in turn also has dependency on the transverse beam length, but of the first order, instead of fourth order – is roughly 35% higher for RISA-3D, i.e.  $\frac{4.753}{2.531} \cdot \frac{210}{220} \cdot \frac{0.92}{1.2} = 1.37$ , when geometry and material properties differences are considered. Note that longitudinal beam deflection is

linearly dependent (though not necessarily with coefficient of 1, which explains a small divergence of two percent) on the transverse beam length because load from piping is transferred to the longitudinal beam through joints via point forces, which in turn linearly depend on the length of a beam, in case of uniform load being a simple product of load and length.

However, it's reported that factor of 1 is applied to the LC10, as seen on Figure 75. Additionally, some simulations indeed apply load with factor of 1, for example previously evaluated 3A and others, that are not reported here to be short.

**Load Combinations**

	Description	Solve	PDelta	SRSS	BLC	Factor	BLC	Factor	BLC	Factor	BLC	Factor	BLC	Factor	BLC	Factor	BLC	Factor	BLC	Factor	BLC	Factor	
1	Operational	Yes	Y		DL	1.35																	
2	Operational Wind X	Yes	Y		DL	1.35	WLY	1.5	SL	1.5													
3	Operational Wind Y	Yes	Y		DL	1.35	WLY	1.5	SL	1.5													
4	Seismic X		Y		DL	1	ELX	1	ELY	.3	ELZ	.3											
5	Seismic Y		Y		DL	1	ELX	.3	ELY	1	ELZ	.3											
6	Seismic Z		Y		DL	1	ELX	.3	ELY	.3	ELZ	1											
7	Seismic X (uplift)		Y		DL	1	ELX	1	ELY	.3	ELZ	-.3											
8	Seismic Y (uplift)		Y		DL	1	ELX	.3	ELY	1	ELZ	-.3											
9	Seismic Z (uplift)		Y		DL	1	ELX	.3	ELY	.3	ELZ	-1											
10	Operational (DEFLECTION)	Yes	Y		DL	1																	
11	Operational Wind X (DEFLECTION)	Yes	Y		DL	1	WLY	1	SL	1													
12	Operational Wind Y (DEFLECTION)	Yes	Y		DL	1	WLY	1	SL	1													

Figure 75. Load combinations (Advise Mechanical Solutions).

### 5.4 Key results

Overall, no explicit correlation between given configuration and results divergence has been found, despite all the possible reasons behind the deviation being discussed, compared and calculated. As a conclusion, both models are acceptably accurate and mostly converge with analytical solutions, but since different boundary conditions are applied to the models, different results are produced. However, Waterleau's suspicions regarding some configurations are not groundless, since previous analysis was performed on a less accurate model.

The applied methods have demonstrated their adequacy when analysing side-by-side with analytical solutions and previous findings. Before choosing Frame Analysis environment other programmes were tested, including Femap and Inventor NASTRAN, but they were eventually discarded due to workflow issues. For this study alone they could be utilised, but their future use would be questionable, which determined the choice as it is. Despite software and model differences, the nature of divergence between the achieved and previous results

is mostly understood. The only missing comparison is related to the wind load, since simulations from Advise Mechanical Solutions included wind only in combined load scenarios, and it's tricky to compare effects of live load alone precisely if results for combined loads are reported. However, it can be observed that deviation in results for combined load follows a similar pattern of the gravity and piping load scenario that has been evaluated previously.

Albeit the difference in the results, both analyses estimate pipe rack as a safe structure. RISA-3D, being a specialised tool, can check all the outputs with the according standards, Advise Mechanical Solutions used Eurocode 1: EN 1991-1 and Eurocode 3: EN 1993-1, and pipe racks passed all the checks. For a model with 1D elements von Mises or Tresca stresses are not calculated. Instead, maximum normal and shear stresses are reported. It is possible to calculate combined stresses, but due to 1D approximation, it's not always clear which combination should be considered, i.e. stress for only one, maximum point is reported, not entire cross-section. For example, vertically applied force to a beam induces both normal stress from internal bending moment and transverse shear stress from the shear force, but highest normal stress occurs on the top and the bottom surfaces, while maximum shear takes place in the neutral plane. On the other hand, axial stress will be uniform, while maximum shear stress from torsion will occur on the outside contour. Additionally, in the pipe rack in some members bending moments and shear forces in two different directions are present, but due to the difference between global and local coordinate systems, it can be tricky to combine them, since only maximum value is reported from the entire distribution of the cross-section. But from the simulations we can also observe that shear stresses are less than normal stresses in the pipe rack, and these two maxima don't coincide, i.e. maximum normal and shear stresses occur in different members. Furthermore, even if we take the highest observed values for stresses, keeping in mind that normal stresses occurred only in one of two orthogonal directions, we can estimate principal stresses in 2D:

$$\sigma_{1,2} = \frac{\sigma}{2} \pm \sqrt{\left(\frac{\sigma}{2}\right)^2 + \tau^2} = \frac{123}{2} \pm \sqrt{\left(\frac{123}{2}\right)^2 + 35^2} \rightarrow \quad (51)$$

$$\rightarrow \{\sigma_1 = 132.26 \text{ MPa}, \sigma_2 = -9.26 \text{ MPa}\}$$

where  $\sigma_{1,2}$  are principal stresses,  $\sigma$  is a normal stress and  $\tau$  is a shear stress. Steel is a ductile material, so von Mises criterion can be used:

$$\begin{aligned}\sigma_{vm} &= \sqrt{\sigma_1^2 - \sigma_1\sigma_2 + \sigma_2^2} = \sqrt{132.26^2 + 132.26 \cdot 9.26 + 9.26^2} = \\ &= 137.124698 \text{ MPa}\end{aligned}\quad (52)$$

where  $\sigma_{vm}$  is von Mises stress. And even more conservative Tresca criterion predicts no failure due to yielding:

$$\sigma_t = \max\{|\sigma_1|, |\sigma_2|, |\sigma_1 - \sigma_2|\} = 141.52 \text{ MPa} \quad (53)$$

where  $\sigma_t$  is Tresca stress. However, it's important to remember that both Frame Analysis and RISA-3D approximated pipe rack with 1D elements, neglecting bolted connections that are usually the weakest areas in such structures, so a separate analysis of fasteners is needed to validate the structure's safety.

In addition, it can be noted that deflection ratios from dead load also pass conservative requirement of  $\frac{L}{360}$  in both analyses. Deflection ratios comparison was shown briefly before, but one can also check (Appendix 3) that deflections no more than 5.4 mm, 3.5 mm and 2.7 mm occur in A, B and C configurations respectively (dead load only). As a conclusion, pipe rack is also serviceable.

## 5.5 Future improvements and usability of results

Compilation of stress and deflection analyses leads us to the conclusion that some pipe rack configurations are indeed overengineered and some structural members are over dimensioned for the defined loads. Therefore, weight and cost reductions are possible. Redesign of the pipe rack itself falls beyond the scope of this thesis, since it will require iLogic model changes, for example considering square channels or L-profiles for lighter versions. However, some general patterns can be outlined. Comparing maximum displacements shows that typically the error decreases for a given geometrical configuration (e.g. A, B or C) with lighter load case (e.g. 1, 2 and 3). Configuration A has the smallest error and its previous analysis is overall similar to the one in this study. However, its deflection ratios are still significantly higher than defined ratio, though it's more likely considered to be a solid safety factor. Overall, the error for A configurations is usually no more than 10%, which is mostly a material properties difference in simulations.

Configuration B is not consistent as A or C – 1B and 2B have significant deviations between current and previous analyses, with up to 64% for 1B, while 3B is closer to configuration A in regard to divergence in different simulations. The excessive safety factors are observed in C configuration. All C versions are similar to 1B and 2B with a very high error up to a little bit over 100% in 2C, where RISA-3D estimates 3.539 mm displacement in the middle of M27, while Frame Analysis predicts 1.747 mm at the same point. As mentioned earlier, there is no point in direct comparison of pure results, since different boundary conditions were used. Nevertheless, taking into account that all pipe racks passed code checks in RISA-3D, it's plausible that those configurations with a higher divergence are more likely to be used with lighter structural profiles without compromising safety and serviceability.

It is obvious that over dimensioning affects configuration C more than A and B. Furthermore, all C versions can be made more lightweight. The general idea is to reduce profiles to the ones below current selections, e.g. switch HEA120 to HEA100, or UPN100 to UPN80, etc. For 1B and 2B it's more complicated. Channels can be reduced similarly to the C, and it's possible to do the same with longitudinal beams and spacers, but columns will require deeper buckling analysis before possible reductions, i.e. more advanced software capable of linear and non-linear buckling simulations (Inventor NASTRAN), or more sophisticated buckling theories (Rankine or Johnson) should be applied, because previous buckling calculations were trivial and basic. Although, as mentioned before, new pipe rack design for the defined loads is not considered in this thesis, it can be shown that existent configurations can carry heavier loads instead. For example, 1B has the same maximum displacements as in Advise Mechanical Solutions report only when load of 1275 kg/m is applied in Frame Analysis (Figure 76).



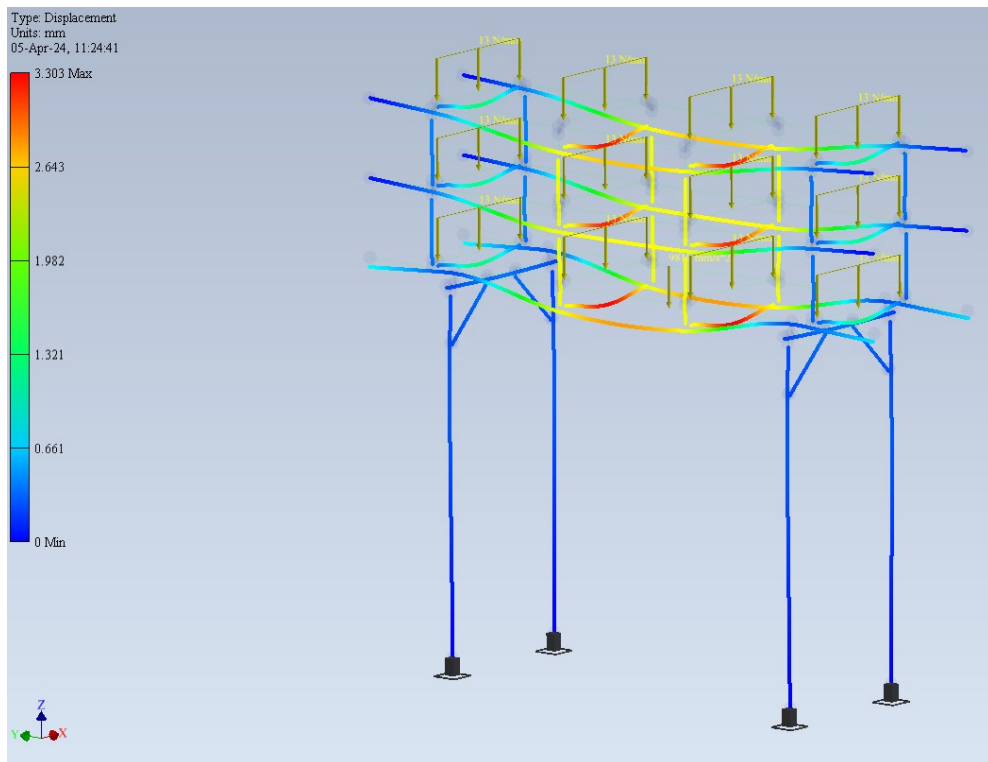


Figure 76. Higher load on 1B.

For 2B this value is 765 kg/m (Figure 77).

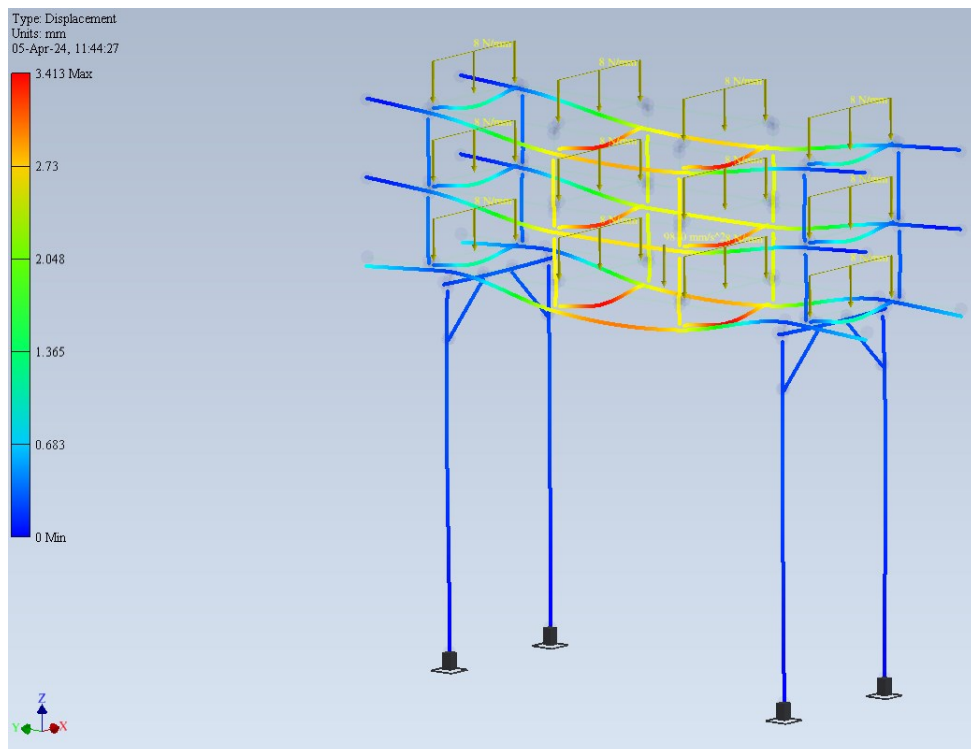


Figure 77. Higher loads on 2B.

Regarding C configurations, current 1C is estimated to experience similar displacement as in RISA-3D with 1530 kg/m of load (Figure 78).

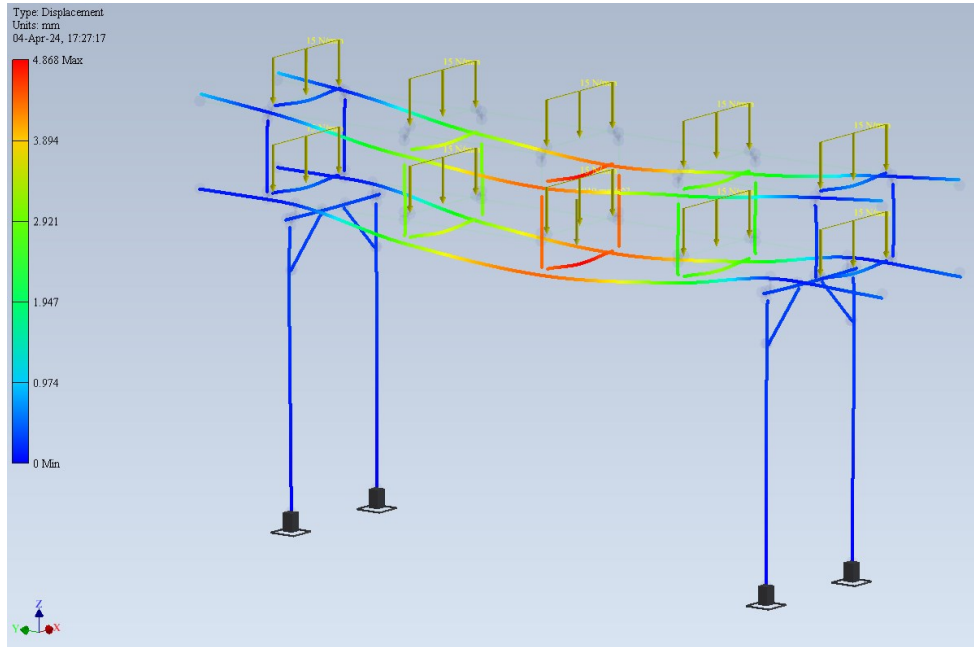


Figure 78. Higher loads on 1C.

At the same time, 2C has similar displacements to RISA-3D only with 1020 kg/m (Figure 79).

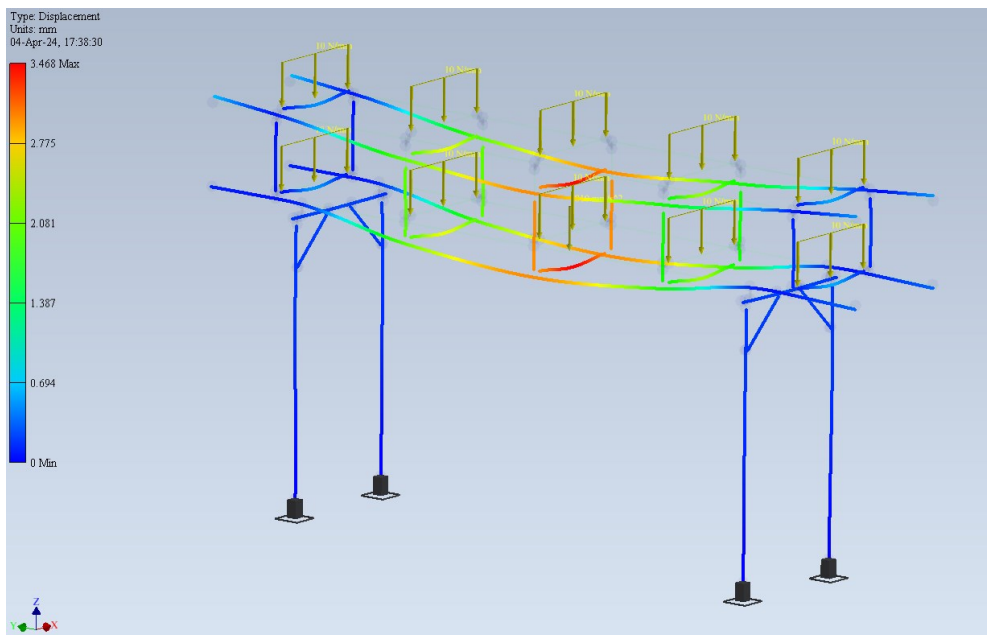


Figure 79. Higher loads on 2C.

Lastly, 3C is estimated to reach previously reported maximum displacements only with 510 kg/m (Figure 80).

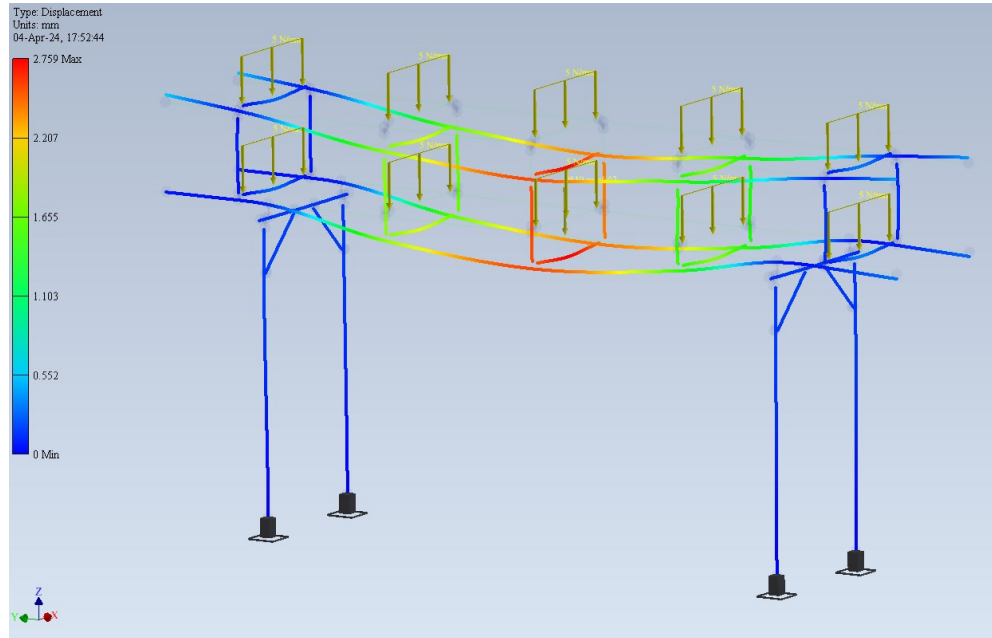


Figure 80. Higher loads on 3C.

Higher loads demonstrate overengineering of 1B, 2B, 1C, 2C and 3C more explicitly. Although loads over one tonne per metre are unrealistic, it's reasonable to state that, say, 2B can be used for loads defined for 1B, or 1C can be replaced with 2C, which in turn can be replaced with 3C. Alternatively, lighter profiles can be chosen, e.g. UPN80 instead of UPN100, etc. Third approach in optimisation can be increase of width limit for the configurations, so more pipes can be fitted on a cheaper version. However, it was previously shown that beam deflection is especially sensitive to the beam's length, so it's recommended to not increase the limit beyond the difference between dimensions used in the thesis and report by Advise Mechanical Solutions without further investigation of applicable safety and serviceability limits. Based on these conclusions, more particular and detailed product proposals are formulated for the commissioner, but due to their confidentiality, they are not reported here.

Last small issue that should be addressed is bolts placement. Figure 18 shows that current iLogic model places bolts upside down on the top structure, while in reality they are placed with bolts on top, so that if nuts are unscrewed, bolts stay in place and provide shear resistance. Otherwise, bolts would fall off, essentially disassembling the structure.

## 6 Conclusions

Despite very limited available information, solid background for the pipe rack structures and context for the parametric design have been established first, including some novel information and examples obtained from the industry. Pipe rack design details have been reported as well. After that, theoretical base and practical aspects of FEM were discussed. Further, detailed and sound analysis of multiple pipe rack configurations has been performed. Multiple areas have been investigated, including reactions, internal forces and moments, stresses, deflections and buckling. Majority of FEA results have been validated with analytical solutions, highlighting limitations of the software and method in general. Moreover, some correction formulae have been derived to compensate for simulation's approximations.

Similar results to the previous report were not achieved. Instead, a close comparison of the results revealed that the previous analysis was performed on the over dimensioned pipe rack, probably due to the differences in engineering and structural analysis measurements that were not settled. Though such an outcome was unexpected, it essentially confirms that some pipe rack configurations are indeed overengineered, confirming the company's suspicions. Therefore, cost reduction for the pipe rack is possible through weight reduction. Pipe rack redesign is not covered, but general ideas for proposals based on current designs are outlined, with details being omitted due to privacy reasons. More particularly, 1B, 2B and all C configurations are estimated to carry much heavier loads than initially intended for, before reaching maximum deflections previously reported. For example, 2B, that is intended for 500 kg/m load, was estimated to carry 750 kg/m safely, basically replacing 1B. Same pattern was observed for all C configurations. Despite difficulties to balance between academic requirements and commissioner's needs, both comprehensive explanations and useful results were produced. However, thesis goals were mostly shifted to developing solid understanding of applied mechanics and FEM, thus limiting coverage of design changes after analysis due to time frame and confidentiality restrictions for Bachelor's theses.

## References

Autodesk (2024). *Frame Analysis Overview*.

<https://help.autodesk.com/view/INVNTOR/2023/ENU/?guid=GUID-302B683F-8CAC-46A4-BD67-E39D4BAC0997>

Aziz, E., Chassapis, C. and Esche, S. (2008). *Online wind tunnel laboratory*. Proceedings of the 2008 ASEE Annual Conference and Exposition, Pittsburgh, Pennsylvania, USA, p. 14.

Bausbacher, E. and Hunt, R. (1994). *Process plant layout and piping design*, pp. 261-265.

CAD/CAM Machine Drawing and Computer Graphics (2013). *LESSON 12. Analytical and synthetic approaches, parametric and implicit equations*.

<http://ecoursesonline.iasri.res.in/mod/page/view.php?id=127526>.

Cook, N. (2007). *Designers' Guide to EN 1991-1-4 Eurocode 1: Actions on structures, general actions part 1-4. Wind actions*.

Dark, R. (2018). *SOLIDWORKS Simulation Elements: Solid vs. Beam Results*.

<https://www.goengineer.com/blog/solidworks-simulation-elements-solid-vs-beam-results>.

Drake, R. M. and Walter, R. J. (2010). *Design of Structural Steel Pipe Racks*. Engineering Journal, American Institute of Steel Construction, Fourth Quarter, pp. 241-242.

Duffin, J., MLC CAD Systems (2023). *Which type of elements should I use? - MLC CAD systems*. <https://www.mlc-cad.com/solidworks-help-center/which-type-of-elements-should-i-use/>.

Harish, A. (2024). *Finite element method – what is it? FEM and FEA explained, SimScale*.

<https://www.simscale.com/blog/what-is-finite-element-method/>.

- Harish, A. (2023). *Tips for meshing your CAD model for structural analysis, SimScale*.  
<https://www.simscale.com/blog/mesh-cad-model-structural-analysis/>.
- Herbert, G. W. (2006). *Descriptive table of structural column effective length (K factor) values*.
- Kleinlogel, A. (1952). *Rigid frame formulas: Explicit Formulas of All Statical Quantities for Those Single-panel Frames which Occur in Practical Steel*, p. 147, 150.
- Kosakowski, A. (2012). *RESULTS - DISPLACEMENT vs. DEFLECTION - Definitions used by Robot*. <https://forums.autodesk.com/t5/robot-structural-analysis-forum/results-displacement-vs-deflection-definitions-used-by-robot/m-p/3505268>.
- LinDapter (no date). *Type AF High Slip Resistance Girder Clamp*.  
<https://www.lindapter.com/product/type-af-high-slip-resistance-girder-clamp>.
- Metinvest (no date). *Steel S235JR: characteristics, properties, analogues - Metinvest*.  
<https://metinvestholding.com/en/products/steel-grades/s235jr>.
- Moran, S. (2016). *Process plant layout*, p. 483. Butterworth-Heinemann.
- Morrison, J. (2018). *Pipe racks: The main artery of a plant - Judith Morrison - Medium*.  
<https://judith-morrison.medium.com/pipe-racks-the-main-artery-of-a-plant-d7df3f8e813d>.
- Polyanin, A.D., Schiesser, W.E. and Zhurov, A.I. (2008). *Partial differential equation, Scholarpedia*. <https://doi.org/10.4249/scholarpedia.4605>.
- Risa (2018). *RISA | A Deeper Understanding of Deflection and Member Deflection Ratios*.  
<https://blog.risa.com/post/a-deeper-understanding-of-deflection-and-member-deflection-ratios>.
- Ucal, M. (2024). *Parametric equation | Definition & Facts*.  
<https://www.britannica.com/science/parametric-equation>.

Younis, W. (2010). *Up and Running with Autodesk Inventor Simulation 2011: A Step-by-step Guide to Engineering Design Solutions*, pp. 383-412. Butterworth Heinemann.

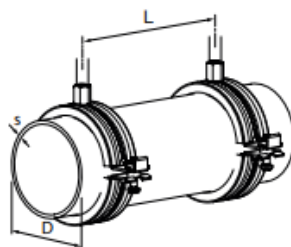
## Appendix 1. Structural profile selection sheet

First digit corresponds to the load case, following letter indicates geometrical configuration as per Table 1 and a letter after a dash means that the setup is prepared for seismic loads, but these are not considered in the thesis.

<b>Piperack_Setup</b>	<b>Base_Profile</b>	<b>Brace_Profile</b>	<b>Span_Profile</b>	<b>Spacer_Profile</b>	<b>Strut_Profile</b>
1A-S	HEB200	HEB140	HEB140	HEB140	UPN160
2A-S	HEB180	HEB120	HEB120	HEB120	UPN140
3A-S	HEB140	HEB100	HEB100	HEB100	UPN120
1B-S	HEB180	HEB140	HEB140	HEB140	UPN120
2B-S	HEB160	HEB120	HEB120	HEB120	UPN100
3B-S	HEB120	HEB100	HEB100	HEB100	UPN80
1C-S	HEA160	HEA140	HEA140	HEA140	UPN100
2C-S	HEA140	HEA120	HEA120	HEA120	UPN80
3C-S	HEA100	HEA100	HEA100	HEA100	UPN80
1D-S	HEB240	HEB140	HEB140	HEB140	UPN160
2D-S	HEB220	HEB120	HEB120	HEB120	UPN140
3D-S	HEB180	HEB100	HEB100	HEB100	UPN120
1A	HEB140	HEB120	HEB120	HEB120	UPN160
2A	HEB120	HEB120	HEB120	HEB120	UPN140
3A	HEB120	HEB100	HEB100	HEB100	UPN120
1B	HEA140	HEA120	HEA120	HEA120	UPN120
2B	HEA120	HEA100	HEA100	HEA100	UPN100
3B	IPE180	IPE140	IPE140	IPE140	UPN80
1C	HEA120	HEA120	HEA120	HEA120	UPN100
2C	HEA120	HEA120	HEA120	HEA120	UPN80
3C	IPE140	IPE140	HEA100	HEA100	UPN80
1D	HEB200	HEB140	HEB140	HEB140	UPN160
2D	HEB180	HEB120	HEB120	HEB120	UPN140
3D	HEB140	HEB100	HEB100	HEB100	UPN120



## Appendix 2. Pipe specifications



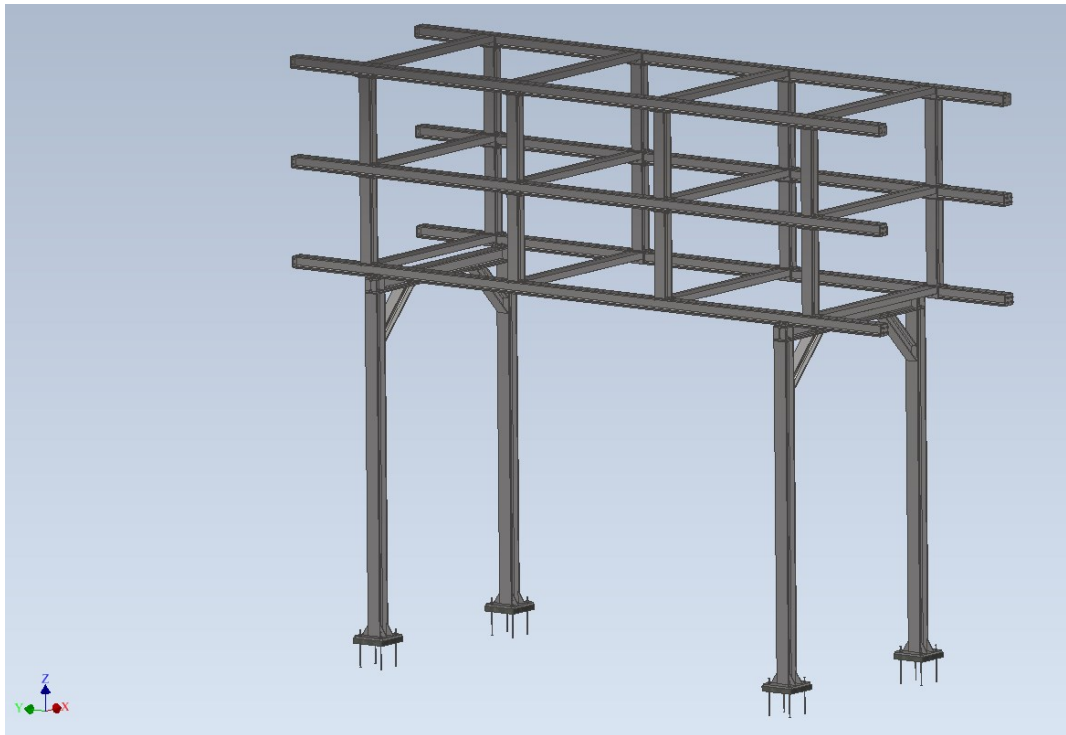
### Seamless steel pipes according to EN 10220 (replaces DIN 2448)

Ø Pipe D		s [mm]	Weight of pipe [kg/m]	Water content [l/m]	Water filled weight [kg/m]	L max. [m]
[DN]	O.D. [mm]					
6	10.2	1.6	0.34	0.04	0.38	1
8	13.5	1.8	0.52	0.08	0.6	1
-	16	1.8	0.63	0.121	0.751	1.1
10	17.2	1.8	0.68	0.145	0.825	1.2
-	20	2	0.89	0.201	1.091	1.2
15	21.3	2	0.95	0.235	1.185	1.3
-	25	2	1.13	0.346	1.476	1.4
20	26.9	2.3	1.4	0.39	1.79	1.5
-	30	2.6	1.76	0.483	2.243	1.8
-	31.8	2.6	1.87	0.555	2.425	1.8
25	33.7	2.6	1.99	0.638	2.628	2
-	38	2.6	2.27	0.845	3.115	2.2
32	42.4	2.6	2.55	1.086	3.636	2.3
-	44.5	2.6	2.69	1.212	3.902	2.4
40	48.3	2.6	2.95	1.458	4.408	2.5
-	51	2.6	3.1	1.647	4.747	2.8
-	57	2.9	3.87	2.058	5.928	3
50	60.3	2.9	4.11	2.332	6.442	3.1
-	63.5	2.9	4.33	2.614	6.944	3.1
-	70	2.9	4.8	3.235	8.035	3.2
65	76.1	2.9	5.24	3.88	9.12	3.3
-	82.5	3.2	6.26	4.546	10.806	3.7
80	88.9	3.2	6.76	5.343	12.103	4.2
-	101.6	3.6	8.7	6.995	15.695	4.3
-	108	3.6	9.27	7.976	17.246	4.4
100	114.3	3.6	9.83	9.004	18.834	4.5
-	127	4	12.13	11.116	23.246	4.7
-	133	4	12.73	12.266	24.996	4.9
125	139.7	4	13.39	13.616	27.006	5.1
-	152.4	4.5	16.41	16.144	32.554	5.3
-	159	4.5	17.15	17.663	34.813	5.5
150	168.3	4.5	18.18	19.921	38.101	5.8
-	177.8	5	21.31	22.103	43.413	6
-	193.7	5.4	25.08	26.26	51.34	6
200	219.1	5.9	31.02	33.734	64.754	6
-	244.5	6.3	37.01	42.215	79.225	6
250	273	6.3	41.44	53.26	94.7	6
300	323.9	7.1	55.47	75.33	130.8	6
350	355.6	8	68.58	90.58	159.16	6
400	406.4	8.8	86.29	118.73	205.02	6
450	457	10	110.24	149.99	260.23	6
500	508	11	134.82	185.51	320.33	6
600	610	12.5	184.19	268.78	452.97	6

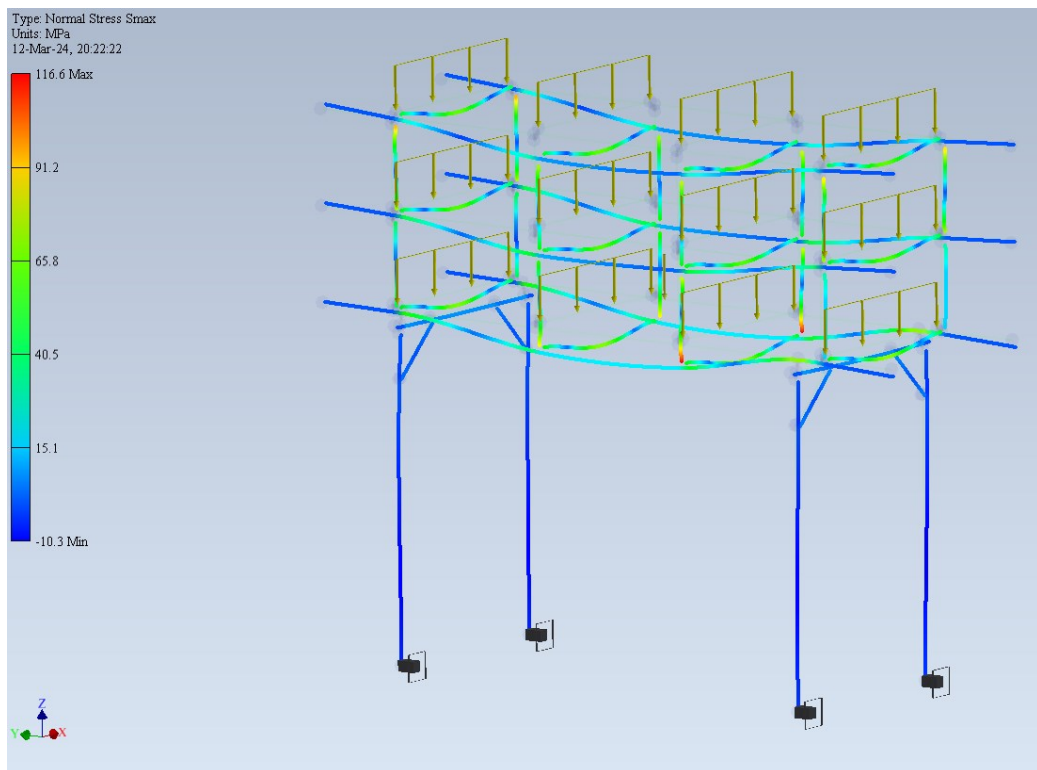
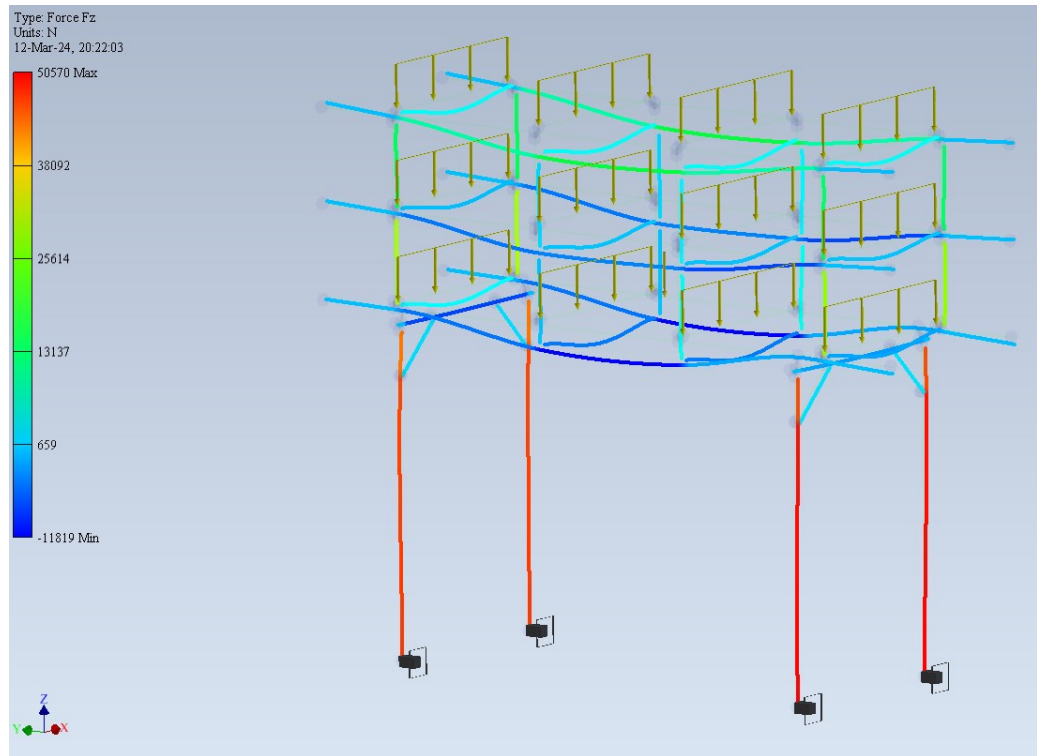
### Appendix 3. Results of simulations

All simulation results are reported in this appendix. Brief description is given first, then applied loads and mass of the assembly are reported. All wind loads are taken from the report by Advise Mechanical Solutions because it was shown that our calculations converge and there is no need to do repetitive calculations for every new beam profile. For all three configurations two scenarios are demonstrated – first, load from gravity and piping only, then with the additional load from the wind. For every scenario displacement, vertical forces and combined normal stresses fields are depicted. All results are shown on the models with twofold exaggerated deformation, and all boundary conditions are visible.

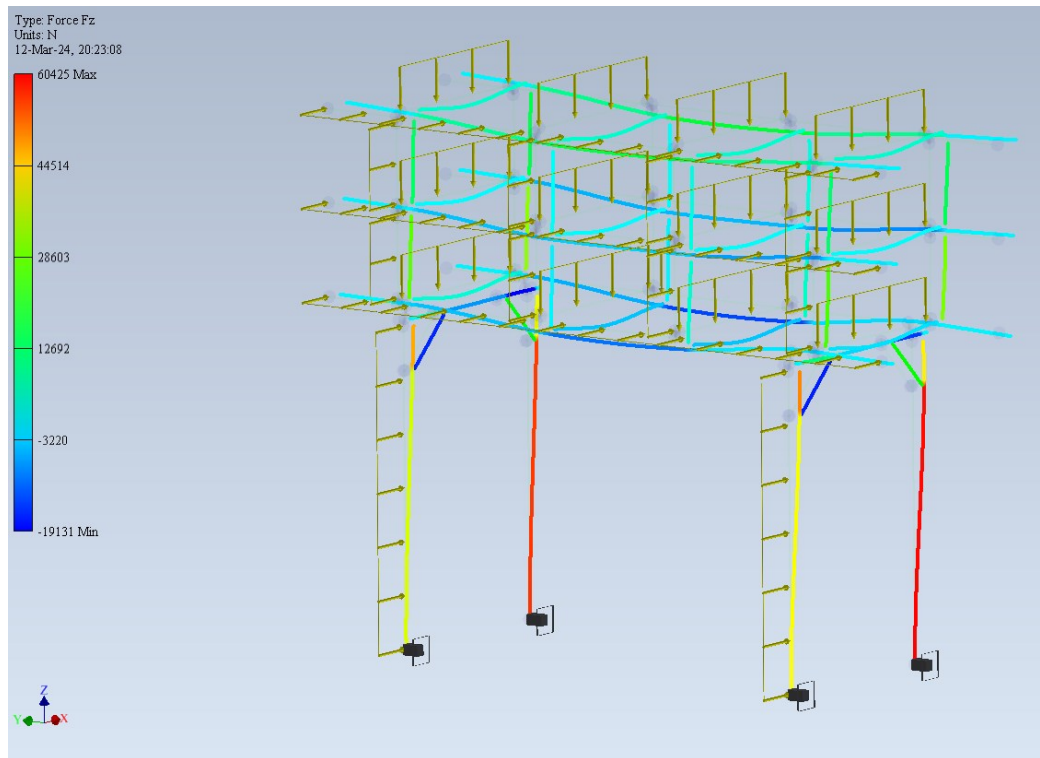
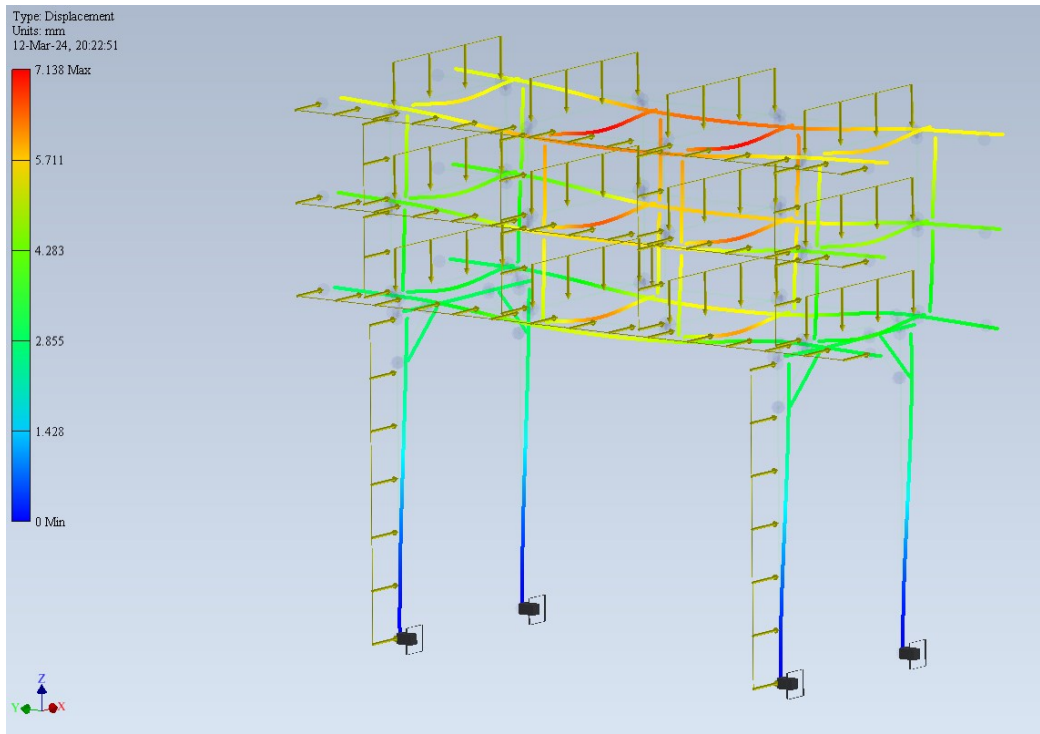
Large and heavy configuration A.

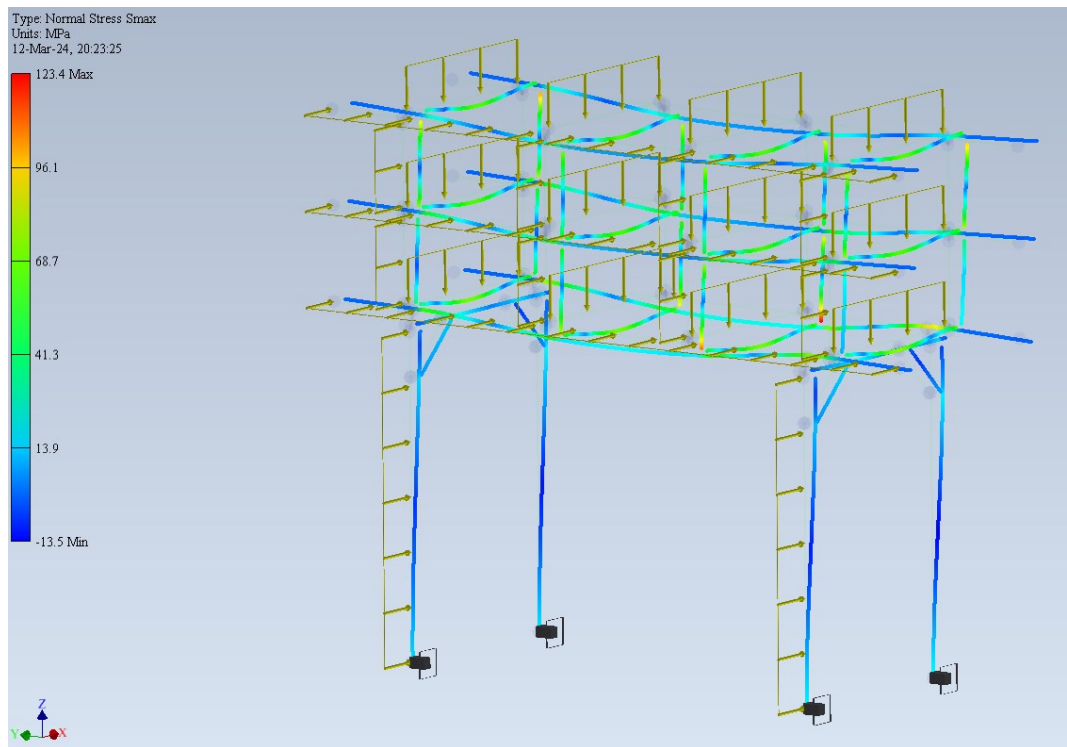


Configuration 1A. Load from piping: 750 kg/m. Mass: 2984 kg. Next two pictures show colour maps of vertical forces and combined normal stresses in dead load scenario respectively.

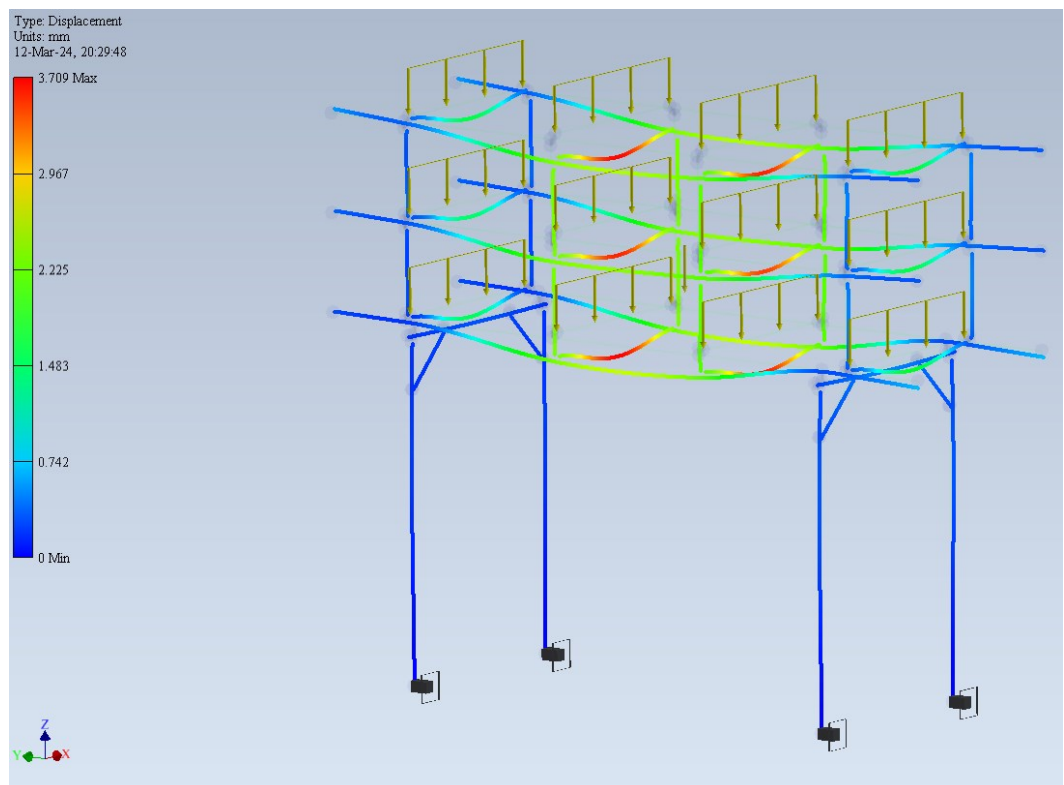


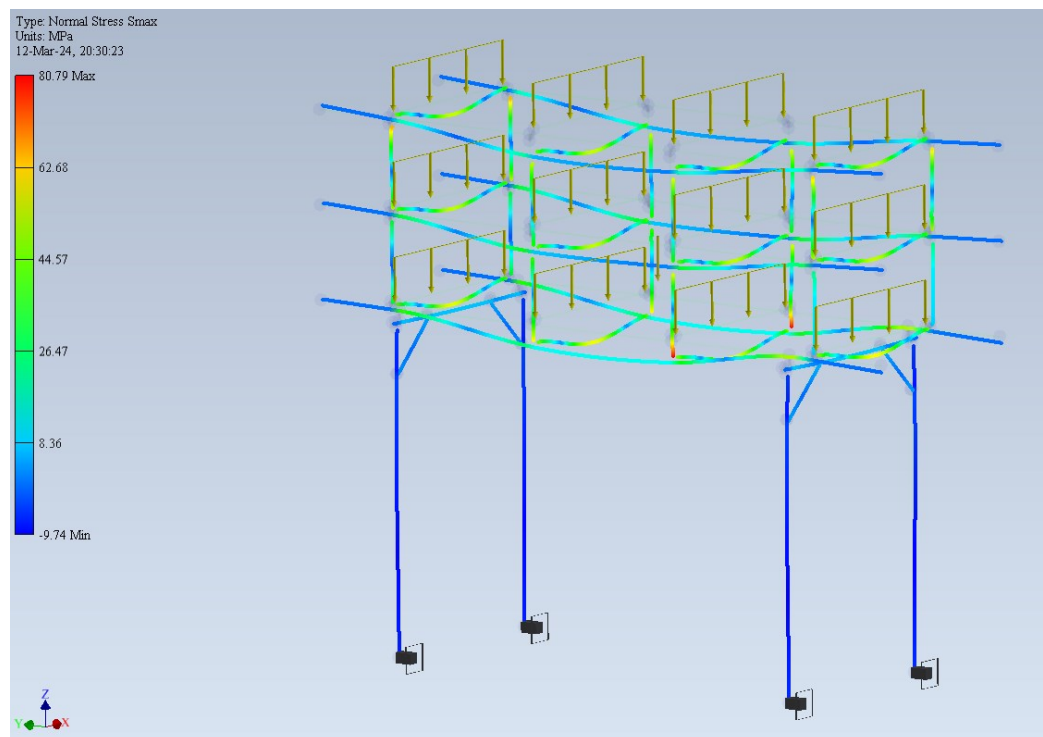
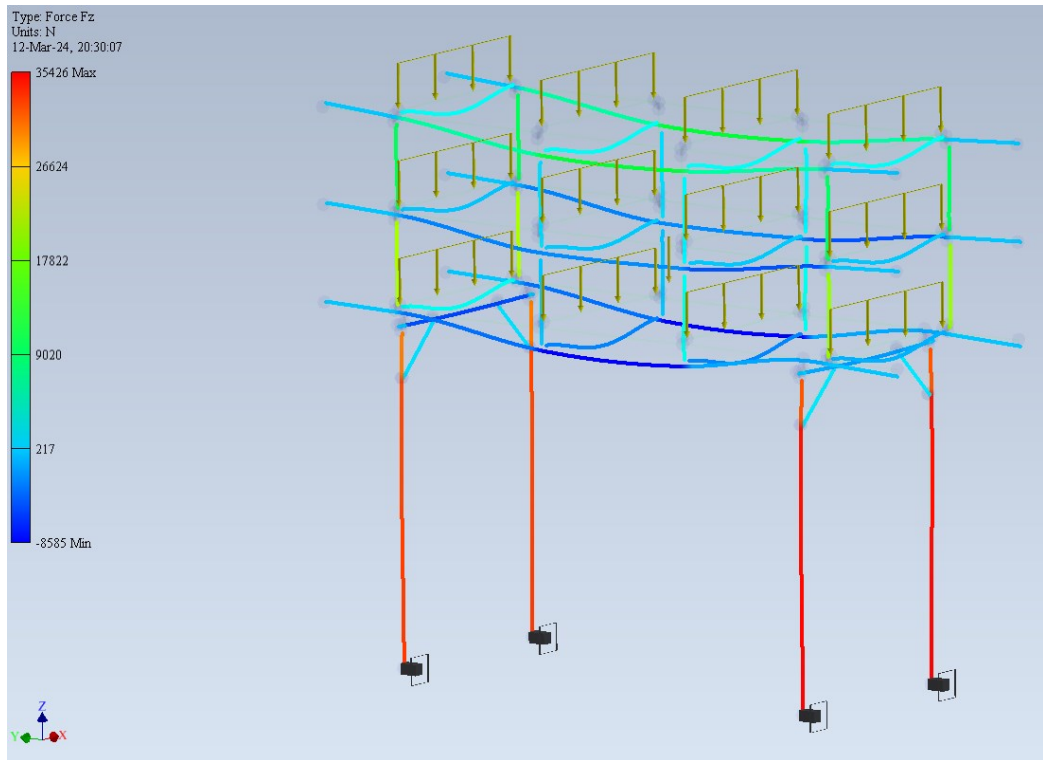
Next three pictures show colour maps of displacements, vertical forces and combined normal stresses in dead load and live load scenario respectively.



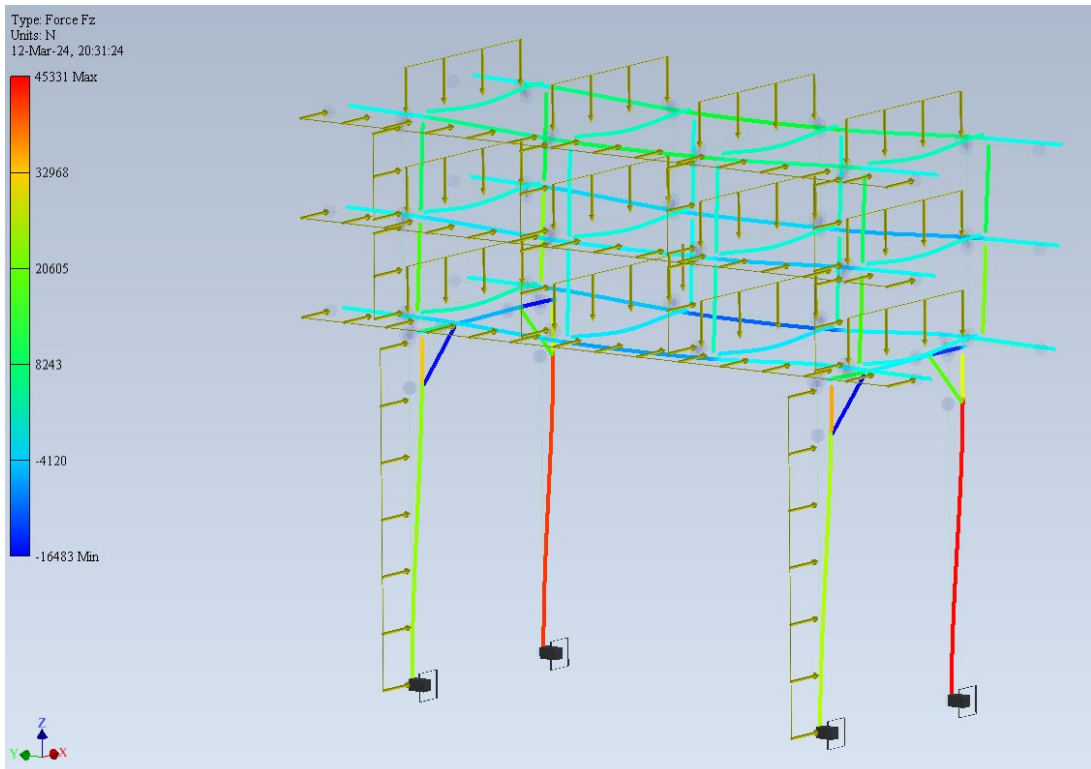
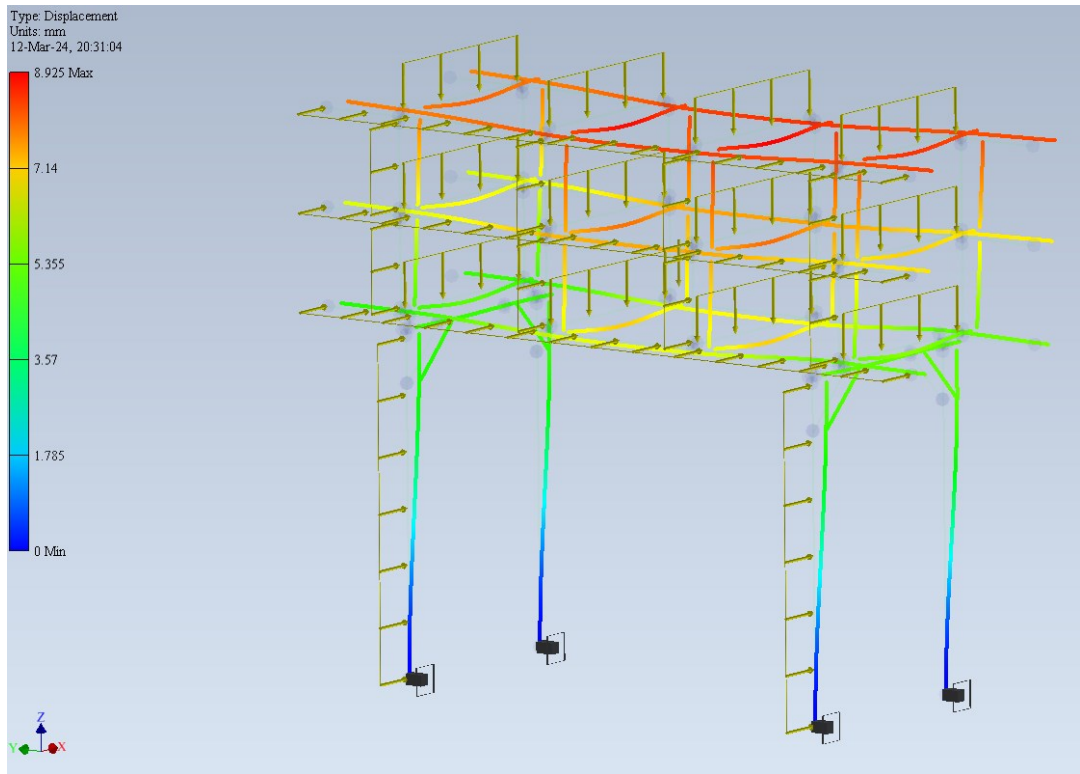


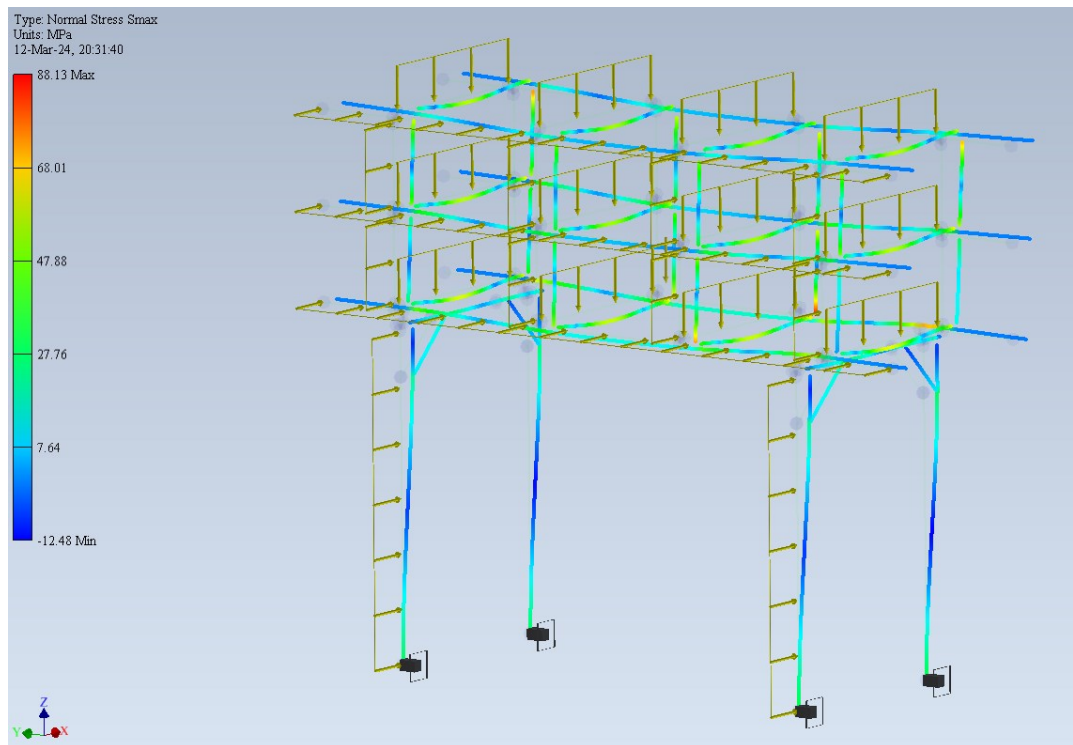
Configuration 2A. Load from piping: 500 kg/m. Mass: 2691 kg. Next three pictures show colour maps of displacements, vertical forces and combined normal stresses in dead load scenario respectively.



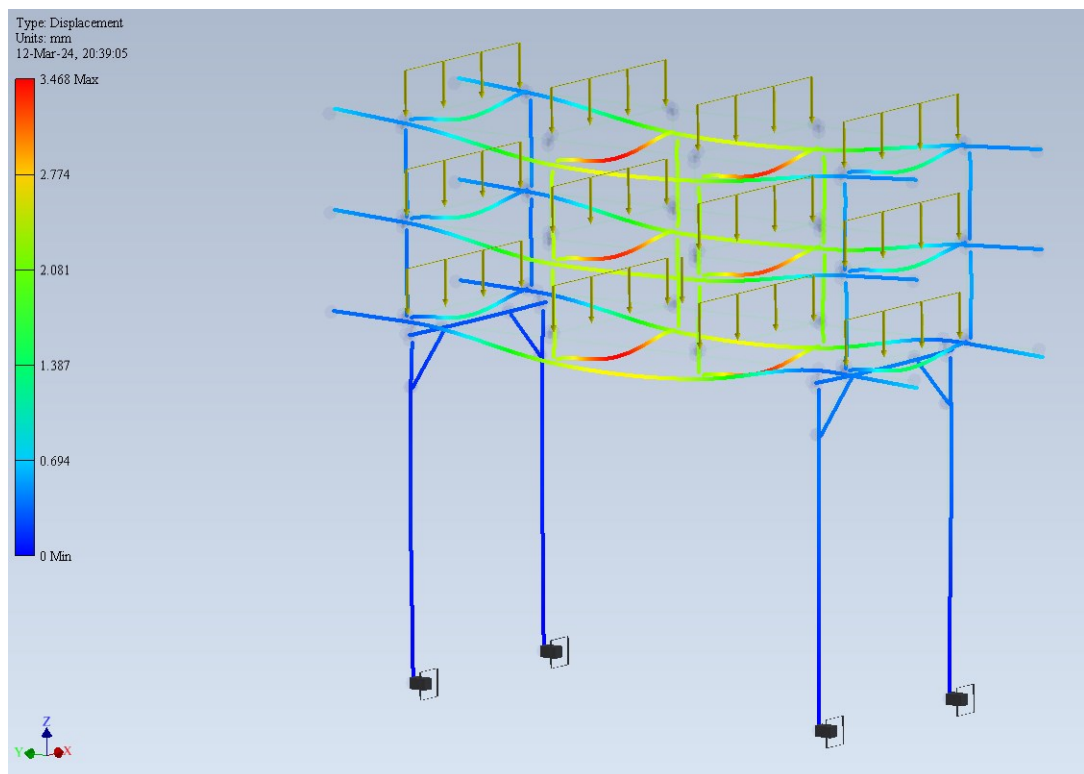


Next three pictures show colour maps of displacements, vertical forces and combined normal stresses in dead load and live load scenario respectively.

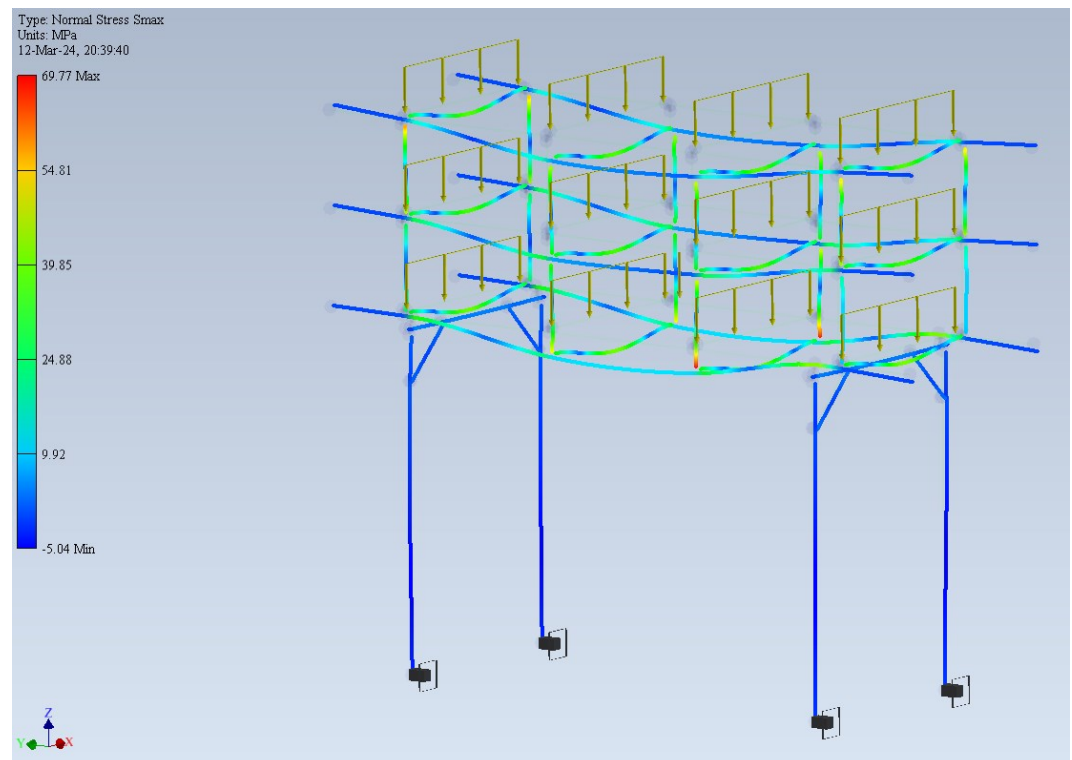
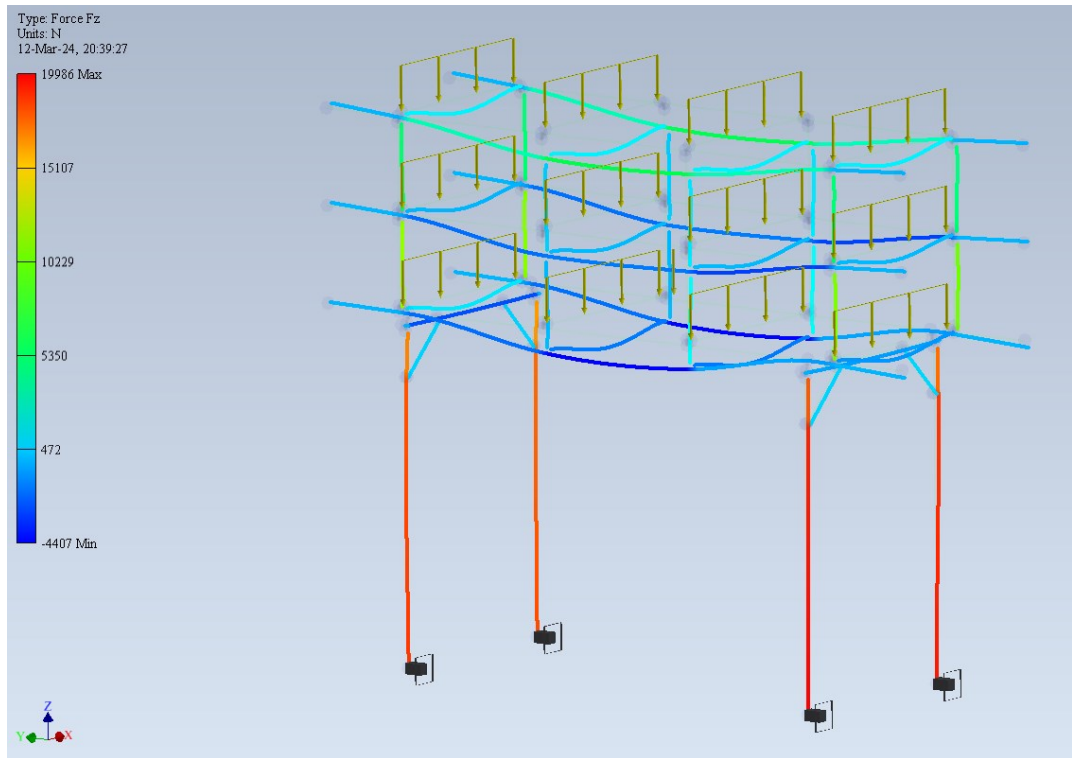




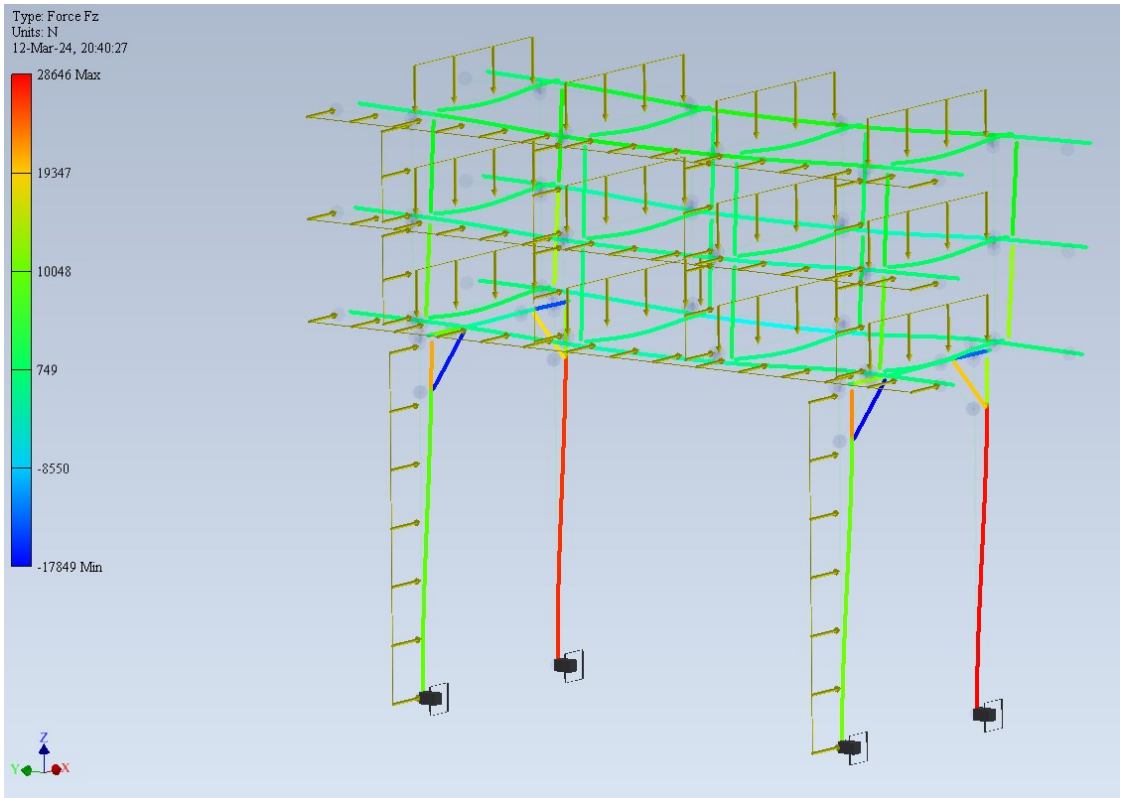
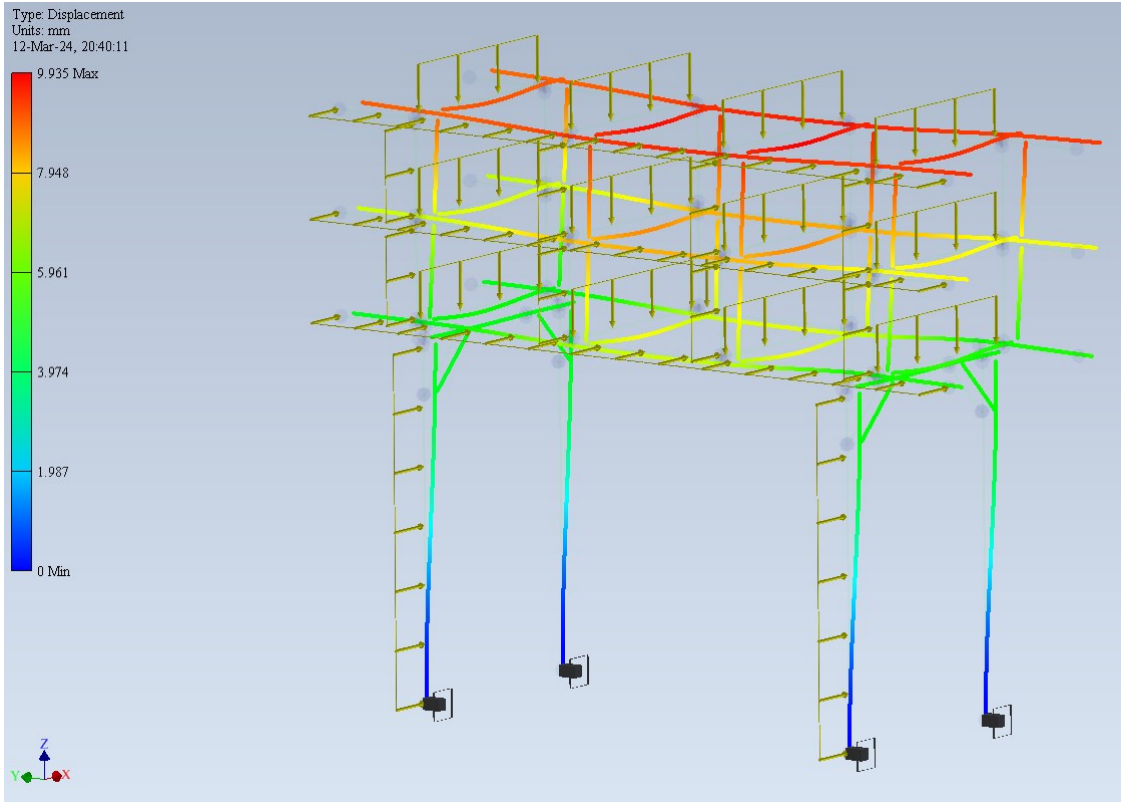
Configuration 3A. Load from piping: 250 kg/m. Mass: 2237 kg. Next three pictures show colour maps of displacements, vertical forces and combined normal stresses in dead load scenario respectively.

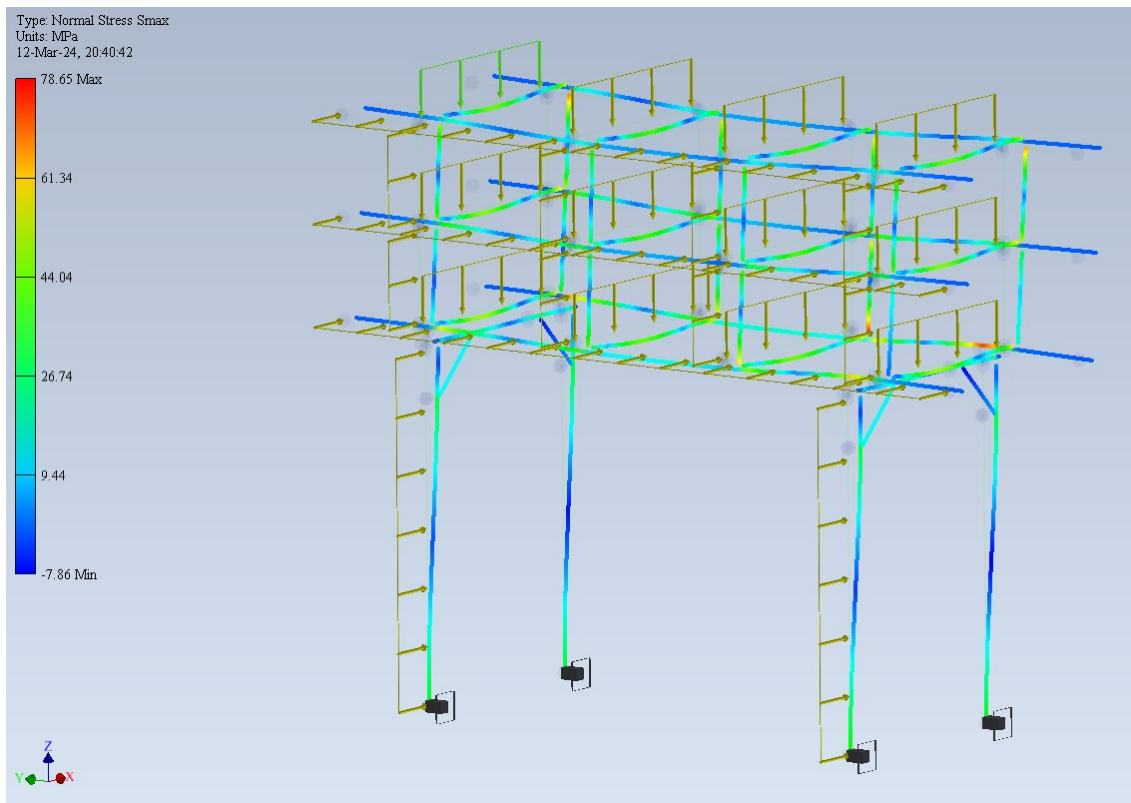




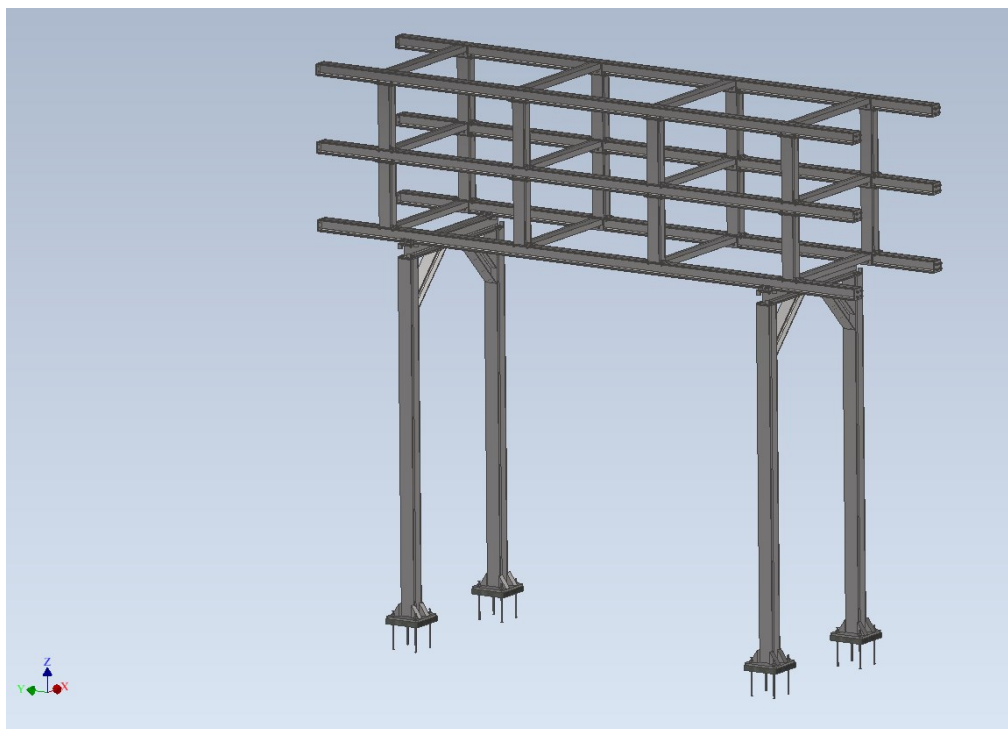


Next three pictures show colour maps of displacements, vertical forces and combined normal stresses in dead load and live load scenario respectively.

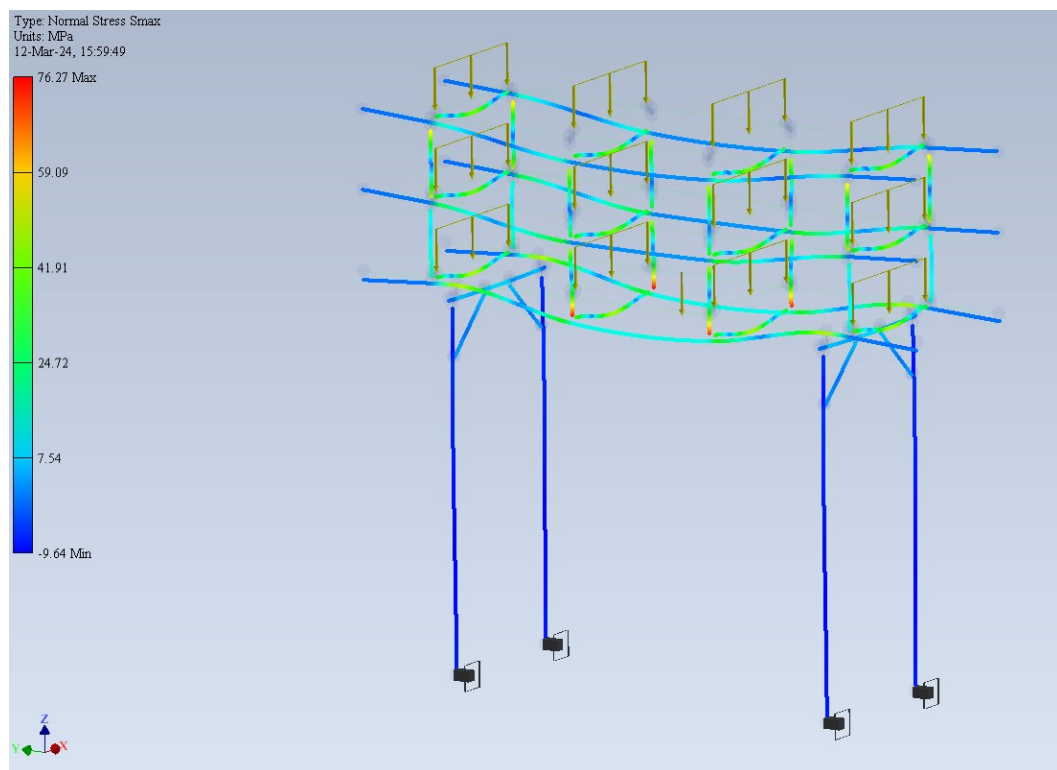
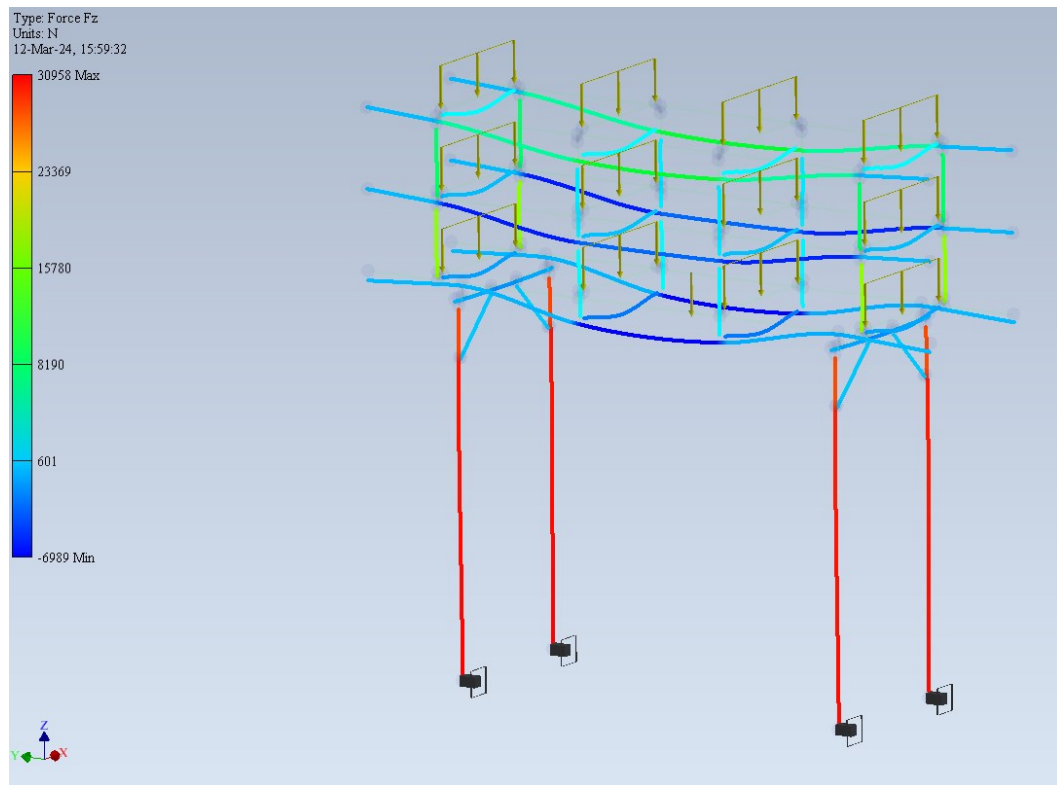




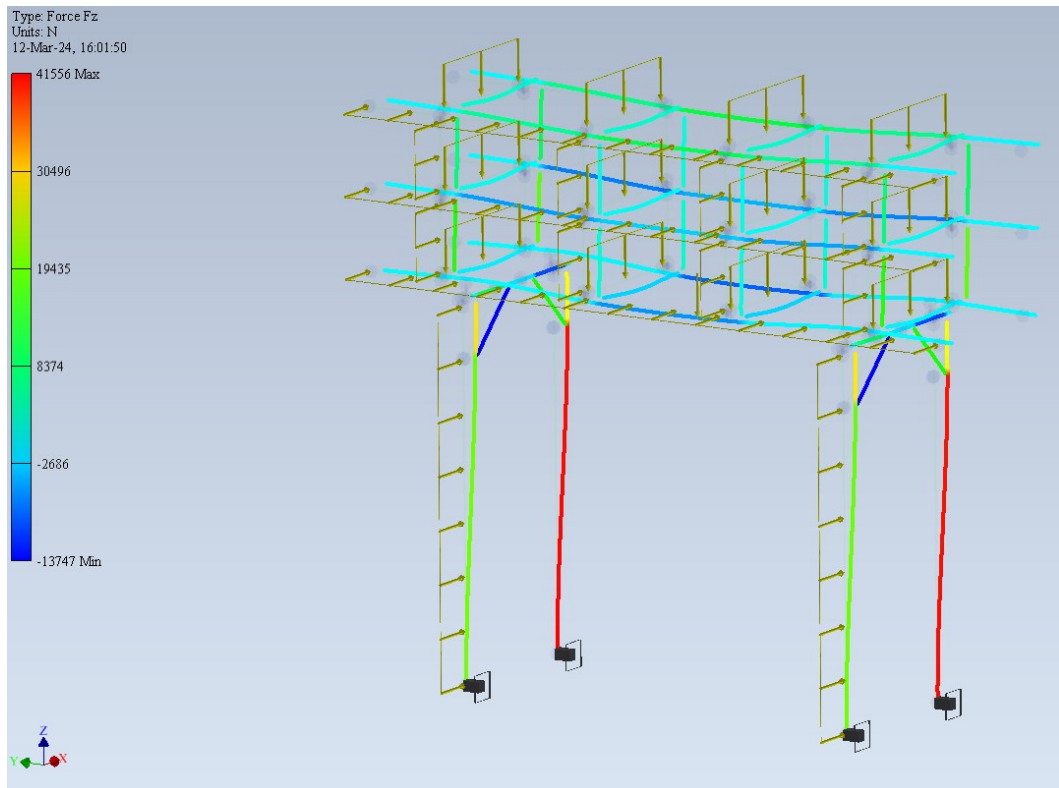
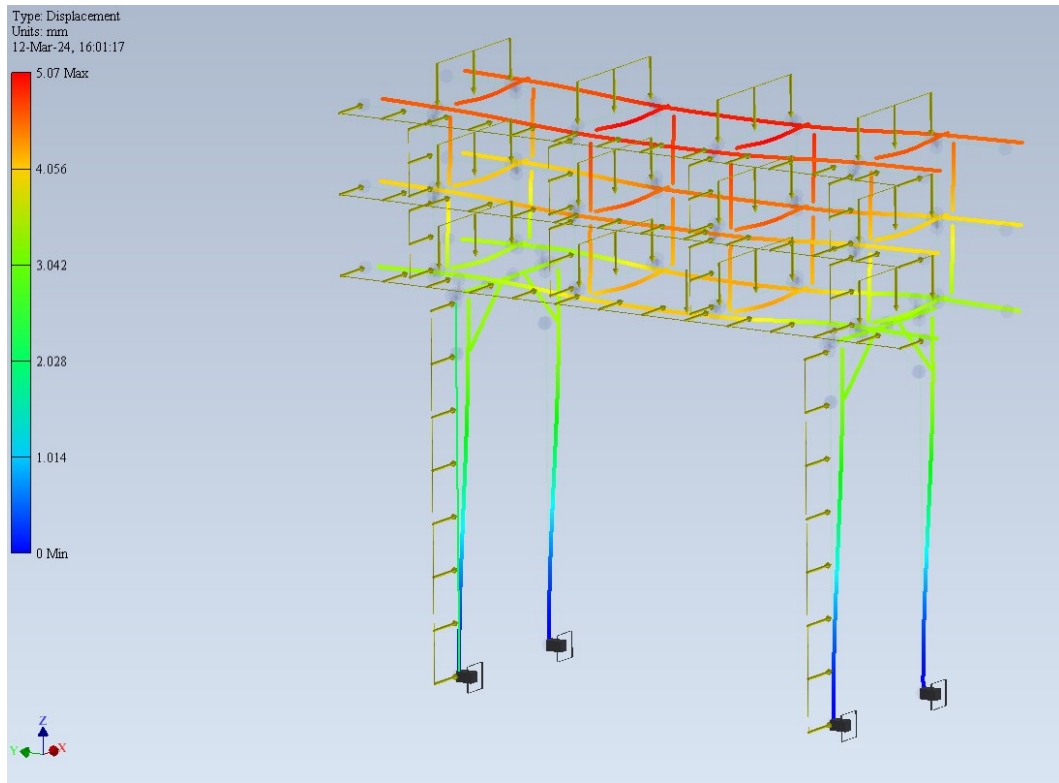
Intermediate design B. It is narrower than A.

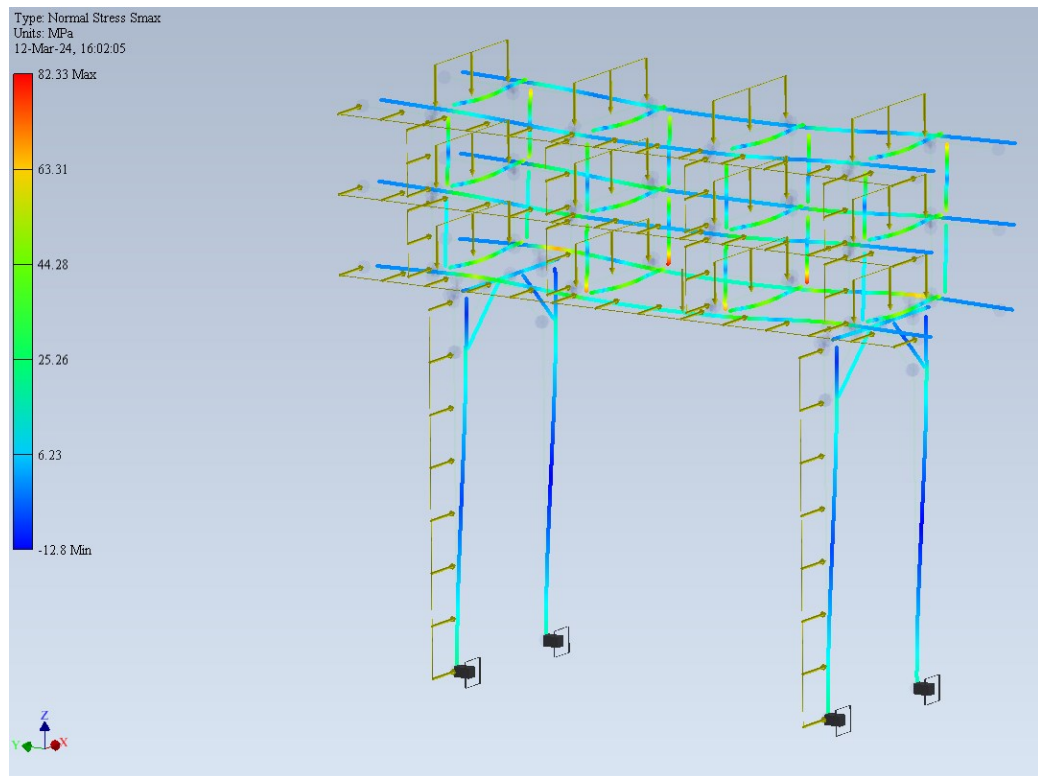


Configuration 1B. Load from piping: 750 kg/m. Mass: 1937 kg. Next two pictures show colour maps of vertical forces and combined normal stresses in dead load scenario respectively.

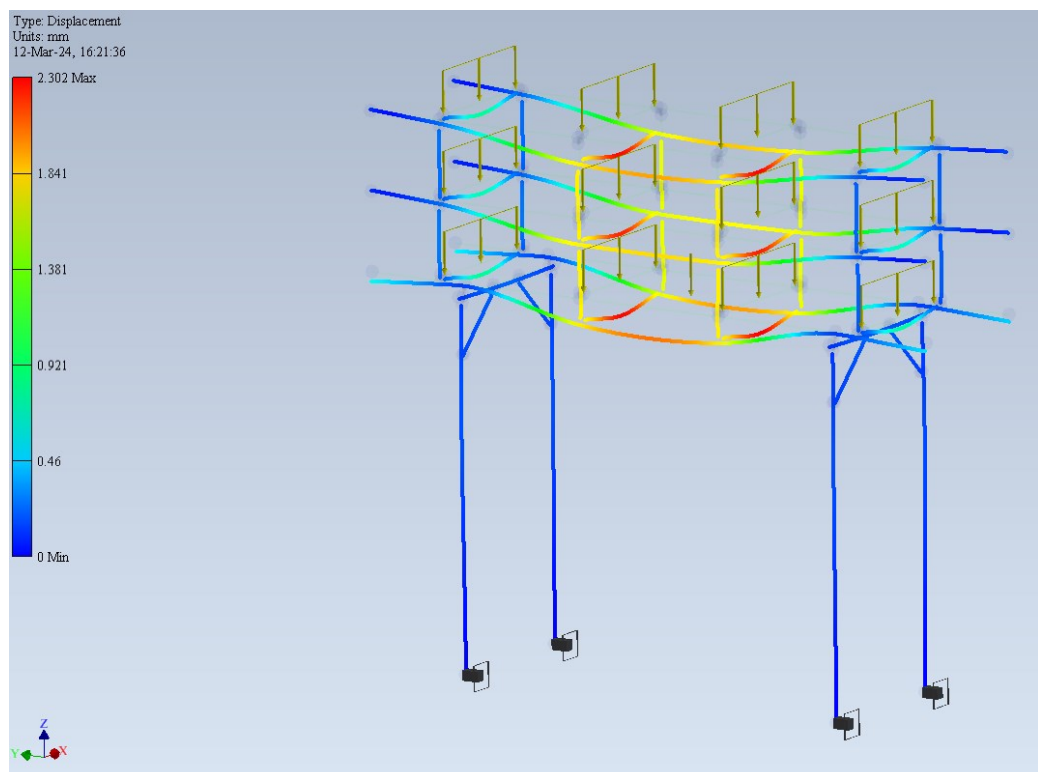


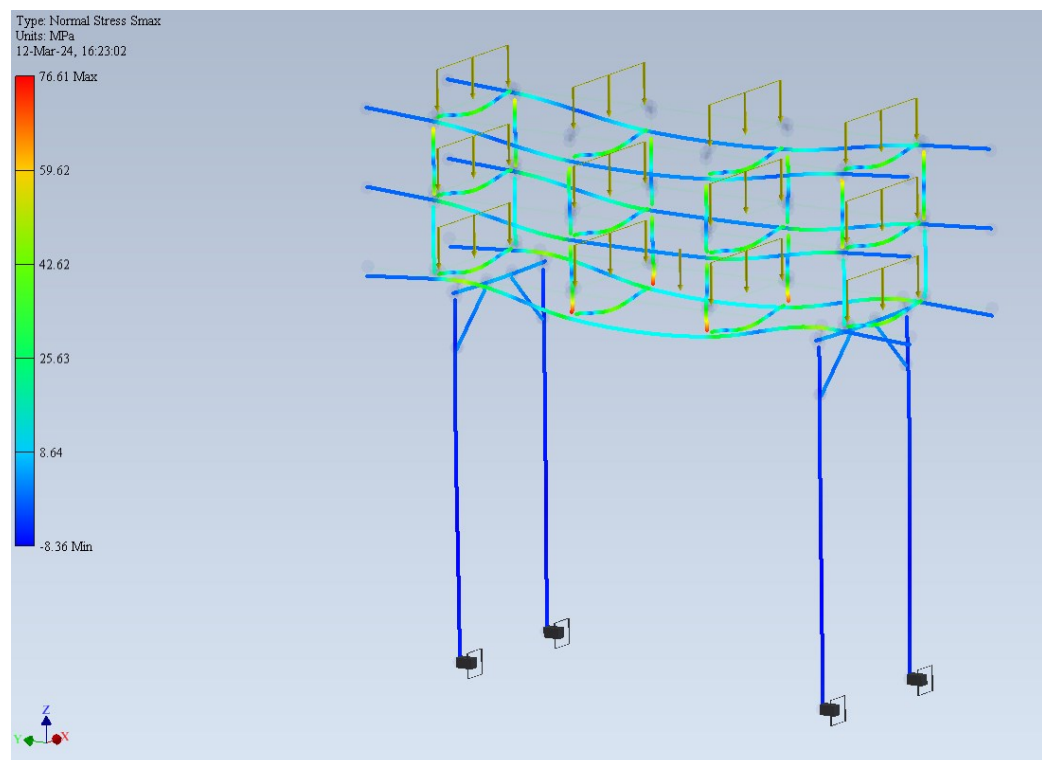
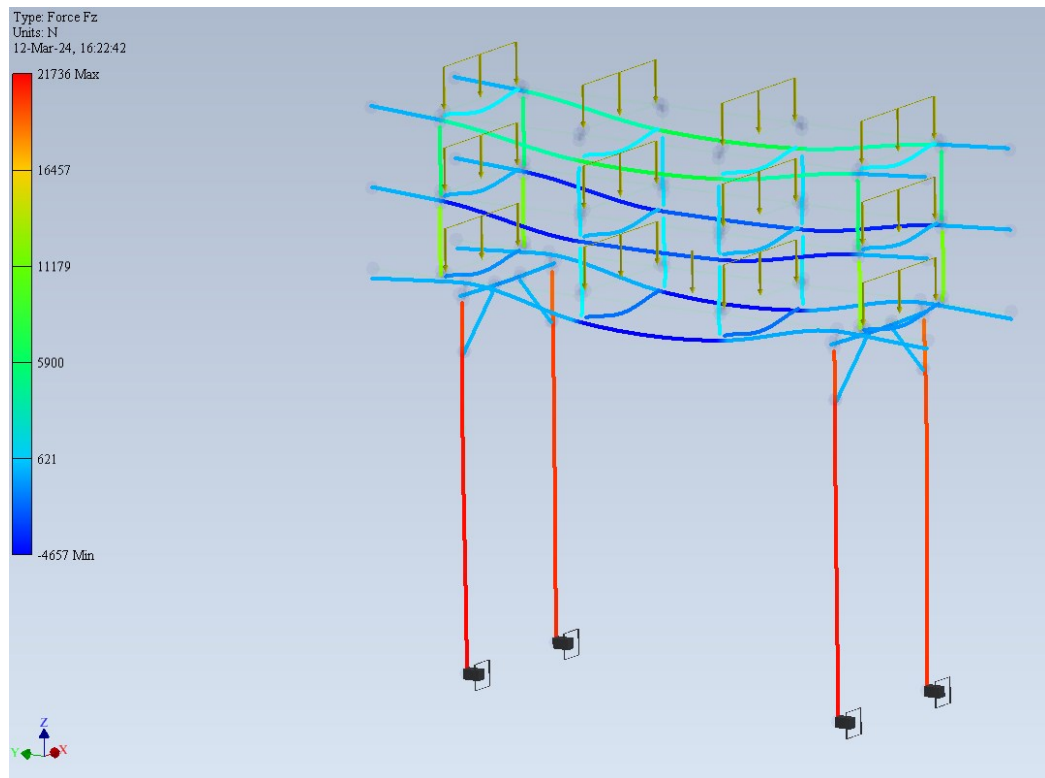
Next three pictures show colour maps of displacements, vertical forces and combined normal stresses in dead load and live load scenario respectively.



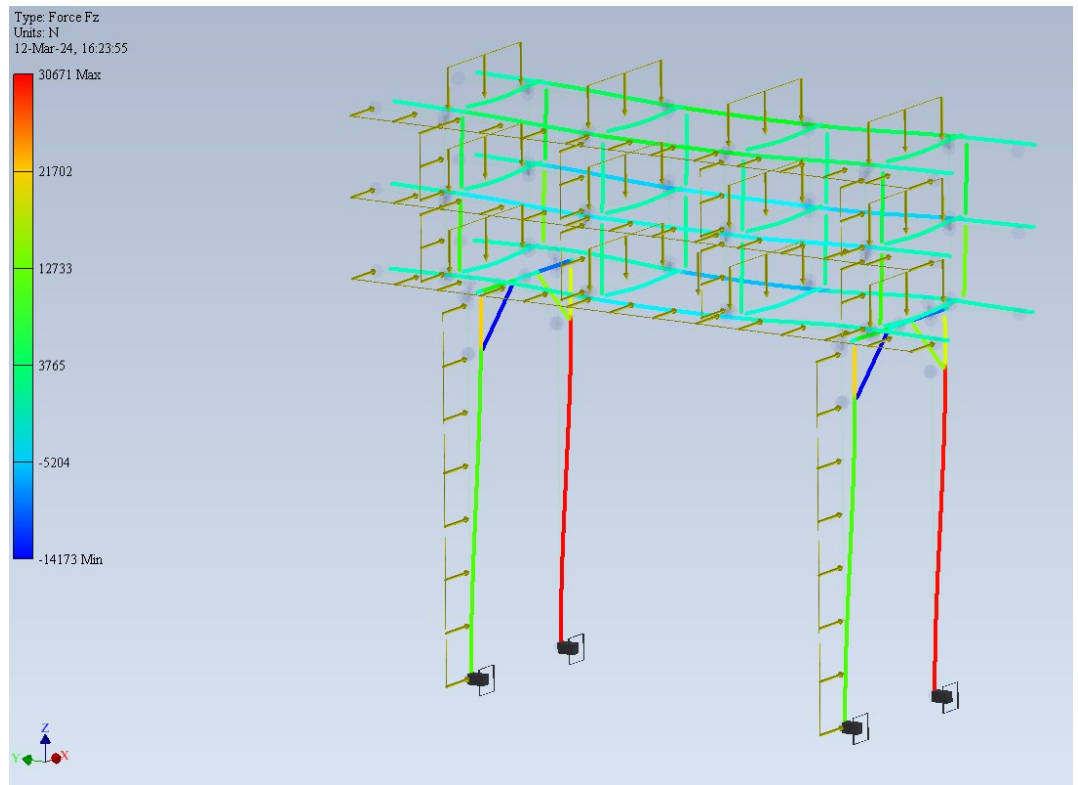
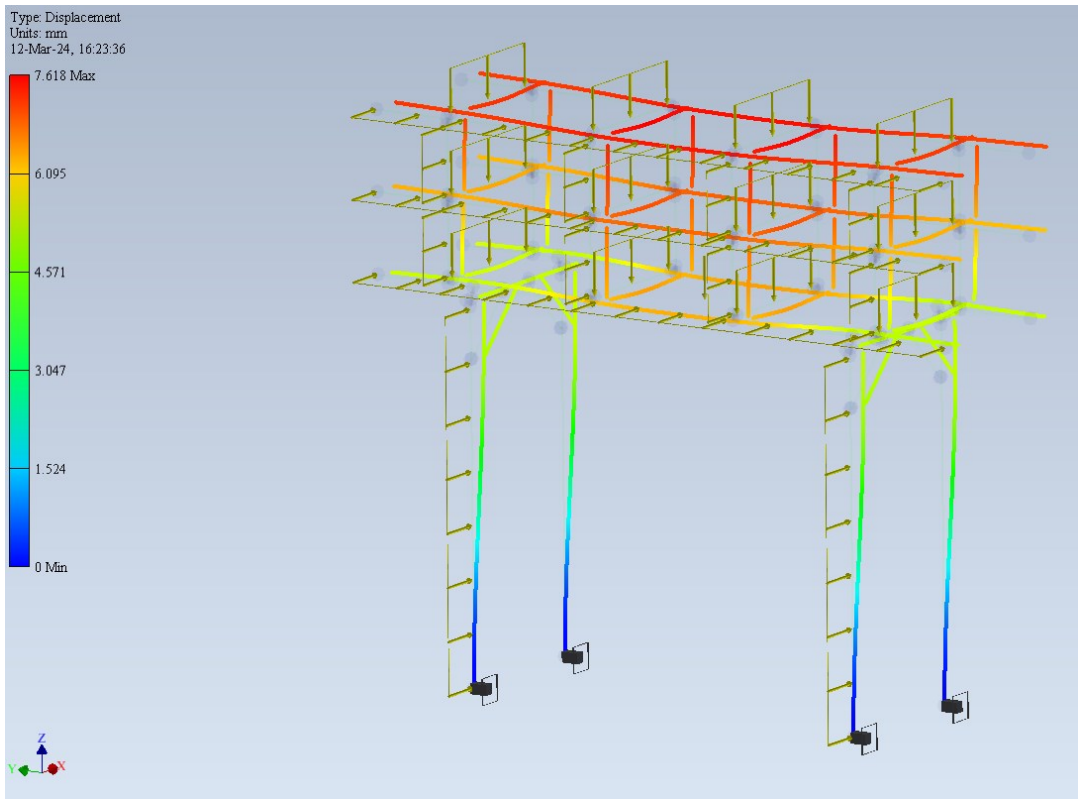


Configuration 2B. Load from piping: 500 kg/m. Mass: 1528 kg. Next three pictures show colour maps of displacements, vertical forces and combined normal stresses in dead load scenario respectively.

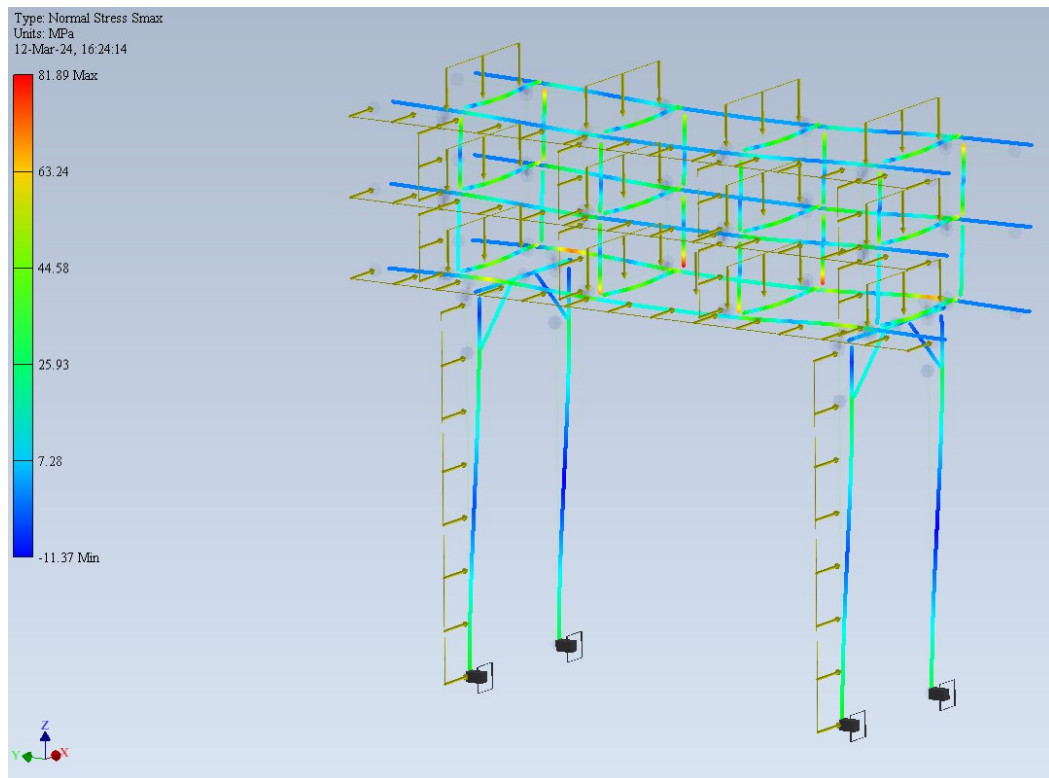




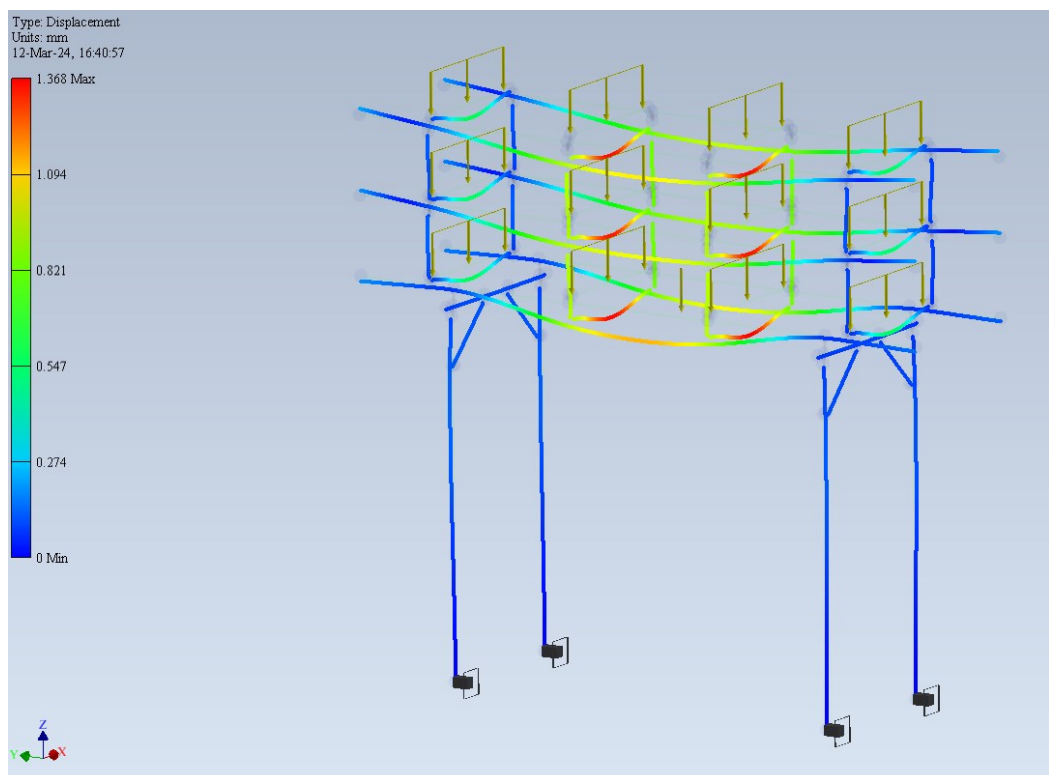
Next three pictures show colour maps of displacements, vertical forces and combined normal stresses in dead load and live load scenario respectively.

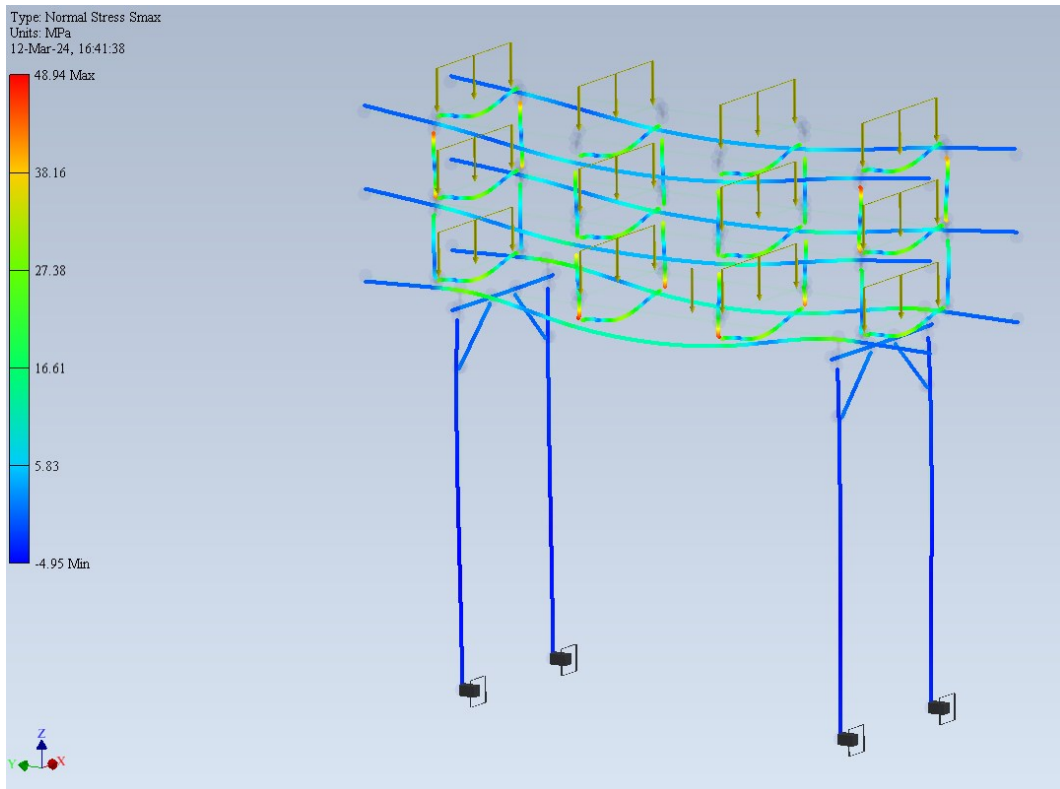
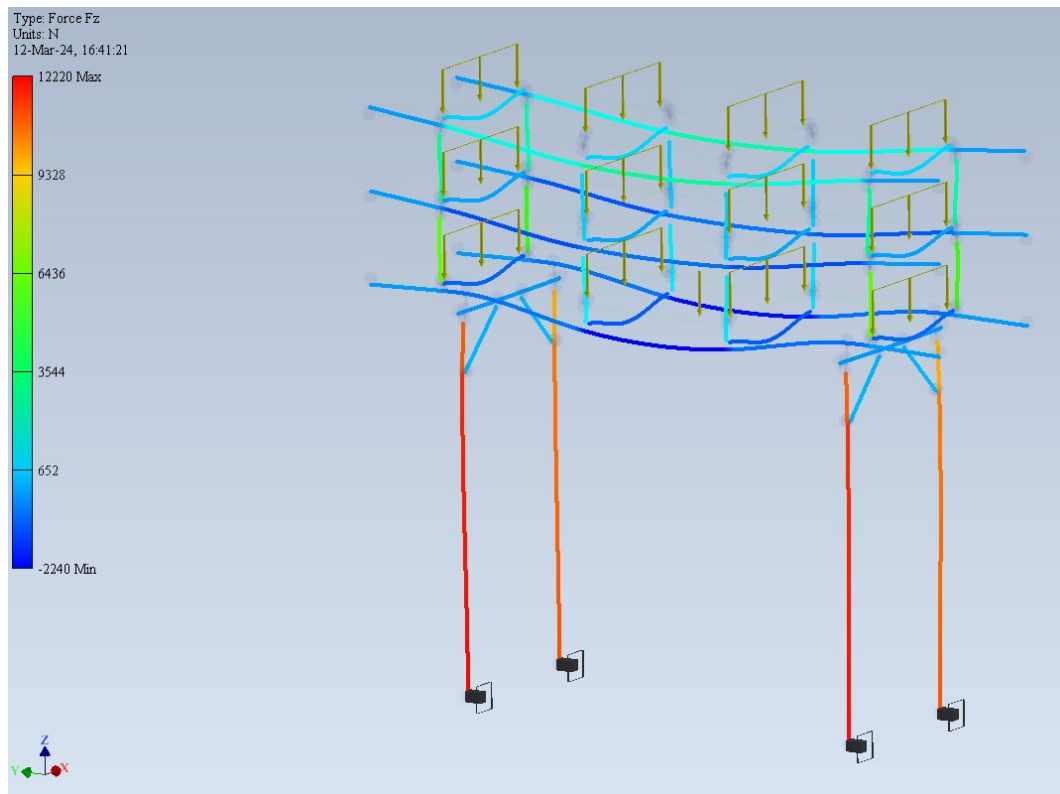




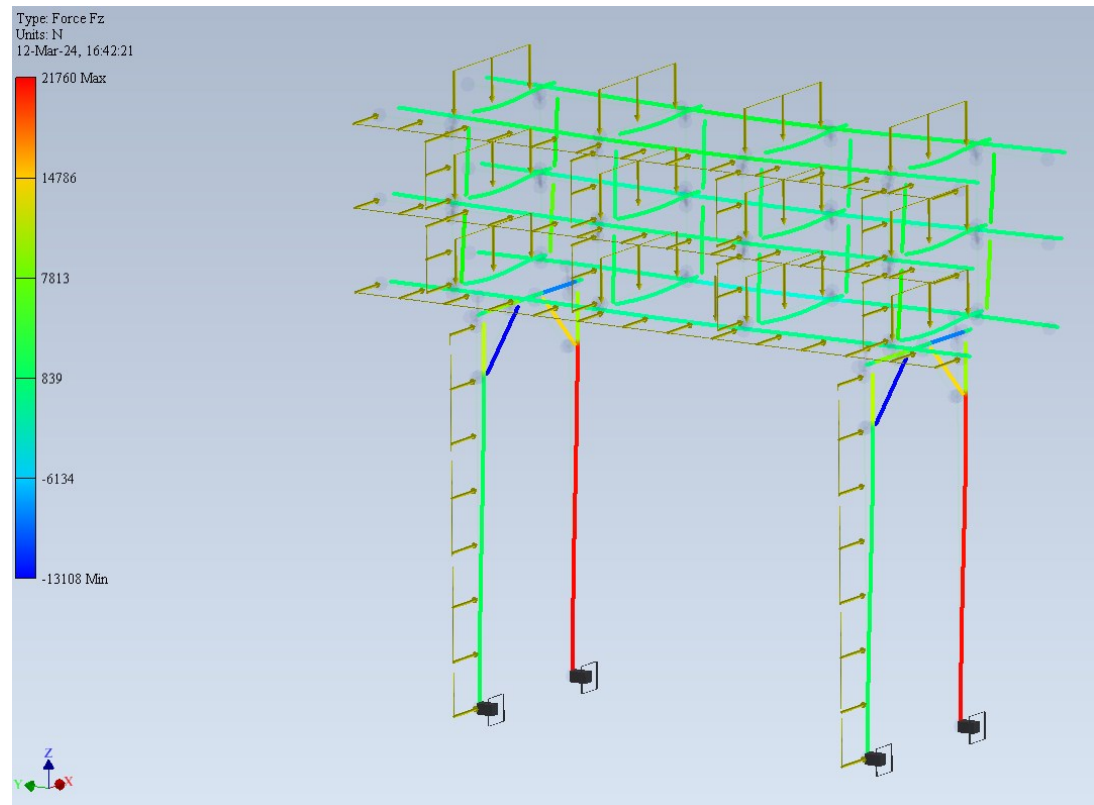
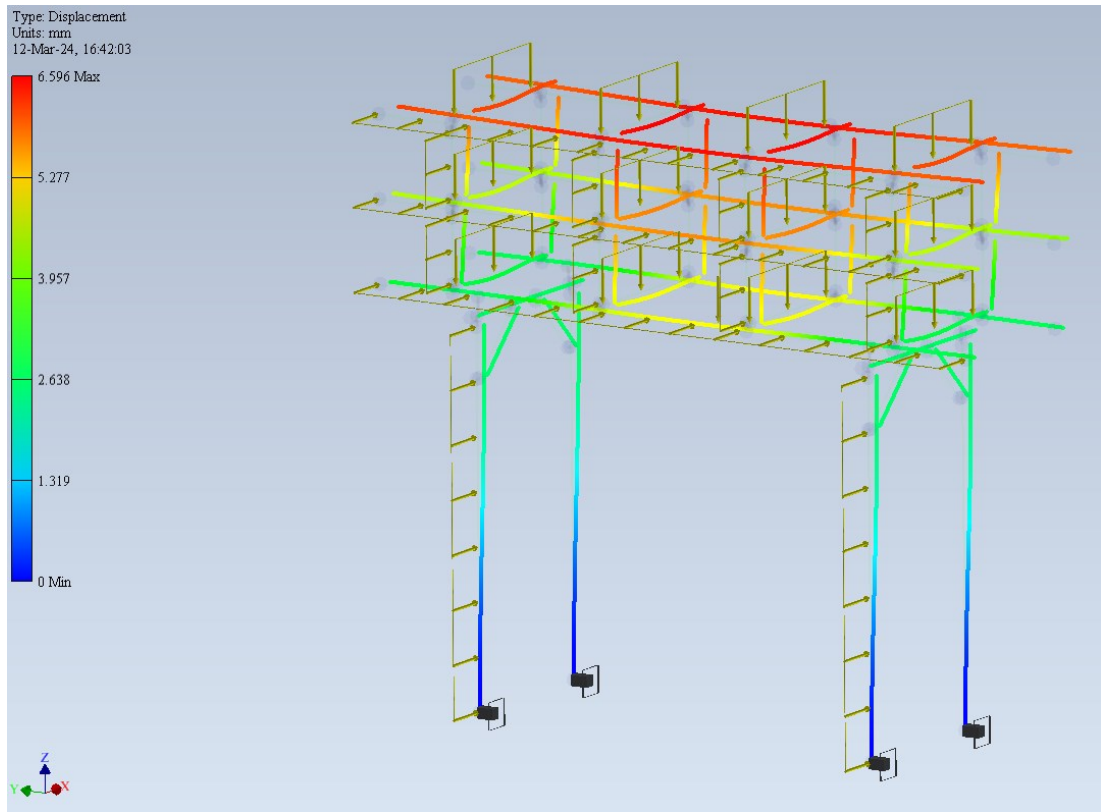


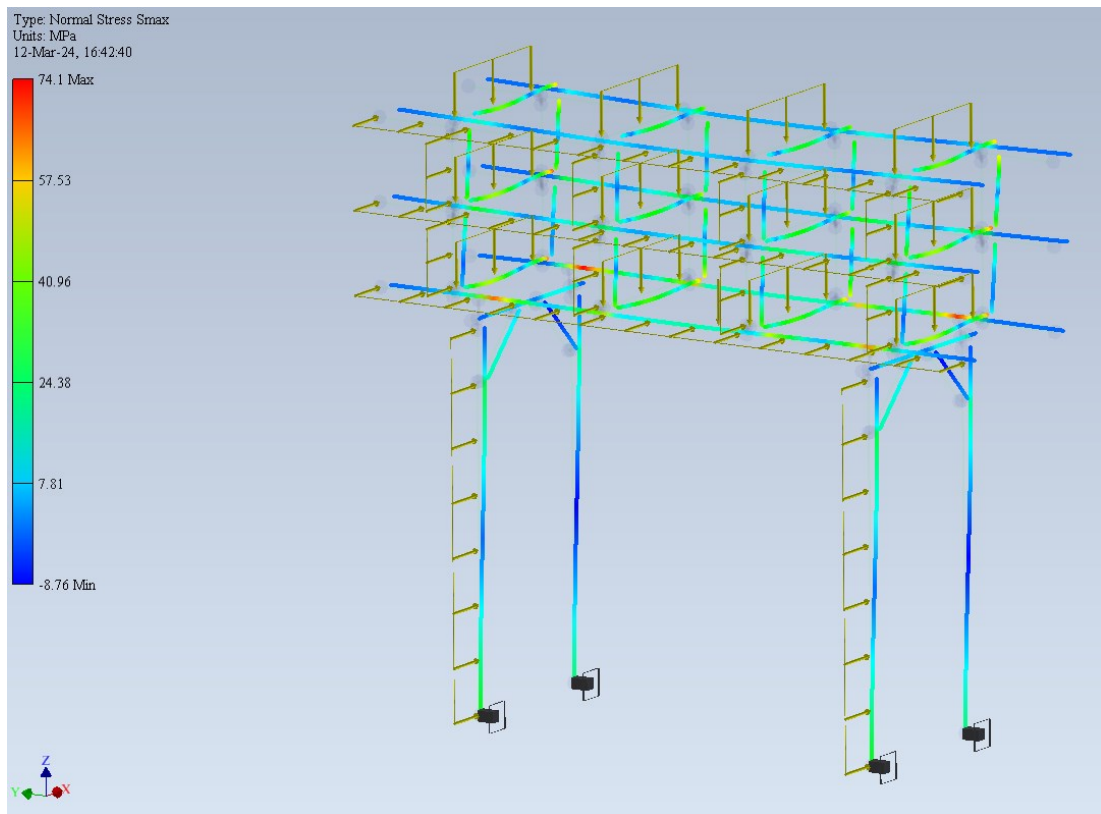
Configuration 3B. Load from piping: 250 kg/m. Mass: 1282 kg. Next three pictures show colour maps of displacements, vertical forces and combined normal stresses in dead load scenario respectively.



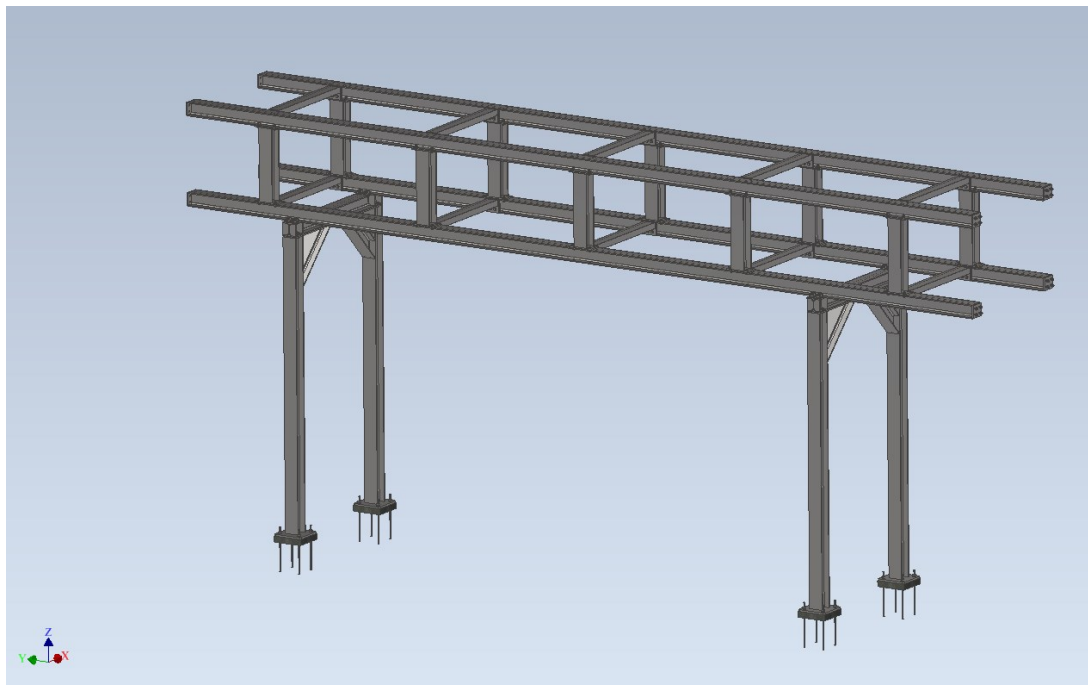


Next three pictures show colour maps of displacements, vertical forces and combined normal stresses in dead load and live load scenario respectively.

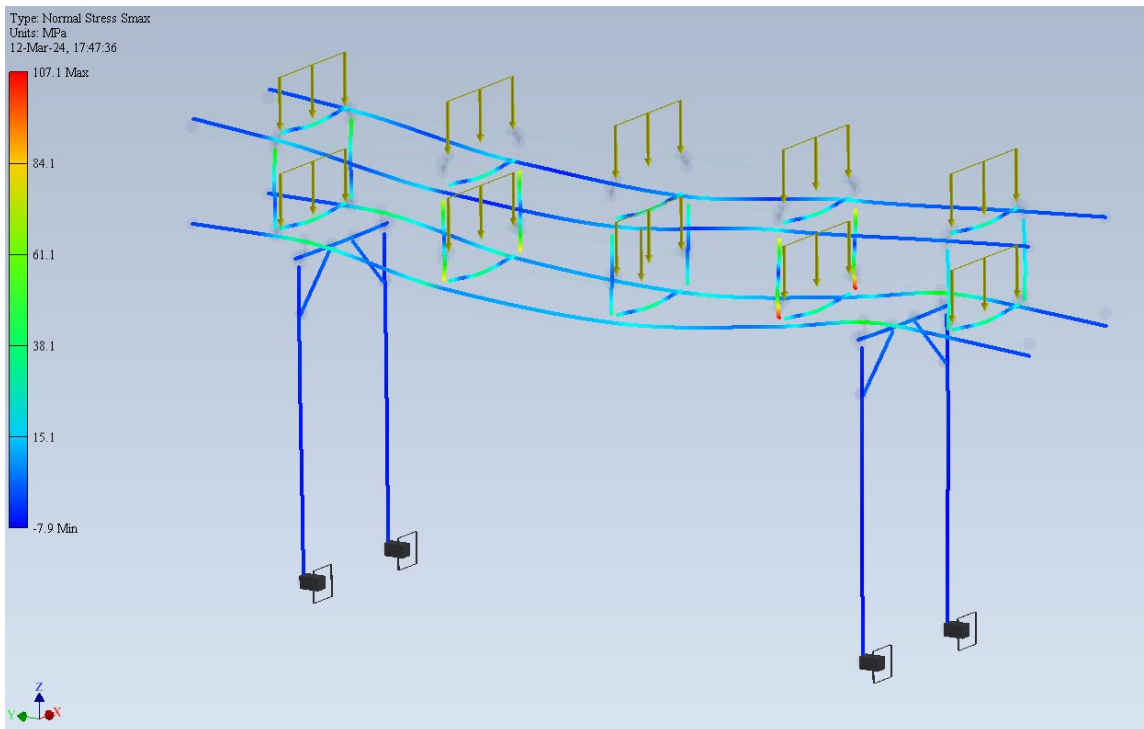
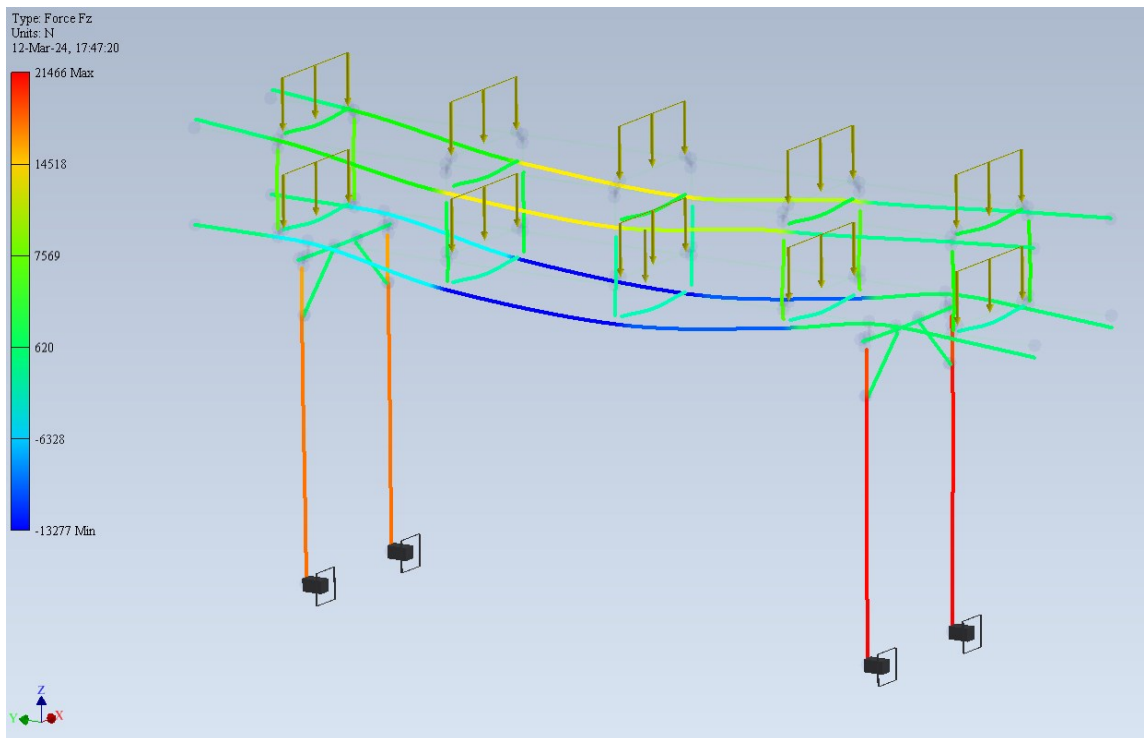




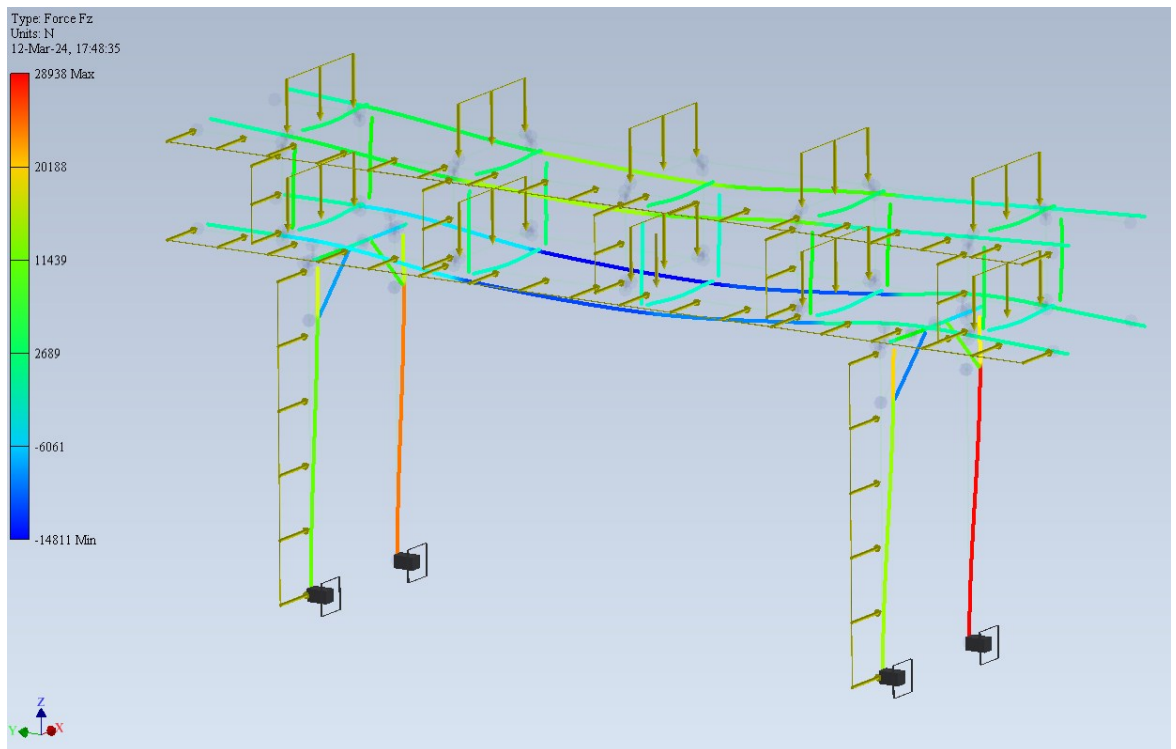
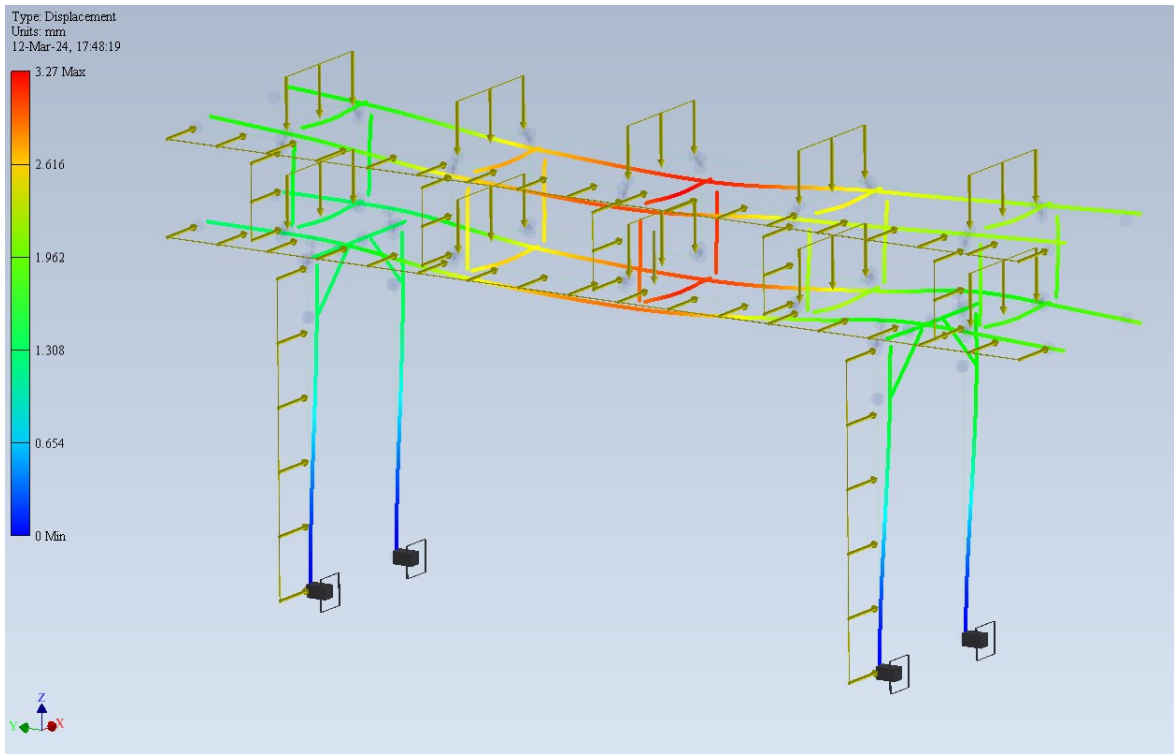
Smaller and lighter version C with two layers for piping and shorter base subassembly.

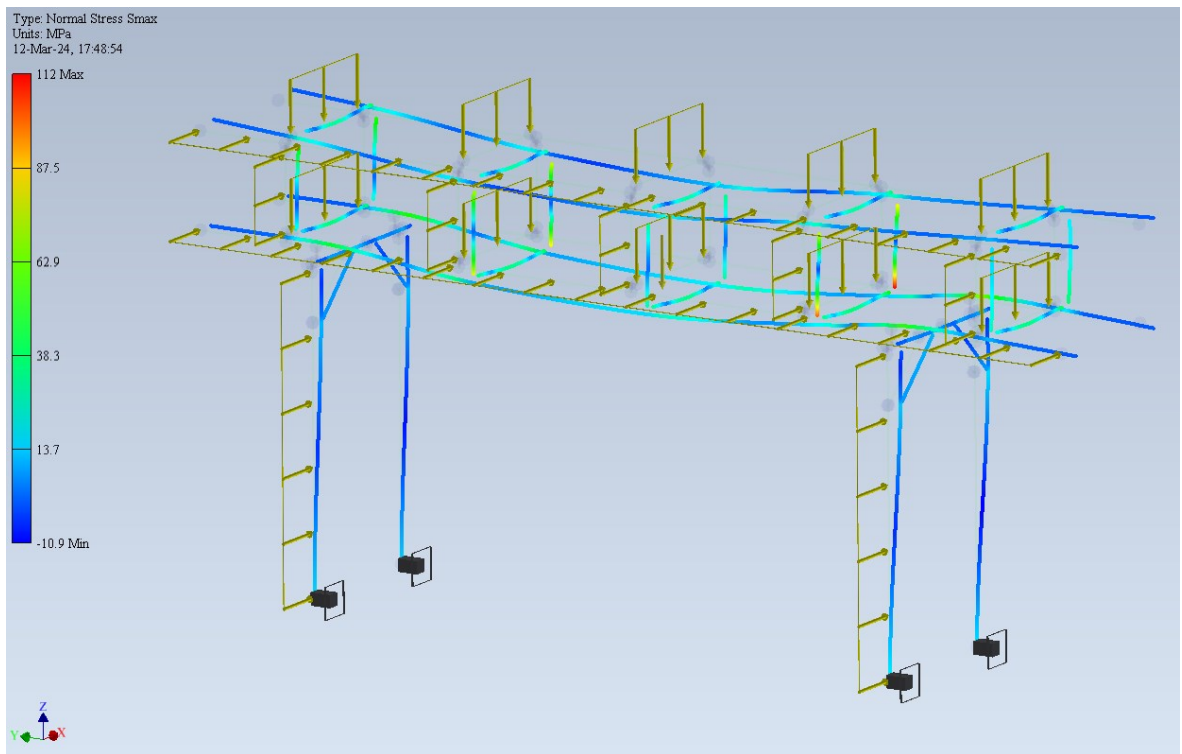


Configuration 1C. Load from piping: 750 kg/m. Mass: 1294 kg. Next two pictures show colour maps of displacements, vertical forces and combined normal stresses in dead load scenario respectively.

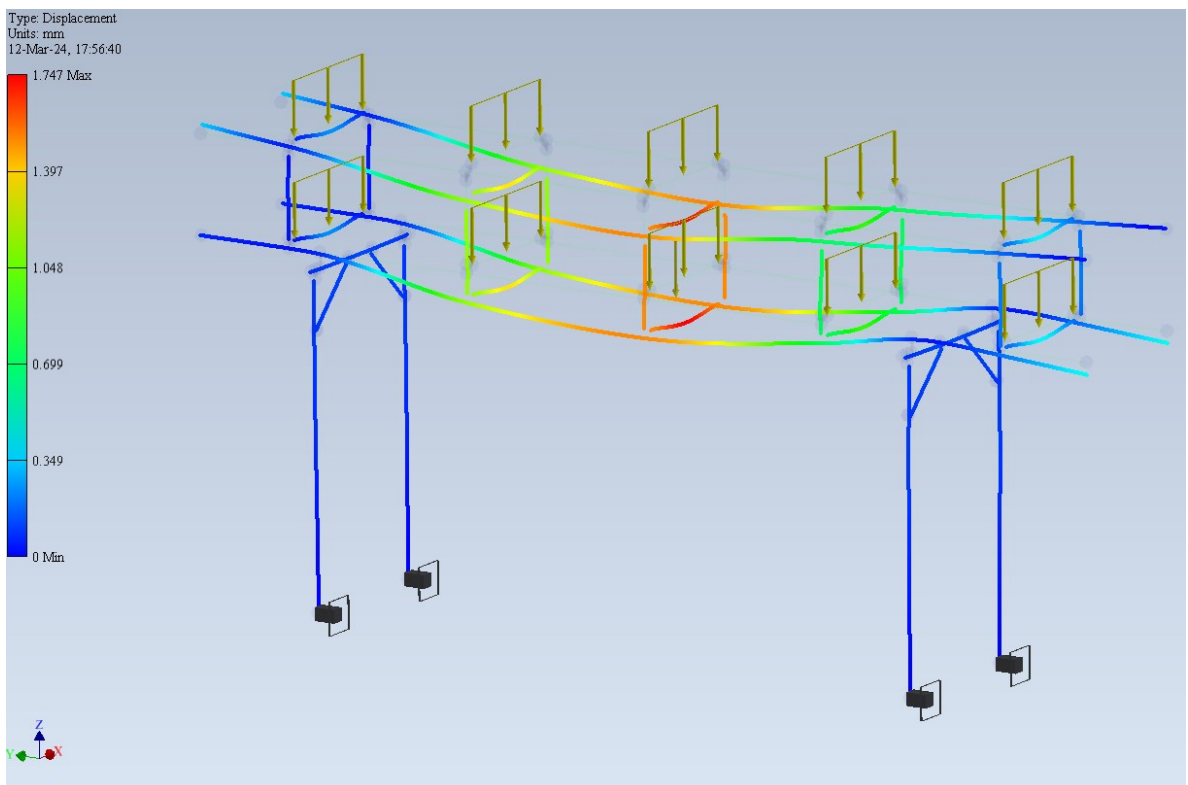


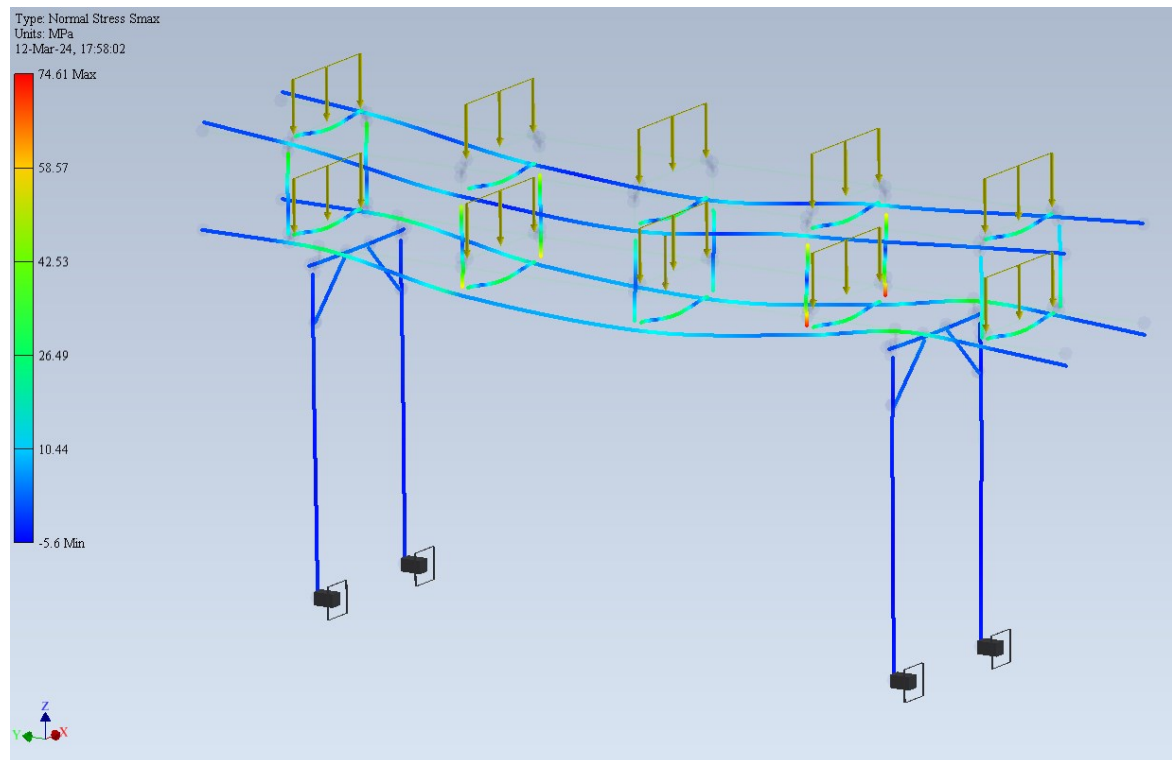
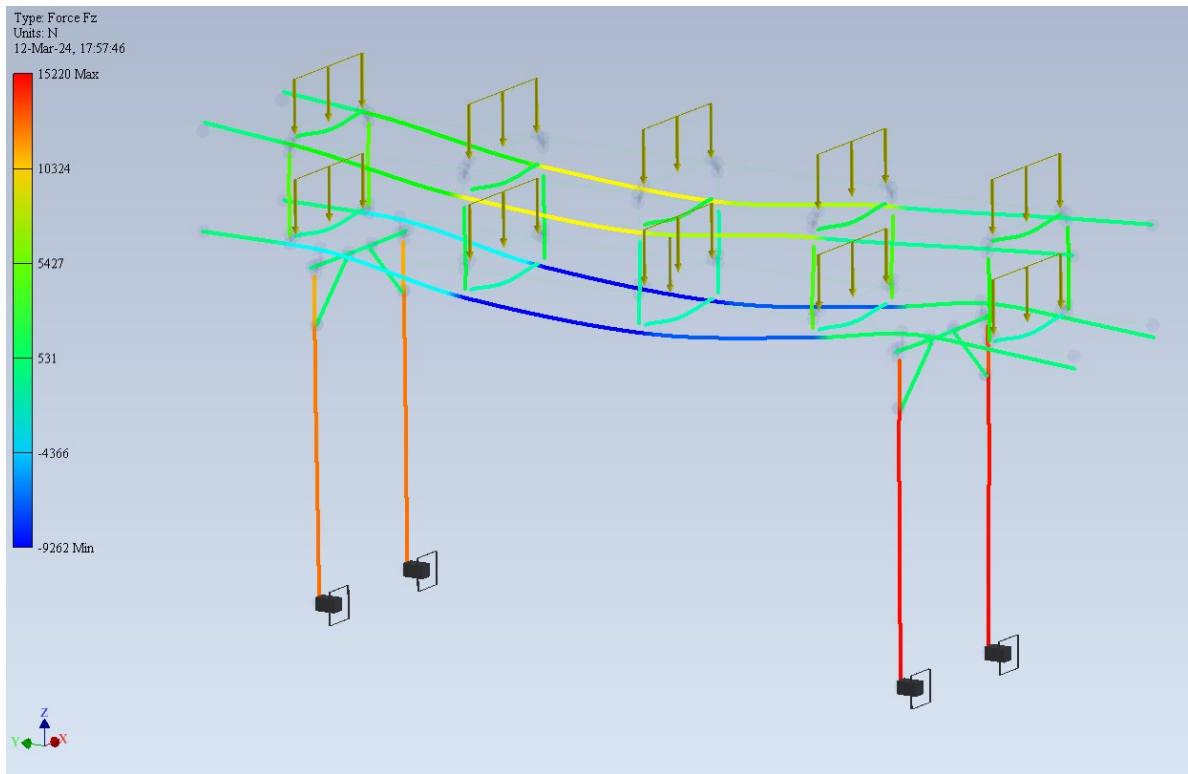
Next three pictures show colour maps of displacements, vertical forces and combined normal stresses in dead load and live load scenario respectively.





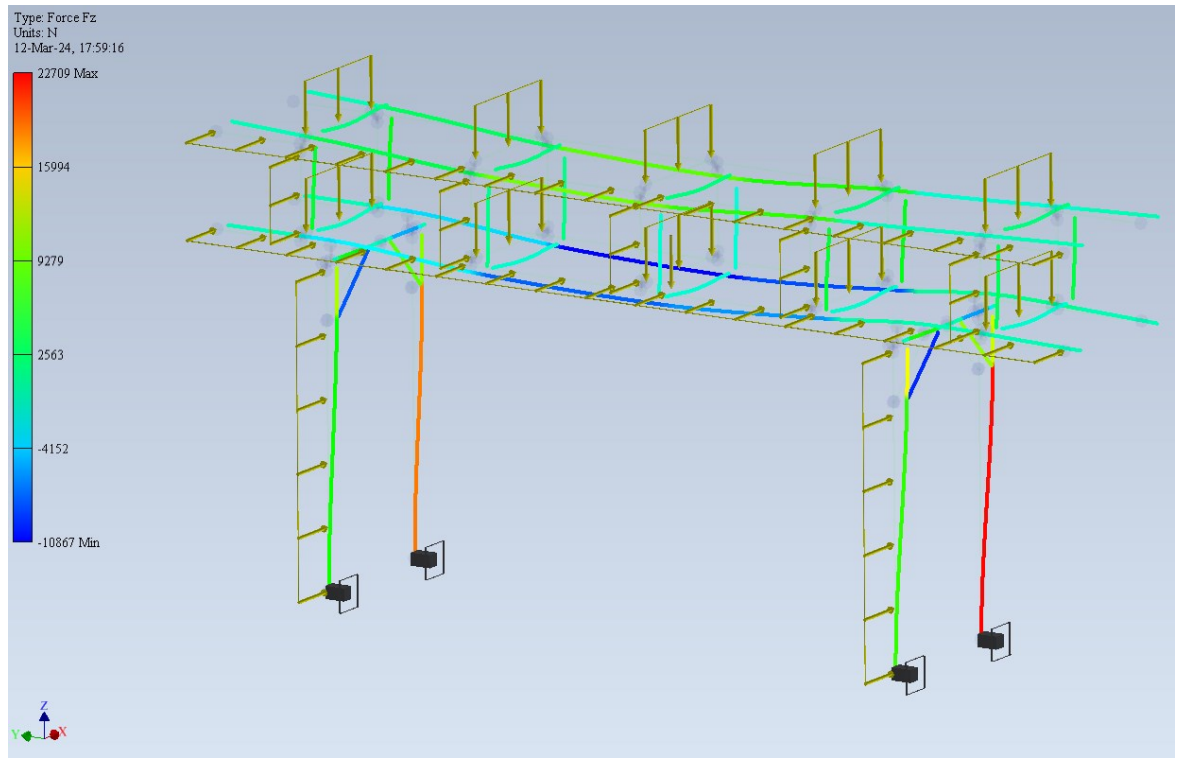
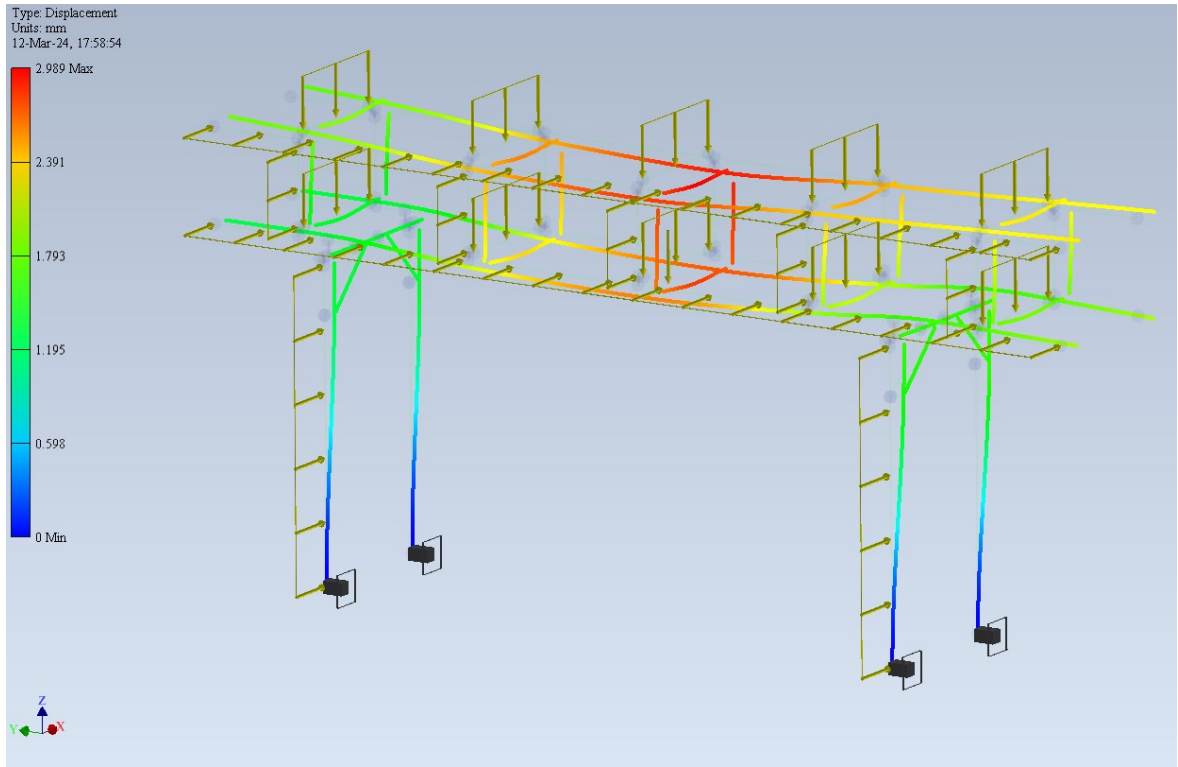
Configuration 2C. Piping load: 500 kg/m. Mass: 1269 kg. Next three pictures show colour maps of displacements, vertical forces and combined normal stresses in dead load scenario respectively.

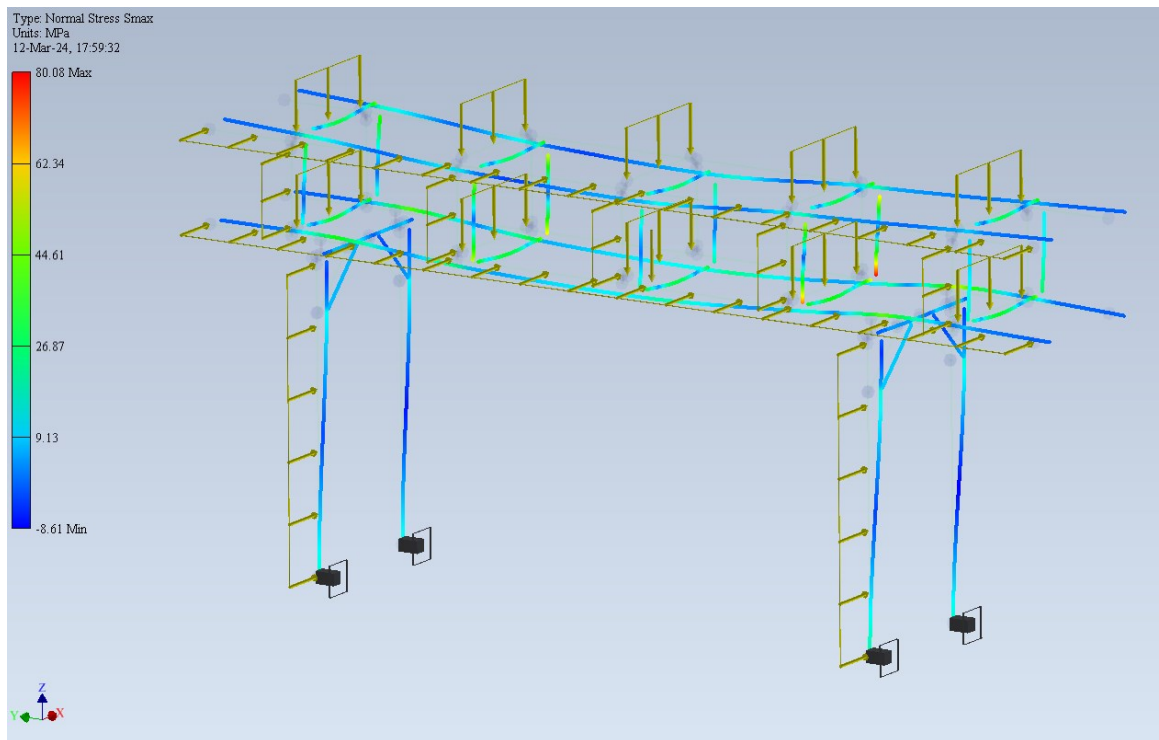




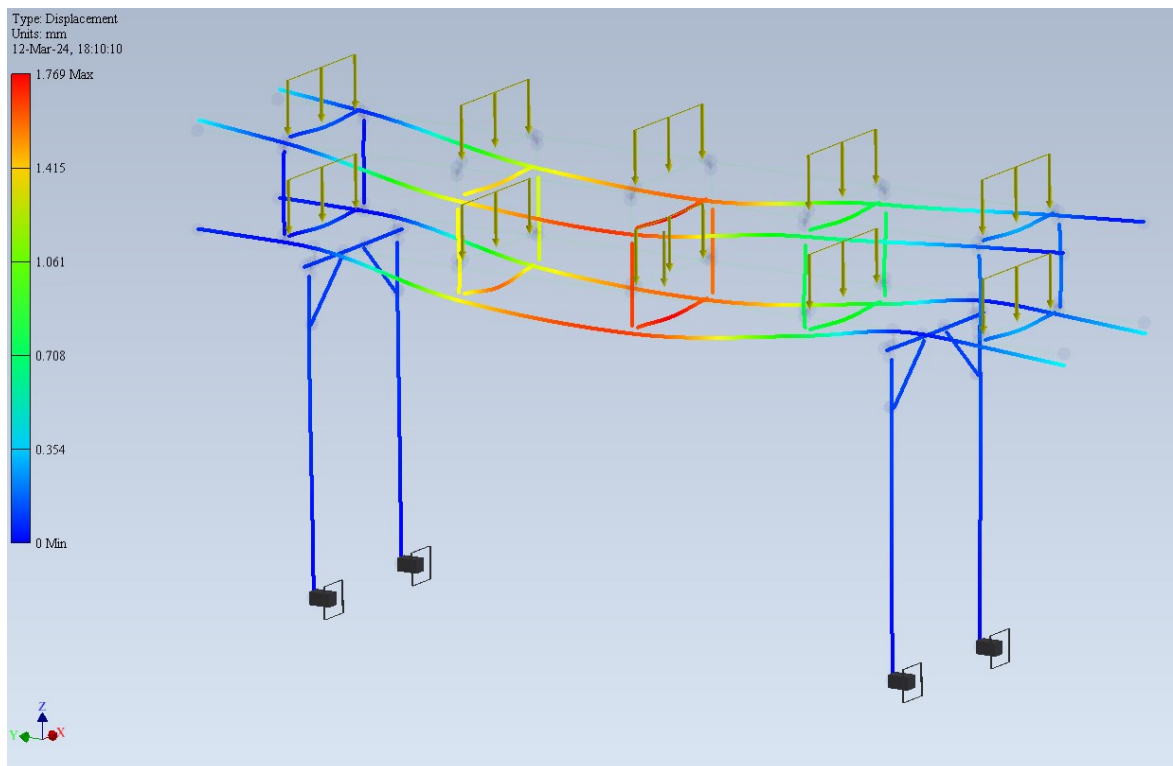
Next three pictures show colour maps of displacements, vertical forces and combined normal stresses in dead load and live load scenario respectively.

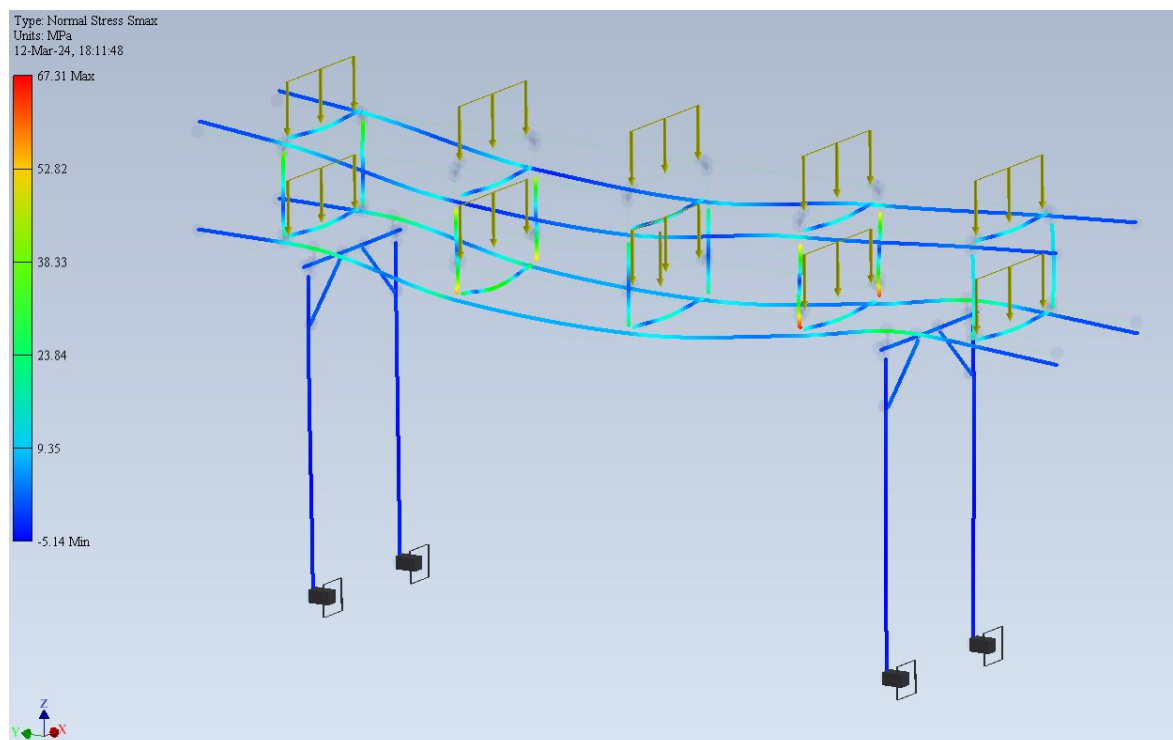
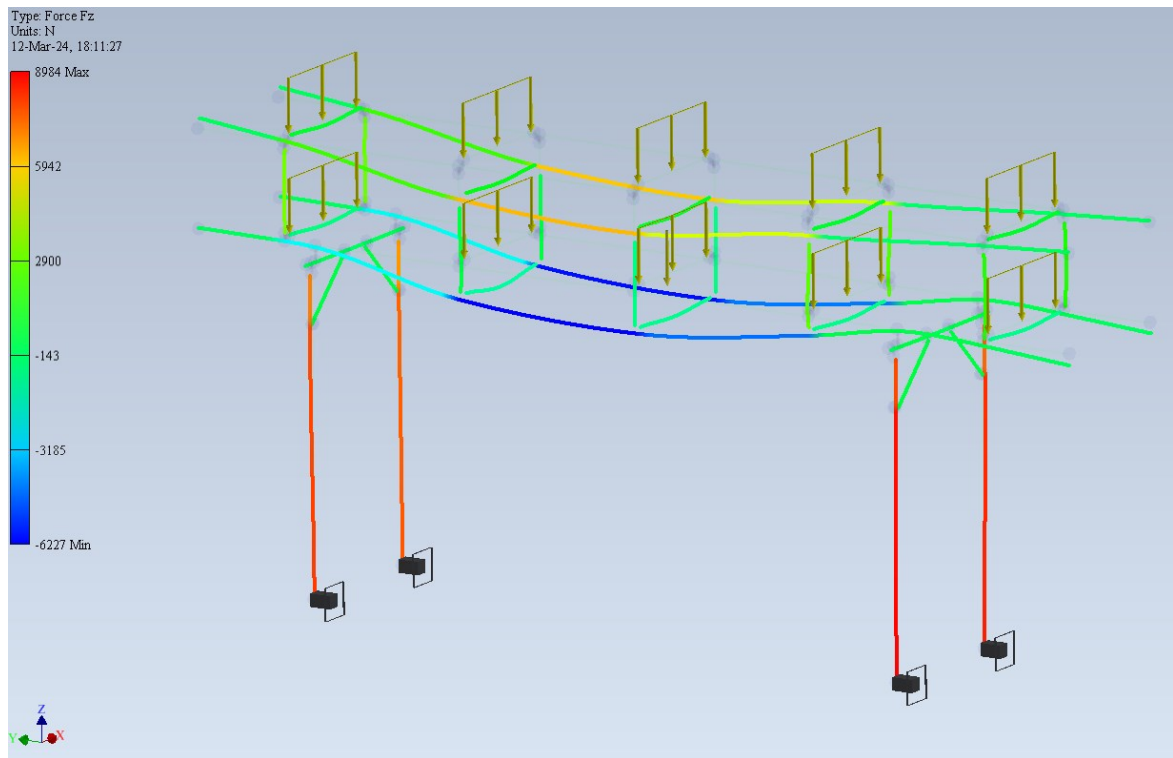






Configuration 3C. Load from piping: 250 kg/m. Mass: 1030 kg. Next three pictures show colour maps of displacements, vertical forces and combined normal stresses in dead load scenario respectively.





Next three pictures show colour maps of displacements, vertical forces and combined normal stresses in dead load and live load scenario respectively.

